THESIS APPROVAL

GRADUATE SCHOOL, KASETSART UNIVERSITY

Doctor of Philosophy (Chemistry)

DEGREE

Chemistry	Chemistry
FIELD	**DEPARTMENT**

TITLE: Experimental and Theoretical Study on the Physical, Photophysical, and Biological Properties of UV Absorbers and Skin Sensitizers

NAME: Miss Malinee Promkatkaew

THIS THESIS HAS BEEN ACCEPTED BY

THESIS ADVISOR

(Professor Supa Hannongbua, Dr.rer.nat.)

THESIS CO-ADVISOR

(Mr. Songwut Suramitr, Ph.D.)

THESIS CO-ADVISOR

(Assistant Professor Thitinun Karpkird, Ph.D.)

THESIS CO-ADVISOR

(Mr. Matthew Paul Gleeson, Ph.D.)

THESIS CO-ADVISOR

(Professor Masahiro Ehara, Ph.D.)

DEPARTMENT HEAD

(Professor Supa Hannongbua, Dr.rer.nat.)

APPROVED BY THE GRADUATE SCHOOL ON _____

DEAN

(Associate Professor Gunjana Theeragool, D.Agr.)

THESIS

EXPERIMENTAL AND THEORETICAL STUDY ON THE PHYSICAL, PHOTOPHYSICAL, AND BIOLOGICAL PROPERTIES OF UV ABSORBERS AND SKIN SENSITIZERS

MALINEE PROMKATKAEW

A Thesis Submitted in Partial Fulfillment of
the Requirements for the Degree of
Doctor of Philosophy (Chemistry)
Graduate School, Kasetsart University
2014

Malinee Promkatkaew 2014: Experimental and Theoretical Study on the Physical, Photophysical, and Biological Properties of UV Absorbers and Skin Sensitizers. Doctor of Philosophy (Chemistry), Major Field: Chemistry, Department of Chemistry. Thesis Advisor: Professor Supa Hannongbua, Dr.rer.nat. 135 pages.

Experimental and theoretical study in this work consists of 3 parts. Firstly, the photophysical properties, photochemistry, and photostablity of various substituted cinnamic acids and cinnamates for UV absorbers were investigated experimentally and theoretically. These series include monohydroxy-, -nitro, and -fluoro derivatives for 18 compounds. Theoretical calculations were performed using both the time-dependent density functional theory (TD-DFT) and symmetry-adapted cluster configuration interaction (SAC-CI) methods. The obtained results showed that *para*-hydroxy derivative was found to be an appropriate UV absorber based on its broad absorption in the UVB/UVA regions, less emission, and higher photostability. Secondly, the photostability of five host-guest inclusion complexes between methoxycinnamic acids (CA) and cyclodextrins (CD) was investigated. All possible conformers were considered and analyzed for their structural and energetic behaviors using quantum chemical calculations. The calculated results revealed that CA and CD can form stable inclusion complexes in both the gas phase and water. Their stability depends on molecular size and shape complementation. Tail orientation showed the most favorable and stable orientation that absorbed in the UVB/UVA regions which is similar to the parent CA. Therefore, the agreement between theoretical results and experimental data can be a potent way to determine the geometry of supramolecular system. Thirdly, a non-animal model for skin sensitization was studied. This work is concerned with the nucleophilic aromatic substitution (S_NAr) domain. A set of 23 halo- and pseudohalobenzenes, 12 of which are reported skin sensitizers and 11 of which are reported nonsensitizers, was investigated using quantum chemical calculations. A model cysteine based nucleoephile was simulated using $-SCH_3$. The reaction coordinate associated with the nucleophilic attack by $-SCH_3$ for the 23 chemicals was evaluated. The barriers and enthalphies were subsequently used to successfully discriminate the sensitizers/reactive molecules from nonsensitizers/unreactive molecules of 23 S_NAr compounds. In these perspectives, the experimental and theoretical investigation provides a useful insight into the physical, photophysical, and biological properties of UV absorbers and skin sensitizers and a useful tool for designing and developing the novel UV compounds and predicting the new compounds for skin sensitizers.

/ /

Student's signature Thesis Advisor's signature

ACKNOWLEDGEMENTS

I would like to express my deep and sincere gratitude to my supervisor, Professor Dr. Supa Hannongbua. Her understanding, encouragement and guidance have provided a good basis for research works. I would like to thank my co-advisors, Dr. Songwut Suramitr, Assistant Professor Dr. Thitinun Karpkird, and Dr. Matthew Paul Gleeson for kindly providing valuable suggestions and helpful guidance on research works. I am deeply grateful to my co-supervisors, Professor Dr. Masahiro Ehara and Professor Dr. Karl Peter Wolschann, for providing me valuable opportunities to learn and gain lots of experiences in short-term research training at their labs, advices and comments.

During studies, I received full financial support from the Royal Golden Jubilee Ph.D. Program (Grant No. 3.C.KU/52/B.1). I also have partial supports from the National Center of Excellence in Petroleums, Petrochemical Technology and Advanced Materials (NCE-PPAM), Thailand Research Fund (TRF), Faculty of Science (ORSE) and Japan Student Services Organization (JASSO). Center of Nanotechnology at Department of Chemistry, Kasetsart University, Institute for Molecular Science (IMS), Japan and University of Vienna, Austria, are gratefully acknowledged for providing research facilities.

My colleagues at Laboratory for Computational and Applied Chemistry (LCAC) are acknowledged for their providing assistance and sharing useful ideas. I would also like to thank all of the staffs at Department of Chemistry, Faculty of Science, Kasetsart University for research facilities. Finally, I would like to thank my parents, who have encouraged me to achieve success in my education.

Malinee Promkatkaew

February, 2014

TABLE OF CONTENTS

Page

LIST OF TABLES

LIST OF TABLES (Continued)

LIST OF TABLES (Continued)

LIST OF FIGURES

LIST OF FIGURES (Continued)

LIST OF FIGURES (Continued)

LIST OF FIGURES (Continued)

LIST OF FIGURES (Continued)

LIST OF FIGURES (Continued)

LIST OF ABBREVIATIONS

E_{ex}	=	Excitation energy
E_{Flu}	=	Fluorescence transition energy
I_{irr}	=	Absorbance of irradiated sample
I_{unirr}	=	Absorbance of unirradiated sample
λ_{abs}	=	Absorption wavelength
λ_{em}	=	Emission wavelength
λ_{max}	=	Maximum wavelength
c	=	Velocity of light
ε	=	Dielectric constant
f	=	Oscillator strength
μ	=	Dipole moment
τ	=	Radiative lifetimes
σ^-	=	Single substituent constants
σ^*	=	Taft value for the leaving group
θ	=	Torsional angle
S	=	Photostability
ΔE_b	=	Binding energy
ΔE_d	=	Deformation energy
pEC3	=	Molar logarithmic parameter of EC3 values
*p*CA	=	*para*-methoxycinnamic acid
245CA	=	*ortho*-, *meta*-, and *para*-trimethoxycinnamic acid
246CA	=	*ortho*- and *para*-trimethoxycinnamic acid
ACD	=	Allergic contact dermatitis
Acyl	=	Acylation
AD	=	Atomic dipole
B3LYP	=	Becke's three parameter hybrid functional using the Lee-Yang-Parr correlation functional
CA	=	Cinnamic acid
CAM-B3LYP	=	Coulomb-attenuating method - B3LYP

LIST OF ABBREVIATIONS (Continued)

CASSCF	=	Complete active space self-consistent field method
CD	=	Cyclodextrin
$CDCl_3$	=	Deuterated chloroform
CIS	=	Singles configuration interaction
CIS(D)	=	Singles configuration interaction (doubles correction)
COOH	=	Carboxylic
CM	=	Cinnamate
D	=	Debye
DFT	=	Density functional theory
DMSO	=	Dimethyl sulfoxide
EC	=	Exchange correlation
EC3	=	Effective chemical concentration values
eV	=	Electron volt
GPT	=	Guinea pig maximization test
HF	=	Hatree fock theory
HOMO	=	Highest occupied molecular orbital
HPLC	=	High performance liquid chromatography
ICCVAM	=	Interagency coordination committee on the validation of alternative methods
ICD	=	Irritant contact dermatitis
ICT	=	Intramolecular charge transfer
int	=	Intermediate complex
KS		Kohn-Sham orbitals
LC	=	Long-range correction
LLNA	=	Murine local lymph node assay
LogP	=	Octanol-water partition coefficient
LUMO	=	Lowest unoccupied molecular orbital
M06-2X	=	Minnesota 06 Functional with 54% HF exchange
MA	=	Michael-type addition

LIST OF ABBREVIATIONS (Continued)

MD	=	Molecular dynamics simulations
MeOH	=	Methanol
MM	=	Molecular mechanics
MOs	=	Molecular orbitals
MOE	=	Molecular operating environment
MWT	=	Molecular weight
nm	=	Nanometer
NMR	=	Nuclear magnetic resonance spectroscopy
MS	=	Mass spectroscopy
NR	=	Non-reactive / Non-sensitizer
OECD	=	Organization for economic co-operation and development
OMC	=	Octyl-*para*-methoxy cinnamate
PCM	=	Polarized continuum model
PECs	=	Potential energy curves
ppm	=	Parts per million
PYP	=	Photoactive yellow protein
QMM	=	Quantitative mechanistic models
QSARs	=	Quantitative structure activity relationships
QSPRs	=	Quantitative structure property relationships
QC	=	Quantum chemical calculations
RAI	=	Relative alkylation index
REACH	=	Registration, evaluation, authorization and restriction of chemical substances regulations
RDS	=	Rate determining step
RMSD	=	Root mean square displacement
S_0	=	Ground state
S_1	=	First excited state
S_2	=	Second excited state
S_3	=	Third excited state

LIST OF ABBREVIATIONS (Continued)

SAC	=	Symmetry adapted cluster
SAC-CI	=	Symmetry adapted cluster-configuration interaction
SAR	=	Structure activity relationships
SB	=	Schiff base formation
SD-R	=	Singles and doubles-R
S_N1	=	First order aliphatic nucleophilic substitution
S_N2	=	Second order aliphatic nucleophilic substitution
S_NAr	=	Aromatic nucleophilic substitution
T_1	=	First triplet excited state
T_2	=	Second triplet excited state
TiO_2	=	Titanium dioxide
TS1	=	Transition state step 1
TS2	=	Transition state step 2
TD-DFT	=	Time-dependent density functional theory
UV–Vis	=	Ultraviolet visible
UVR	=	Ultraviolet radiation
ZnO	=	Zinc oxide

EXPERIMENTAL AND THEORETICAL STUDY ON THE PHYSICAL, PHOTOPHYSICAL, AND BIOLOGICAL PROPERTIES OF UV ABSORBERS AND SKIN SENSITIZERS

INTRODUCTION

Ultraviolet (UV) radiation is part of the electromagnetic spectrum (200-400 nm). These wavelengths are classified as UVA (320-400 nm), UVB (280-320 nm), and UVC (200-280 nm). UVC radiation is absorbed by the ozone layer of the atmosphere and does not reach the earth. UVA and UVB radiation both reach the earth's surface in amounts sufficient to have important biological consequences from exposure of the skin and eyes. Most UVA radiation can penetrate into the deeper layers to play a major part in tanning, skin aging, eye damage, and immune suppression. UVB wavelength tends to cause damage in more superficial epidermal layers. It is responsible for burning, tanning, and acceleration of skin aging and plays a very key role in the development of skin cancer.

Sunscreens have become the most popular choice of photoprotection. These are two broad categories of sunscreens: organic (absorbers) and inorganic (blockers). Most UV filters are organic and protect by absorbing UV, for example, cinnamate, salicylate, and aminobenzoate derivatives. They form a thin protective film on the surface of the skin and take the energy from UV radiation and then go back to a relaxed state by release the energy as heat before it penetrates the skin. The inorganic sunscreens, such as metal oxides, are often termed "physical" or "mineral". The metal oxides, namely titanium dioxide (TiO_2) and zinc oxide (ZnO), are insoluble particles which absorb, reflect, or scatter UV away from the skin.

Cinnamates have received much attention, as they are the most widely used as UVB absorber due to their photophysical properties in particular the absorption efficiency in the UVB region is an important factor. In order to achieve the favorable optical properties, molecular design using the variation of the substituents has been

extensively performed. Recently, 2-ethylhexyl-*para*-methoxycinnamate, as well as other cinnamate derivatives, has been developed as a commercial product. However, only few photophysical properties and photoisomerization mechanisms have been studied on experimental and theoretical investigation of cinnamic acid and some unsubstituted cinnamate.

In parallel, quantum chemical calculations based on semi-empirical, *ab-initio*, density functional theory (DFT), or higher levels of theory are used to determine the geometrical, energetic, and vibrational characteristics of these molecules. All the possible conformers will be considered and analyzed by various theoretical methods and basis sets. Then, single-point electronic calculations are used to determine the absorption/emission spectra, oscillator strengths, molecular orbital contribution, and dipole moments by using the time-dependent density functional theory (TD-DFT) and symmetry adapted cluster configuration interaction (SAC-CI) levels of theory. The effects of solvent inclusion are analyzed by comparisons between gas-phase and solution systems.

Therefore, quantum chemical calculations provide a useful insight into the physical, photophysical, and biological properties and a useful tool for designing and developing the novel UV absorbers and predicting the skin sensitizers. Whereas, the experimental data will be accompanied by theoretical prediction at different level of approximation in order to set up the conclusion on the quantitative structure-activity/property relationships (QSARs/QSPRs) models. These models will be used to predict of the structure, properties and toxicity effects of the other analogous molecules for development as cosmetics products and industries in Thailand.

OBJECTIVES

Firstly, we experimentally and theoretically investigated the photophysical properties and photochemistry of the monohydroxy-, -nitro-, and -fluoro-substituted cinnamic acids (**1A**–**9A**) and cinnamates (**1E**–**9E**) substituted at the *ortho*, *meta*, and *para* positions, as shown in Figure 1. In particular, we are interested in the substitution effects of electron-donating (hydroxy) and electron-withdrawing (nitro and fluoro) group at three positions on the photoabsorption and photostability aiming at the fine chemical modification. The absorption and fluorescence spectra were observed for all the derivatives and detailed assignments were performed by the TD-DFT and SAC-CI methods to elucidate the characteristics of the spectra of these compounds over a wide energy range. The measurement of molar extinction coefficient provides the direct comparison of UVB/UVA blocking performance. The present reliable theoretical results enabled the discussion on the differences in absorption spectra among these derivatives with various substitutions. The solvent effect was also considered in methanol solution for each excited state. The relaxation in the excited state was examined by the fluorescence measurement including oxygen quenching and the photostability was examined using UVB irradiation. The *cis–trans* photoisomerization pathways that lead to the nonradiative decay were also investigated. Based on the comprehensive analysis, the effective substitution in the cinnamate derivatives was proposed.

(a)

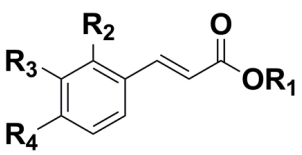

1A-9A: R_1 = H
1E-9E: R_1 = CH_3

(b)

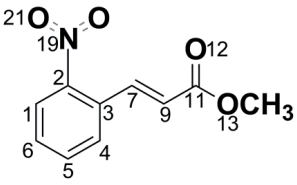

Compound	R_2	R_3	R_4
1	**OH**	H	H
2	H	**OH**	H
3	H	H	**OH**
4	**NO_2**	H	H
5	H	**NO_2**	H
6	H	H	**NO_2**
7	**F**	H	H
8	H	**F**	H
9	H	H	**F**

Figure 1 Molecular structures of (a) substituted cinnamic acids (**1A**–**9A**) and methyl cinnamates (**1E**–**9E**) and (b) the calculated model compounds and atom numbering of *ortho*-nitro methyl cinnamate (**4E**).

Secondly, we investigated the interaction between methoxycinnamic acid and cyclodextrins, to quantify the host-guest inclusion complexation and to determine the driving forces for the complexation process. Five host-guest inclusion complexes between methoxycinnamic acid and cyclodextrins including **[1]** *p*CA-αCD (*para*-monomethexycinnamic acid and α-cyclodextrin), **[2]** *p*CA-βCD (*para*-monomethexycinnamic acid and β-cyclodextrin), **[3]** 245CA-βCD (*ortho*-, *meta*-, *para*-trimethoxycinnamic acid and β-cyclodextrin), **[4]** 246CA-βCD (*ortho*- and *para*-trimethoxycinnamic acid and β-cyclodextrin), and **[5]** 246CA-γCD (*ortho*- and *para*-trimethoxycinnamic acid and γ-cyclodextrin) as shown in Figure 2. The structural and energetic behaviors of all five complexes were studied using quantum chemical calculations. Whereas, molecular docking and molecular dynamics simulations were investigated the most photostability complex **[3]** 245CA with βCD (Karpkird and Wanichweacharungruang, 2010). All possible conformers have been considered and analyzed by theoretical investigations. The agreement between theoretical results and experimental data can be a potent way to determine the geometry of supramolecular system. So, we expect that the theoretical results would provide valuable information for developing effective UV blocking compounds.

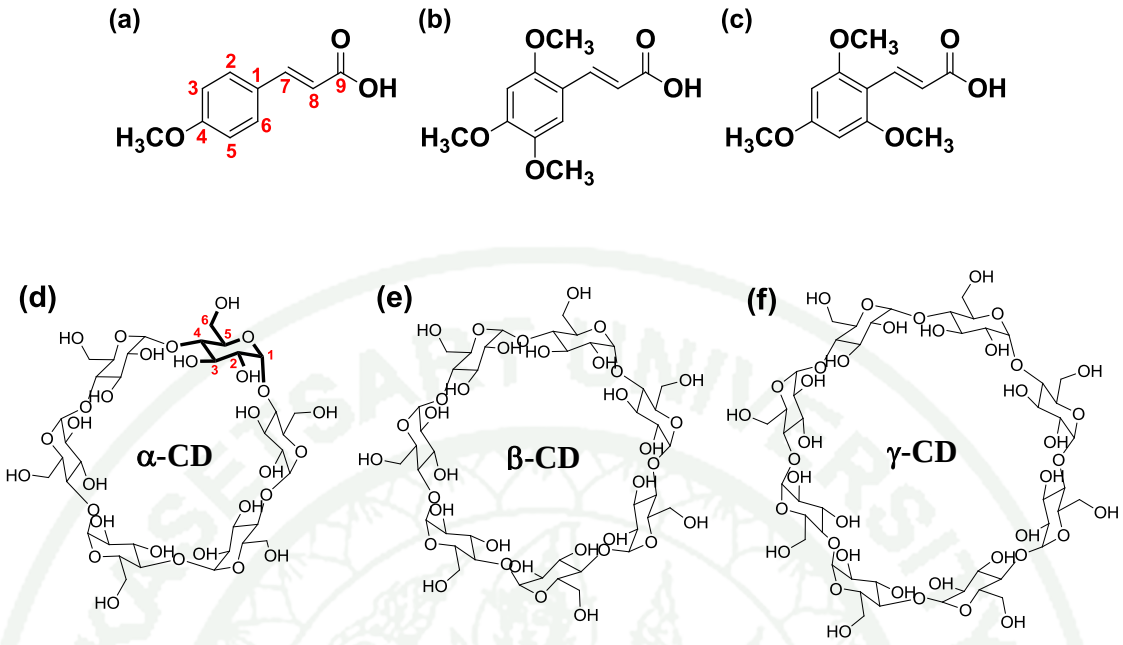

Guest	Host	Complex
para-methoxycinnamic acid (*p*CA)	αCD	**[1]** pCA-αCD
para-methoxycinnamic acid (*p*CA)	βCD	**[2]** pCA-βCD
ortho-, meta- and para-trimethoxycinnamic acid (245CA)	βCD	**[3]** 245CA-βCD
ortho- and para-trimethoxycinnamic acid (246CA)	βCD	**[4]** 246CA-βCD
ortho- and para-trimethoxycinnamic acid (246CA)	γCD	**[5]** 246CA-γCD

Figure 2 Chemical structures and atom numbering of methoxycinnamic acid and cyclodextins: (a) *para*-methoxycinnamic acid, (b) *ortho*-, *meta*-, and *para*-trimethoxycinnamic acid, (c) *ortho*- and *para*-trimethoxycinnamic acid, (d) α-CD, (e) β-CD, and (f) λ-CD.

Thirdly, we investigate the use of QC methods in attempt to rationalize the sensitization potential of chemicals. We focus on the S_NAr reaction domain. The electrophilic reactivity of the S_NAr domain is determined by a combination of the effects of the leaving group X and the activating groups Y. In fact, the reaction can occur when X is any halogen or pseudohalogen or a range of other X groups which are not usually considered as leaving groups (i.e. NO_2, SO_2Ph, SOPh, and SO_3). We calculate the full reaction profile for 23 chemicals reported in the QMM study (Roberts *et al.*, 2011), providing complete details of the reaction kinetics and thermodynamics using a model sulphur nucleophile (Figure 3). This is because it is not clear as to what extent the reactions of different chemicals are influenced by kinetic and thermodynamic factors. Thus, computing the complete energy profile is preferable to rationalize its reactivity. We then use the kinetic and thermodynamic data to try and rationalize the experimentally reported LLNA sensitization results for the compounds in question. We also compare the discriminating potential of the approximated barrier as used by Enoch and Roberts (Enoch and Roberts, 2013) as well as the commonly used HOMO-LUMO band gap. We are particularly interested in determining whether the extra cost of the detailed profile is in any way beneficial over the latter two more approximate representations of reactivity.

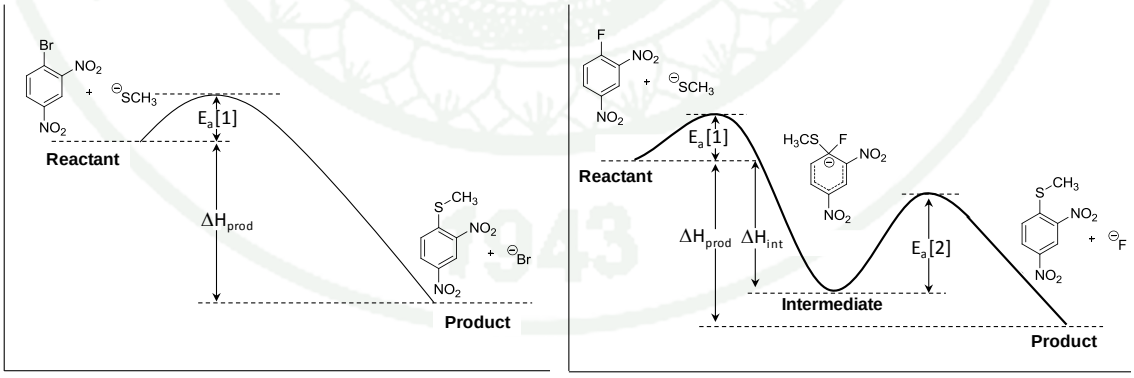

Figure 3 Nucleophilic aromatic substitution (S_NAr) by addition-elimination via S_N1 (right) and S_N2 processes.

LITERATURE REVIEW

1. Cinnamic acid and cinnamate derivatives

Cinnamic acids and their derivatives can be found in many plant products such as foods, medicines, and cosmetics (De *et al.*, 2011; Li *et al.*, 2010). These molecules generally exist in both, *cis* and *trans* configurations. Moreover, the ester derivatives of cinnamic acid also act as optical active molecules in liquid crystal devices. Light induced *cis–trans* isomerization of olefins is a major area of interest in modern photochemical research. Photochemistry of these compounds can be utilized in a variety of applications, such as optoelectronics, storage devices, and light-driven molecular switches (Lendlein *et al.*, 2005; Rehab and Salahuddin, 1999; Zhang *et al.*, 2002; Zuniga *et al.*, 2010). Recently, there has been considerable interest in the photophysical properties and photochemistry of 4-methoxycinnamic acid and 2-ethylhexyl-4-methoxycinnamate; both have been widely used as ultraviolet B (UVB) blocking compounds in cosmetic sunscreens (Huong *et al.*, 2007; Monhaphol *et al.*, 2007; Serpone *et al.*, 2007). However, photostability studies on the derivatives of cinnamic acid and cinnamate showed that they decompose into other compounds when exposed to ultraviolet radiation (Karpkird and Wanichweacharungruang, 2010; Pattanaargson and Limphong, 2001; Pattanaargson *et al.*, 2004b; Rodil *et al.*, 2009; Smith and Miller, 1998). They achieve photoabsorption in the UVB region followed by a *cis–trans* isomerization at the propenyl double bond and relax to the ground state with nonradiative decay. The photochemistry of this process has also been studied, and the involvement of an intramolecular charge transfer (ICT) state resulting from a rotation at the carbon carbon double bond (C=C) has been recognized (Chakraborty *et al.*, 2006; Singh *et al.*, 2008).

In particular, among the various derivatives of cinnamates, methyl 4-hydroxycinnamate has been extensively studied as a model chromophore of photoactive yellow protein (PYP), a cytoplasmic photoreceptor protein found in the *Halorhodospira halophila* bacterium (Hellingwerf *et al.*, 2003; Sprenger *et al.*, 1993). In the UV–Vis absorption of this molecule, three excited states, namely, two $\pi\pi^*$ and

one nπ* transitions, were found to be relevant (Changenet-Barret *et al.*, 2004; de Groot *et al.*, 2008; Gromov *et al.*, 2005; Shimada *et al.*, 2012). The *cis–trans* photoisomerization and nonradiative decay have also been extensively studied both experimentally and theoretically. Recently, the excited-state dynamics of the nonradiative decay and the effect of hydrogen bonding with a water molecule has been investigated using picosecond pump-probe spectroscopy and theoretical calculations (Shimada *et al.*, 2012). There is some discussion about the relaxation pathway; namely, relaxation via conical intersection and nπ* exited state (de Groot *et al.*, 2008; Shimada *et al.*, 2012).

To improve the UVB blocking function and photostability of cinnamate derivatives, chemical modification is necessary. However, only a few studies have reported the effects of substituents at the *para* position. Ishigami (Ishigami *et al.*, 1979) reported that the *cis–trans* photoisomerization of methyl cinnamate occurs via a triplet state in the derivatives with electron-withdrawing groups such as nitro, acetyl, and cyano groups at *para* positions, while those with electron-donating groups such as methyl, isopropyl, methoxy, chloro or dimethylamino groups at the *para* position occur via the singlet excited state (Lewis *et al.*, 1989). Herein, we reported the photophysical and photochemical properties of cinnamic acids and cinnamates with both electron-donating groups, e.g. hydroxy and electron-withdrawing groups, e.g. nitro and fluoro groups at *ortho, meta* and *para*-positions. Interestingly, some derivatives might be useful for optically addressable devices. In our previous studies, we investigated the photophysical properties and photochemistry of *cis* and *trans* isomers of the methoxy-substituted 2-ethylhexylcinnamates at various positions on an aromatic ring experimentally (Karpkird *et al.*, 2009) and their model compounds theoretically (Promkatkaew *et al.*, 2009).

Theoretical investigations of the absorption and emission spectra by means of quantum chemical calculations have become a standard approach with being widely used to help the assignment of the experimental spectra and to get insights of the underlying optical and electronic properties. The advantages of Density Functional Theory (DFT) and time-dependent formalism are combined in Time-Dependent

Density Functional Theory (TD-DFT) (Marques and Gross, 2004; Petersilka *et al.*, 1996; Runge and Gross, 1984) to make it well-suited for efficient and reasonably accurate determination of the excited state properties. The method has been successfully applied to various types of the molecular excited states compared with the experimental results (Fabian, 2001; Meeto *et al.*, 2010; Meeto *et al.*, 2008; Zaleśny *et al.*, 2007). The solvent effects on the absorption and emission spectra are also relevant; therefore, we estimated in this study solvent effects on the electronic spectra with the polarizable continuum model (PCM) (Bader and Berne, 1996; Scalmani *et al.*, 2006; Tomasi *et al.*, 2005). The PCM-TD-DFT is one of the most common and effective model among theoretical methods in supporting the analysis of experimental data for a better understanding of the photophysical properties in solution.

As for TD-DFT, it is generally recognized that the global hybrids describe the valence excitations well, while the range-separated hybrids are necessary for the charge-transfer excitations (Jacquemin *et al.*, 2009; Peach *et al.*, 2008). The cinnamate derivatives have both valence and charge reorganization excitations that are responsible for the photoabsorption in UVB and UVA regions from the dipole moment analysis. The reliable calculation of oscillator strength (spectrum shape) is also important for the development of proper UV absorbers. In the previous study, both global hybrid (B3LYP) and range-separated hybrid (CAM-B3LYP) were adopted for the calculations, however, there were some deviations to experimental results and the calculated spectra were not satisfactory for the definitive assignments and the detailed discussion on the difference among the different derivatives. Thus, further theoretical work based on more accurate wave function theory is necessary to understand the details of photophysical properties and to provide reliable information for molecular design. Theoretical studies of the photochemistry and photostability of these compounds are also important, especially for *cis–trans* photoisomerization in the relaxation pathways.

The symmetry-adapted cluster-configuration interaction (SAC-CI) (Nakatsuji, 1979; Nakatsuji, 1978) method was developed to obtain a detailed interpretation and prediction of the molecular spectroscopy and photochemistry of organic and inorganic

molecules The SAC-CI method has been utilized for the accurate theoretical spectroscopy of many π-conjugated systems and has also been applied to the photochemistry of biological systems(Ehara *et al.*, 2005). Recently, the photophysical properties and excited state dynamics of molecules for organic light-emitting diodes (OLEDs) (Poolmee *et al.*, 2005; Poolmee *et al.*, 2011; Saha *et al.*, 2007; Suramitr *et al.*, 2011). and dye-sensitized solar cells (DSSC) (Namuangruk *et al.*, 2012) were investigated and the absorption and emission spectra of these molecules were elucidated. These studies confirm that the SAC-CI method is useful for investigating the electronic excitations and excited state dynamics of large π-conjugated systems.

2. Methoxycinnamic acid and cyclodextrin inclusion complexes

The most popular organic UV absorber, octyl methoxycinnamate (OMC) is widely used as UVB filter in sunscreen and many cosmetic formulations. OMC can absorb the UVB (280-320 nm) and UVA-II (320-340 nm). It is an ester formed from methoxycinnamic and 2-ethylhexanol. The photoisomerization of *trans*-OMC to *cis*-OMC causing a decrease of absorption efficiency was studied both in solutions and formulations (Chawla and Mrig, 2009). Several studies suggested ways to improve the photostability of cinnamates (Centini *et al.*, 2007). To be ideal UV filters, the UV absorbers should remain unchanged after UV irradiation. The photostability of UV filters has been studied mainly to guarantee a long protection function by optimized dosage and formulation (Gaspar and Maia Campos, 2006). Encapsulation of OMC into nanoparticles consisting of polyvinylalcohol was studied for example (Klinubol *et al.*, 2008; Luadthong *et al.*, 2008; Pattanaargson *et al.*, 2004a; Sasiwilaskorn *et al.*, 2008).

Cyclodextrins (CDs) and their derivatives are cyclic oligosaccharides consisting of several (α-1,4)-linked α-D-glucopyranose units. The most common CDs are α-, β-, and γ-CDs having six, seven, and eight α-D-glucopyranose units, respectively. These non-toxic compounds have elicited an interest not only in pharmaceutical industry, food industry, separation technique, and molecular recognition, but also in environmental protection (Brewster and Loftsson, 2007; Davis

and Brewster, 2004; Szejtli, 1998; Valle and Martin, 2004). CDs, unique in characteristics due to their relative hydrophilic outer surface and comparatively hydrophobic inner cavity, are soluble in water and are able to form inclusion complexes with a variety of guest molecules of partly hydrophobic character (Chen and Jiang, 2011; Szejtli, 1996; 1998).

OMC is used as an oil-soluble sunscreen. In these formulations a slow release of OMC from the complex takes place, resulting in a long-lasting protection of the skin. CD complexes are used to increase the solubility of substances secreted by the skin and thus they are used in products for skin cleaning. Moreover, they are able to complex and to dissolve skin fat. The fat complex formed with CDs can be easily removed from the skin. All these and further advantages of CDs and their complexes can be used for the formulation of cosmetic products (Buschmann and Schollmeyer, 2002; Centini *et al.*, 2007; Numanoglu *et al.*, 2007).

Recently, a number of literature reports discussed the increased photostability of organic UV filters by forming inclusion complexes with CDs (Fenyvesi *et al.*, 2004; Sarveiya *et al.*, 2004; Scalia *et al.*, 2004). The stability of OMC was increased to 26.1% after forming an inclusion complex with β-CD (compared to free OMC) (Scalia *et al.*, 2002). The designing and synthesis of modified CDs have been shown to improve the original binding ability and increase the molecular selectivity of parent CDs. β-CD modified with *trans*- and *cis*-cinnamide, in which only one isomer exhibited the molecular recognition and performed work, so the photoisomerization turns the machine on and off (Coulston *et al.*, 2006). Karpkird and Wanichweacharungruang have synthesized the CD inclusion complex by functionalization of their primary hydroxyl rims with various methoxycinnamoyl moieties. Their behavior and conformations were investigated by 2D NMR ROESY experiments and other spectroscopic techniques. A photostability study of methoxycinnamoyl moieties attached to the cyclodextrins indicated that size matching played an important role in the molecular recognition process of the methoxycinnamoyl modified cyclodextrins. The results indicated that the inclusion complexation could improve photostability of the cinnamoyl moieties and are not

cytotoxic compared to their parent methoxycinnamic acids. Fluorescence and NMR measurements give new insights into inclusion of the hydrophobic moiety of amphiphiles into the cavity of CDs. Their apparent stability constants were well correlated with the structure of the hydrophobic moiety of amphiphiles (Du *et al.*, 2006).

In order to get a better understanding of the binding events, a lot of theoretical methods including molecular mechanics (MM), molecular dynamics simulations (MD) (Cezard *et al.*, 2011; Lawtrakul *et al.*, 2003), and more recently, quantum chemical calculations (QC) (Attoui Yahia and Khatmi, 2009; Fu *et al.*, 2002; Liu and Guo, 2004; Madi *et al.*, 2009; Nascimento *et al.*, 2007; Snor *et al.*, 2009), have been used to study the CD complexes. All experimental and theoretical methods, when properly utilized in combination with each other, have proven to be extremely powerful in solving the structural, energetic, and dynamic problems associated with CD complexes. The aim of this work is to explain the improvement of the chemical stability of complexed methoxycinnamic acid and cyclodextrins by studying the inclusion properties and factors affecting the complexation selectivity between CDs and CA.

3. Skin sensitization

Contact dermatitis is a common environmental and occupational health concern that arises from exposure to certain chemical substances. Contact dermatitis can be caused by the physical effects of chemical irritants on tissue directly (irritant contact dermatitis, ICD), which includes solvents, acids or bases. An irritation may also result from a more extreme allergic response (allergic contact dermatitis, ACD), a complex phased response of the immune system to an allergen (Kimber *et al.*, 2002). Experimental methods for the detection of sensitizers include the Guinea Pig Maximization test (GPT) and the more recent Murine Local Lymph Node Assay (LLNA) (Kimber and Weisenberger, 1989). The LLNA assay is now the method of choice following extensive validation, and has been adopted by the OECD as a standard protocol (Anderson *et al.*, 2011). The assay works by identifying compounds

with the capacity to provoke a T lymphocyte proliferative response within the lymph nodes. Chemicals are classified as sensitizers if they show a 3-fold or greater proliferative response in inducing the draining in lymph nodes compared with controls. While the EC3 is not an absolute response, it can be used to rank order compounds in terms of their relative toxicity (Table 1). EC3 can be sub classified into strong, weak and moderate sensitizers as shown in Table 1. According to the European Union registration, evaluation, authorization and restriction of chemical substances regulations (REACH), greater effort is needed to reduce the numbers of animal tests and costs associated with toxicity testing. This requires the greater use of chemical assay surrogates (Gerberick *et al.*, 2008; Roberts *et al.*, 2009), and theoretical methods such as QSAR models and read-across methods (Patlewicz *et al.*, 2011; Schaafsma *et al.*, 2009).

Table 1 Classification boundaries for LLNA EC3 values of skin sensitizers.

EC3 value (% weight)	Potency classification
NR	Non-sensitizer
≥ 10 to ≤ 100	Weak
≥ 1 to < 10	Moderate
≥ 0.1 to < 1	Strong
≤ 0.1	Extreme

It is widely accepted that skin sensitization begins with the sensitizer in question forming a covalent adduct with a protein electrophile or nucleophile. From the pioneering work in this field by Roberts and Aptula, skin sensitizing chemicals can be assigned to the 5 separate chemical classes (or domains) capable of causing protein adducts; aromatic nucleophilic substitution (S_NAr), Schiff base formation (SB), Michael-type addition (MA), aliphatic nucleophilic substitution (S_N2) and acylation (Acyl) (Aptula *et al.*, 2005; Aptula and Roberts, 2006). The presence of structural or reactive features alone are not reliable indicators of toxicity (Park *et al.*, 2011; Stepan *et al.*, 2011), which is perhaps unsurprising given such that a classification scheme

neglects the overall molecular and local electronic characteristics of a molecule and the fact that a degree of target recognition may be present.

Attempts to develop truly global (i.e. covering a wide diversity of sensitizer types)quantitative structure-activity relationships (QSAR), either by the relative alkylation index (RAI) approaches (Roberts *et al.*, 1991), or by theoretical descriptor - based QSAR approaches (Li *et al.*, 2006; Miller *et al.*, 2005), have not yet met with sufficient success to conform with the complete set of OECD QSAR guidelines (Patlewicz *et al.*, 2011; Roberts *et al.*, 2007). These guidelines are: (a) a defined endpoint, (b) an unambiguous QSAR model, which is (c), mechanistically interpretable. In addition the model must have (d) predictivity that is fit for purpose and (d) a defined domain of applicability for which the model can be used for. QSAR models that currently best fit the OECD principles are termed quantitative mechanistic models (QMM), are restricted to chemicals from an individual reaction domain, thus resemble the simple but functional QSARs first reported by Hansch and Fujita in the 1960s (Hansch and Fujita, 1964). These QSAR methods typically make use of experimentally derived physico-chemical descriptors and are generally accurate for the particular chemical series under investigation (Aptula *et al.*, 2005; Aptula and Roberts, 2006; Roberts *et al.*, 2006a; b; Roberts *et al.*, 2009). Conversely, the main issue however is that given these methods rely on experimentally derived descriptors (i.e. σ electronic and π Taft steric parameters) novel compounds cannot be predicted without first determining these parameters directly. A QMM-like approach based on purely theoretical methods would therefore be desirable if it could match the performance of that obtained with experimentally derived descriptors.

In a recent paper, Enoch and Roberts reported the development of a theoretically based QMM. This method relied on quantum chemical (QC) and an empirically based molecular descriptor to derive an LLNA QSAR for Michael acceptors (Enoch *et al.*, 2008). The authors approximated the rate determining barrier to reaction by using the energy of the high energy intermediate formed following attack by the negatively charged nucleophile (i.e. relying on the Hammond Postulate to estimate the barrier (Hammond, 1955)), and included an additional solvent

accessible surface area term. The QM based protocol is a significant improvement over the use of the similar HOMO-LUMO energy as an estimate for reactivity (Miller *et al.*, 2005). The model led to good discrimination between sensitizers and non-sensitizers for 26 compounds, with only 4 outliers.

MATERIALS AND METHODS

1. Synthesis and characterization

1.1 Materials

2-Ethylhexanol and malonic acid were purchased from Fluka Chemical Company (Buchs, Switzerland). Piperidine was purchased from Sigma (Sigma Chemical Co., Steinheim, Germany). All benzaldyhydes, pyridine and 2-hydroxycinnamic acid (**1A**) were purchased from Acros (Geel, Belgium). Solvents used in syntheses and spectroscopic techniques were reagent or analytical grades purchased from Labscan (Bangkok, Thailand).

1.2 Instruments

UV–Vis absorption spectra were recorded in a quartz cell (light path, 10 mm) on a UV–Vis spectrophotometer (Perkin-Elmer, CT, USA) in methanol solution. Fluorescence emission spectra were recorded in a fluorescence spectrophotometer (Cary Eclipse; Varian, CA, USA) in acetonitrile solution. All ^{1}H NMR spectra were obtained in $CDCl_3$ or DMSO-d_6 on a Varian Mercury NMR spectrometer, which operated at 400 MHz for ^{1}H and 100 MHz for ^{13}C nuclei.

1.3 Preparation of *trans*-substituted cinnamic acids

All *trans*-cinnamic acids were synthesized as described in the previous work using the Knoevenagel–Doebner condensation between substituted benzaldehydes and malonic acid in the presence of piperidine as a catalyst (Figure 4) (Allen and Spangler, 1943; Koo *et al.*, 1944) In short, malonic acid (0.02 mol) and substituted benzaldehyde (0.015 mol) were dissolved in 5 ml of pyridine and piperidine (0.15 ml) was added. The reaction mixture was refluxed at 70°C for 5 hrs. After the mixture had been cooled, 5 ml of conc. HCl and 40 ml of cold water were

added. The solid was separated by suction filtration, washed with cold water and recrystallized with ethanol. Only the synthesis of 2-hydroxycinnamic acid (**1A**) failed and the commercial product was used: the hydrogen bond between the hydroxyl group and the carbonyl group decreases the reactivity of the carbonyl group of the aldehyde.

1.4 Preparation of 2-ethylhexyl-*trans*-substituted cinnamates

All *trans*-cinnamates were then prepared by esterification between *trans*-cinnamoyl chloride, which was prepared *in situ* from cinnamic acids, oxalylchloride, and 2-ethylhexanol (Figure 4) (Womack and McWhirter, 1955). *Trans*-substituted cinnamic acid (0.01 mol) was dissolved in dichloromethane. Oxalylchloride (0.015 mol) was then added slowly under N_2. The reaction mixture was stirred at room temperature for 1.5 hrs. Residue oxalylchoride was removed by rotary evaporator before 2-ethylhexanol (0.01 mol) was added. The mixture was stirred overnight at room temperature. The residue obtained after solvent evaporation was washed with 10% $NaHCO_3$. A crude reaction product was purified by silica gel column eluting with hexane-ethylacetate to give 2-ethylhexyl-*trans*-substituted cinnamate.

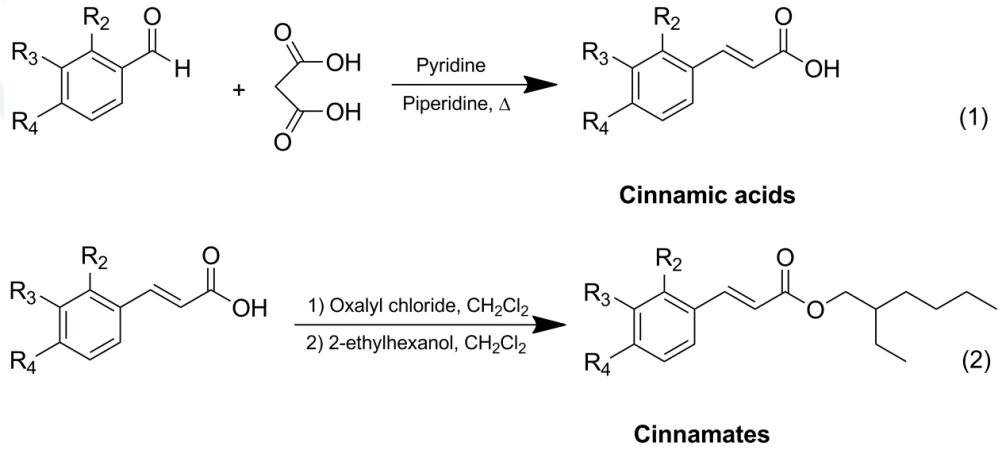

Figure 4 Synthesis pathways of cinnamic acids and cinnamates.

2. Theoretical calculations

2.1 TD-DFT and SAC-CI investigation of cinnamic acids and cinnamates

To investigate the functions of the UVB blocking molecules, the low-lying two ππ* and one nπ* excited states were calculated for the substituted cinnamic acids (**1A**–**9A**) and methyl cinnamates (**1E**–**9E**). These model compounds were investigated to reduce the computation time without losing the essence of the excitations, as the electronic structure relevant to the photophysical properties can be described well with these models; the side alkyl chain does not affect photophysical properties so much. In this article, we use the term "cinnamate" rather than "methyl cinnamate" (model system) except for some computational results because the experimental observation is done for 2-ethylhexyl cinnamate derivatives. The excited states of nitro derivatives whose excitation is localized around nitro group were excluded from the solutions because they do not contribute to the absorption significantly. To calculate vertical absorption and emission spectra, the geometry optimization was performed for the ground (S_0) and the first excited (ππ*, S_1) states. The ground state geometries were fully optimized without restricting the symmetry using the B3LYP (Becke, 1988; Lee *et al.*, 1988) /6-31G(d) (Hehre *et al.*, 1972) method. On the other hand, the optimization of the first ππ* excited-state geometries was performed while restricting the planar structure as Cs symmetry using the CIS/D95(d) (Dunning and Hay, 1976) method except for *ortho*-nitro-substituted derivatives. Based on the S_0- and S_1-state geometries, the vertical absorption and emission energies were calculated. To simulate the absorption spectra, the vertical excitation energies were calculated at the S_0 optimized geometries using the TD-DFT method with B3LYP/6-311G(d,p) and CAM-B3LYP(Yanai *et al.*, 2004)/6-311G(d,p) and the SAC-CI/D95(d) level of theories. To calculate emission spectra, the geometry optimization was performed for the first excited state (S_1) using the SAC-CI/D95(d) method. The solvent effects were evaluated by using the polarizable continuum model (PCM) in methanol solution.

In the SAC/SAC-CI calculations, the singles and doubles (SD)-*R* method with the direct calculation of the σ vectors, i.e., the direct SAC-CI approach (Fukuda and

Nakatsuji, 2008), was used. The perturbation selection technique (Nakatsuji, 1983) was used to reduce the computational cost and level-two accuracy was adopted. The threshold of the linked terms for the ground state was set to $\lambda_g = 5.0 \times 10^{-6}$. All the product terms generated by the doubles were included in the SAC calculations. For the excited states, the threshold of the linked doubles was set to $\lambda_e = 5.0 \times 10^{-7}$. All the product terms generated by the R_1S_2 and R_2S_2 operators were included in the SAC-CI calculations.

The angle of the nitro group relative to the cinnamate unit θ (C_1=C_2–N_{19}=O_{21}) affects the optical properties as it relates to the π-conjugation. In particular, the *ortho*-nitro derivatives have non-planar structures in the S_0 state because of steric effects, as discussed later. Therefore, the ground state potential energy curves (S_0 PECs) along the angle θ of the nitro group with respect to the phenyl ring were calculated using the B3LYP/6-31G(d) method. Molecular structures were partially optimized at fixed angles (θ = 0° to 180° in steps of 15°) with all the other coordinates optimized. With these structures, the excitation energies were calculated to examine their dependence on the angle.

To examine the pathway of nonradiative relaxation in the excited states, the PECs of the singlet excited states (S_1 and S_2), both of which could be involved by UVB absorption (280-320 nm), were calculated for **1E**, **2E**, and **3E** along the torsion angle ω(C_3–C_7=C_9–C_{11}). These S_1 and S_2 PECs were calculated using the CIS(D)/6-31G(d)//CIS/6-31G(d) calculations; namely, the CIS/6-31G(d) partial optimization in which the torsion angle ω was fixed with all the other coordinates optimized and followed by the CIS(D)/6-31G(d) calculations. Triplet excited states may also be involved in the relaxation and they are actually observed in oxygen quenching. Therefore, vertical transition energies of triplet excited states (T_1 and T_2) were also calculated by CIS(D)/6-31G(d) at the ground state geometries.

The B3LYP geometry optimizations, TD-DFT and SAC-CI calculations were performed using the Gaussian 09 suite of programs (Frisch *et al.*, 2009) version B.01.

2.2 Methoxycinnamic acid and cyclodextrin inclusion complexes

Five host-guest inclusion complexes between methoxycinnamic acid and cyclodextrins including **[1]** *p*CA-αCD, **[2]** *p*CA-βCD, **[3]** 245CA-βCD, **[4]** 246CA-βCD, and **[5]** 246CA-γCD. The geometries of all five complexes were studied using quantum chemical calculations. Whereas, molecular docking and molecular dynamics simulations were investigated the most photostability complex **[3]** 245CA with βCD, the most widely used one of the natural CDs (Karpkird and Wanichweacharungruang, 2010).

Despite the efforts that have been devoted to solve the local minimum problem, there is still no method to guarantee the finding of the global minimum for any CD complex. Therefore, a lot of conclusions from the quantum mechanics (QM) and molecular mechanics (MM) studies on CD complexes should be considered qualitative and not absolute. Further studies on the local minimum problem are needed. An important driving force for the CD complex formation in aqueous solution is the hydrophobic effect. The solvation is considered as a continuum medium with certain dielectric constant (ε). Using this method one can easily obtain the solvation free energies and it has been shown that under many circumstances the calculated solvation free energies are quite reliable. However, one needs to add a sufficient number of solvent molecules into the system. This method is advantageous in that the results are easy to visualize. Using this method one often ends up with an extremely large system which is discussed in the molecular dynamics simulations section. By carrying out quantum chemistry calculations, we present the structural and energetic behaviors of the host-guest interactions both in gas phase and water which used the dielectric constant to account for the solvent effect. By performing molecular docking and molecular dynamics simulations, we show the molecular behavior of the host-guest interaction in water.

2.2.1 Quantum chemical calculations

The starting geometries of methoxycinnamic acid (*p*CA, 245CA, and 246CA), cyclodextrins (α-CD, β-CD, and γ-CD), and the inclusion complexes were manually built with the help of GaussView program. In this study, the inclusion complexes between methoxycinnamic acid (CA) and cyclodextrin (CD) were for two possible orientations of CA in the cavity. In the first structure, the modified CDs (by functionalization of their primary hydroxyl rims with CA) are compared with the experimental data (Karpkird and Wanichweacharungruang, 2010). In the second structure, the CD/CA inclusion complex which does not contain any covalent bond between host and guest molecules and their stability depends on molecular size and shape complementation.

The ground-state geometries for all structures were fully optimized by using density functional theory (DFT) calculations with the M06-2X functional (Valero *et al.*, 2008; Zhao and Truhlar, 2011) with the 6-31G(d,p) (Hehre *et al.*, 1972) basis set without any symmetry restrain. All optimized structures were investigated in both gas phase and aqueous solution. The effect of solvent has been included the dielectric constant ε (water = 78.4) using a polarized continuum model (PCM) (Bader and Berne, 1996; Tomasi *et al.*, 2005). To investigate the UV−Vis spectra, the vertical excitation energies were performed for the ground state optimized geometries using the time-dependent density functional theory (TD-DFT) with the same M06-2X/6-31G(d,p) method. The solvent effect was calculated with dimethyl sulfoxide (DMSO) (ε = 46.8) in order to compare with the experimental data.

2.2.2 Molecular docking and molecular dynamics simulations

Molecular docking is frequently used to predict the binding orientation of small molecule drug candidates to their protein targets with the aim to achieve an optimized conformation for both the protein and ligand and relative orientation between protein and ligand such that the free energy of the overall system is minimized.(Lengauer and Rarey, 1996). In this study, molecular docking was

carried out with the MOE 12 (Molecular Operating Environment) program to find the more stable conformation. MOE strongly supports drug design through molecular simulation, protein structure analysis, data processing of small molecules, docking study of proteins and small molecules, and so on under the unified operations.

Molecular docking calculations were employed to predict the potential binding mode of CA to CDs cavity for complex **[3]** 245CA-βCD. The initial structures of 245CA and βCD were optimized by using the M06-2X/6-31G(d,p) calculations. The docking of the inclusion complex between 245CA and βCD were performed with the MOE-dock system. During the refinement step, the ligand was free to move within the binding pocket. After MOE docking, all docked complexes have been re-optimized by using the M06-2X/6-31G(d,p) methods in order to find the global minimum and the driving force for the inclusion complex formations in gas phase and aqueous solution.

Molecular simulation is a very powerful toolbox in modern molecular modeling, and enables us to follow and understand structures and dynamical behavior in detail. Macroscopic properties measured in an experiment are not direct observations, but averages over billions of molecules representing a statistical ensemble. For small gas-phase molecules, advanced molecular orbital theory is more accurate and more useful than molecular mechanics. The real power of molecular dynamics simulations is in the ability to handle explicit solvent molecules. The conformation of a molecule can depend strongly on the presence of solvent. In addition, studies of molecular recognition and binding require careful consideration of solvent effects. When dissolved in water, water molecules will fill the cavity of the host. Then when a guest interacts with the cavity of the host, water molecules are displaced. The binding affinity depends on the interactions of guest with the host and the difference in the interactions of bound water and water with the bulk solvent. Therefore, solvation plays a very important role in molecular binding (Furuki *et al.*, 1993).

To obtain high accuracy and good reliability of the binding mode information, complex **[3]** showing the most photostability was selected for MD simulations. The

initial coordinates of the selected compounds complexed were taken from QC calculations using M06-2X/6-31G(d,p) method and were served as the initial coordinates for MD simulations. MD simulations were performed using the SANDER module of the AMBER12 (Case *et al.*, 2012) program. CDs were solvated in a truncated octahedral box with a buffer distance of 12.0 Å. The parameters used for water were taken from the TIP3P (Jorgensen *et al.*, 1983) model. The GLYCAM06 (Kirschner *et al.*, 2008) force field was used to simulate native CDs. When using GLYCAM, the scaling factors for 1–4 non-bonded interactions have been set to unity. Coordinates and energy outputs during molecular dynamics simulation were sampled every 2 ps. MD trajectories were evaluated in terms of the root mean square displacement (RMSD), complex structure and binding free energy. Visualization of the trajectories was achieved using the Chimera program.

2.2.3 Binding (ΔE_b) and deformation (ΔE_d) energies

The structures and thermodynamic stabilities of the host-guest complexes formed by cyclodextrins and additives vary with the nature of the guests. These inclusion complexes do not contain any covalent bond between host and guest molecules and their stability depends on molecular size and shape complementation but also on the external medium and environmental conditions. The most important driving forces in the inclusion complexes are electrostatic, van der Waals and hydrophobic interactions, hydrogen bonding and release of conformational strain (Liu and Guo, 2002).

In order to investigate the driving forces leading to the actual complex between CA and CDs, we made use of binding and deformation energies, defined as follow (Equations (5)–(8)):

$$\Delta E_{\mathrm{b}} = \quad E_{\mathrm{complex}} - (E[\mathrm{CD}]_{\mathrm{opt}} + E[\mathrm{CA}]_{\mathrm{opt}}) \qquad (5)$$

where E_{complex}, $E[\text{CD}]_{\text{opt}}$, and $E[\text{CA}]_{\text{opt}}$ stand for the minimum energy structures of host, guest, and the inclusion complex, respectively. The more negative binding energy (ΔE_{b}) gives the more thermodynamically favorable inclusion complex.

Furthermore, in order to investigate the host-guest complexation induced deformation of the host and guest molecules, we defined the deformation energy of the host and guest (ΔE_{d}), as according formula:

$$\Delta E_{\text{d}} = \ E_{\text{complex}} - (E[\text{CD}]_{\text{sp}}^{\text{opt}} + E[CA]_{\text{sp}}^{\text{opt}}) \quad (6)$$

$$\Delta E_{\text{d}}(\text{CD}) = \ E[\text{CD}]_{\text{sp}}^{\text{opt}} - E[\text{CD}]_{\text{opt}} \quad (7)$$

$$\Delta E_{\text{d}}(\text{CA}) = \ E[\text{CA}]_{\text{sp}}^{\text{opt}} - E[\text{CA}]_{\text{opt}} \quad (8)$$

where $\Delta E_{\text{d}}(\text{CD})$ stands for the deformation energy of the host, $E[\text{CD}]_{\text{sp}}^{\text{opt}}$ is the single point energy of the host using its geometry in the optimized complex, and $E[\text{CD}]_{\text{opt}}$ is the energy of the optimized geometry of the host. Low deformation energies could indicate favorable processes.

2.3 Skin sensitization prediction using quantum chemical calculations

Three different datasets of chemicals were extracted in order to determine whether the actual application affects prevalence. Topical drugs were obtained from chEMBL, the top 200 drugs (primarily oral) were taken from Stepan *et al*. (Stepan *et al.*, 2011) and an LLNA dataset was created from 3 sources as follows. A dataset of 494 unique chemicals were obtained from three sources (1) ICCVAM (Interagency Coordination Committee on the Validation of Alternative Methods), (2) Kern *et al.* (Kern *et al.*, 2010) and (3) Enoch *et al.* (Enoch *et al.*, 2008) The data was merged and cleaned using the following protocol: CAS numbers and/or smiles were rechecked, LLNA data for smiles duplicates were averaged; compounds with contradictory measurements were excluded. The EC3 values of the LLNA dataset were converted to

the molar logarithmic parameter pEC3 (=log (MWT/EC3)). Compounds were assigned manually to its particular reaction domain if not already specified in the original source. Compound that were clearly assigned to a single reaction class were used for categorization only.

The S_NAr domain chemicals under investigation here consist of 23 halo- and pseudohalobenzenes form the publication of Roberts *et al.* (Roberts *et al.*, 2011) Of these, 12 are reported to be skin sensitizers and 11 are non-sensitizers. A $-SCH_3$ cysteine based model for a protein as nucleophile was used to estimate the reaction profile for these 23 compounds in line with others (Enoch and Roberts, 2013). We evaluate the following states for each chemical, (a) the isolated reactants, (b) the non-bonded reactant complex, (c) the bonded intermediate complex (if stable), (d) the non-bonded product complex and (d) the isolated products, as well as (e) the transitions state(s) connecting the different complexes. The reaction coordinates were modeled using a density functional theory (DFT) based QC model in Gaussian 09 (Frisch *et al.*, 2009), Revision C01. In this case we use the extensively validated M06-2X functional developed by Truhlar and co-workers (Valero *et al.*, 2008; Zhao and Truhlar, 2011) which has been used here in conjunction with the double zeta 6-31+G(d,p) basis set. The effect of solvent has been included using a polarized continuum model (PCM) consisting of water. Stationary points were confirmed as such using vibrational frequency analysis. All minima showed zero negative frequencies and all transitions states just one. Significant properties (MWT and clogP) were calculated using Chemaxon JChem software package.

RESULTS AND DISCUSSION

1. Photophysical properties and photochemistry of substituted cinnamic acids and cinnamates, based on TD-DFT and SAC-CI investigations

1.1 Ground- and excited-state geometries

The ground (S_0)- and excited ($\pi\pi^*$, S_1)-state geometries of the monohydroxy-, -nitro-, and -fluoro-substituted cinnamic acids (**1A–9A**) and cinnamates (**1E–9E**) at the *ortho*-, *meta*-, and *para*-positions were obtained using the B3LYP/6-31G(d) and CIS/D95(d) levels of theory, respectively. Although the local minimum of the $n\pi^*$ state is located below that of the $\pi\pi^*$ state in the cinnamate (Gromov *et al.*, 2005), the fluorescence from the $\pi\pi^*$ excited state is considered. Eight substituted cinnamic acids and eight substituted methyl cinnamates except the *ortho*-nitro substituted derivatives **4A** and **4E** have their local minimum at the coplanar structure in both the S_0 and S_1 states because of the π-conjugation. The *ortho*-nitro-substituted derivatives have non-planar structures as discussed in the potential energy curves section. A comparison of the bond lengths along the π-conjugation between the S_0- and S_1-state geometries of **1A**–**9A** and **1E**–**9E** is shown in Figure 5. The detailed molecular structures of **1A**–**9A** and **1E**–**9E** are given in Figure 6.

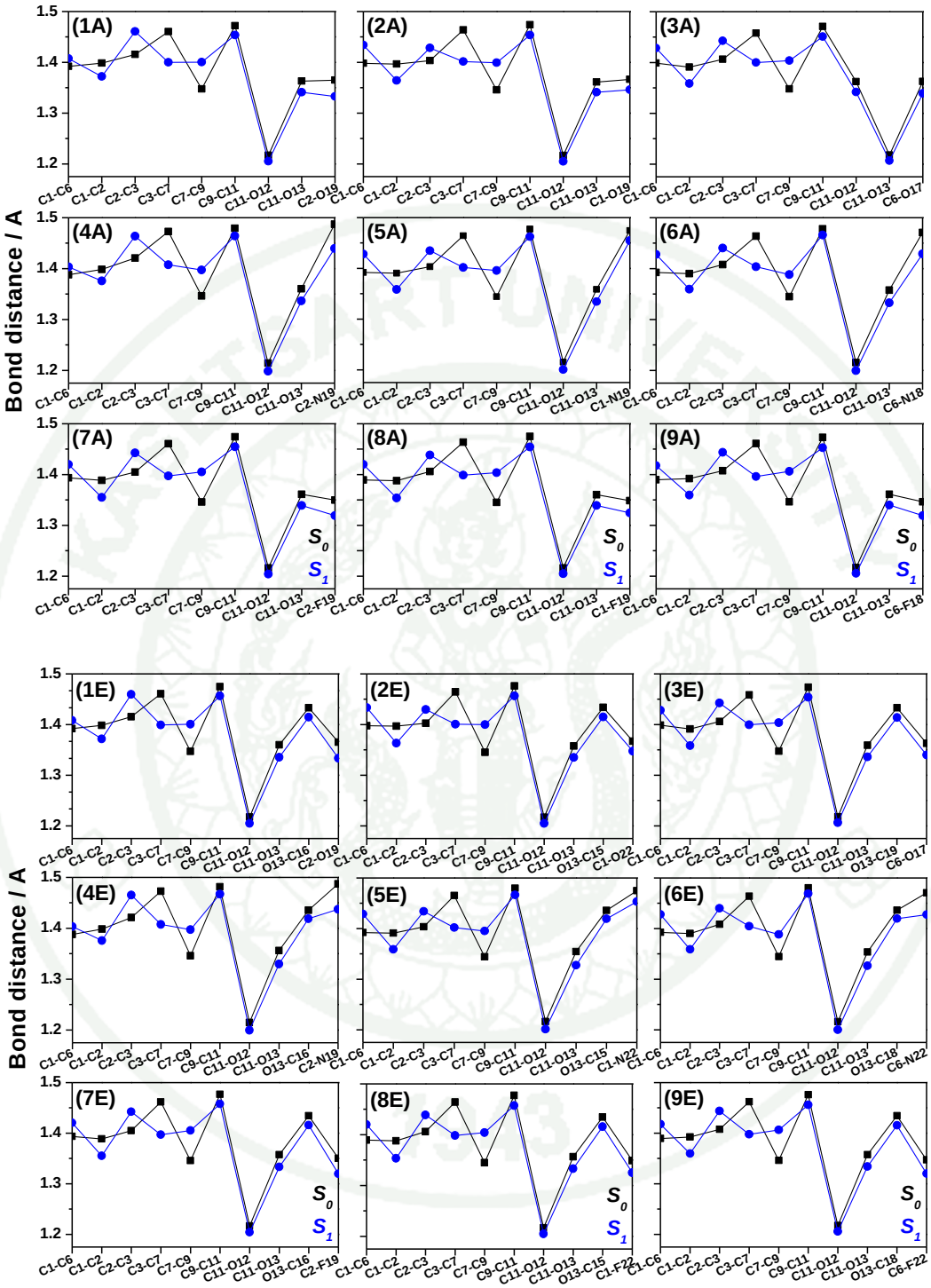

Figure 5 Bond lengths of substituted cinnamic acids (**1A**–**9A**) and cinnamates (**1E**–**9E**) in the S_0 and S_1 states calculated using the B3LYP/6-31G(d) and CIS/D95(d) methods, respectively.

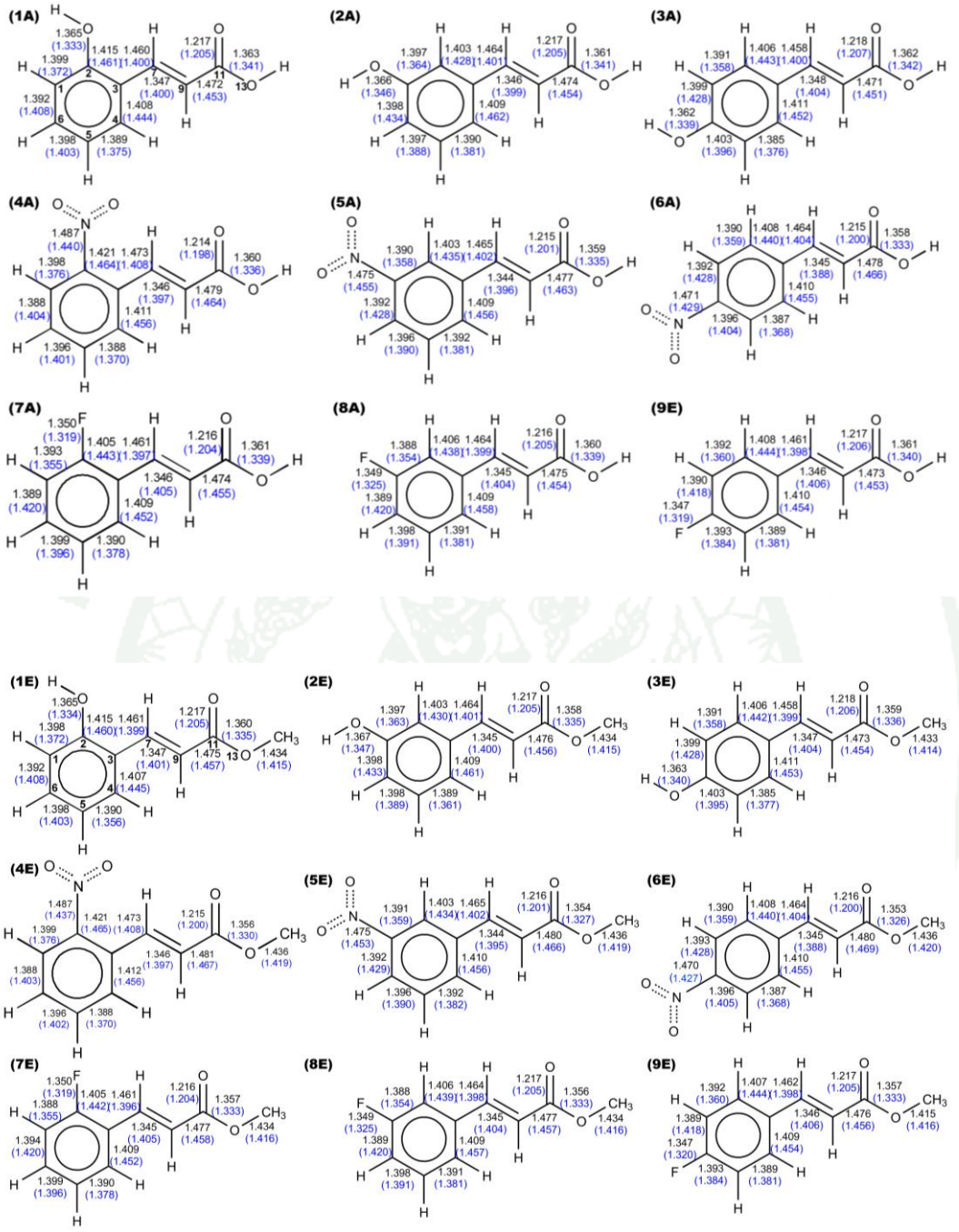

Figure 6 A comparison of the bond lengths (Å) between the S_0 and S_1 (in parentheses) states for substituted cinnamic acids (**1A**–**9A**) and cinnamates **(1E**–**9E)** calculated using the B3LYP/6-31G(d) and CIS/D95(d) methods, respectively.

Based on the geometry changes, the ππ* excitation of the hydroxy-, nitro-, and fluoro-substituted derivatives of both cinnamic acids and methyl cinnamates is localized in the central unit, except for the nitro substituted at the *ortho* and *para* positions of cinnamic acids (**4A**, **6A**). and methyl cinnamates (**4E**, **6E**). For example, in the **1E** derivative, the changes in carbon–carbon (C–C) bond lengths are Δr = +0.044, +0.038, –0.062, and +0.054 Å for C_2–C_3, C_3–C_4, C_3–C_7, and C_7–C_9, respectively. In general, the C_2–C_3, C_3–C_4, C_1–C_6, and C_7–C_9 bond lengths increase and the lengths of the other bonds decrease in the first ππ* excited state compared with those in the ground state. The derivatives with a nitro group at the *ortho* or *para* positions, on the other hand, have a moderate change in C–N bond length between the S_0- and S_1-state geometries. In the **4E** and **6E** derivatives of methyl cinnamates, for instance, the changes in C–N bond length are Δr = –0.050 and –0.043 Å, respectively, and those of **4A** and **6A** of cinnamic acids are Δr = –0.048 and –0.043 Å, respectively. The geometry change of these *ortho*- and *para*-derivatives reflects the bonding nature of LUMO in the C–N bond, while the change is not so large in *meta*-derivatives. This geometry change can be understood by the character of molecular orbital (MO) nodal patterns. The nodal patterns of Kohn-Sham (KS) orbitals around the highest occupied MO (HOMO) and lowest unoccupied MO (LUMO) did not depend on the computational methods or functions. Therefore, the ππ* excitation is predominantly described as the H–L (HOMO–LUMO) transition. The HOMO and LUMO of all the derivatives are shown in Figures 7, 8 and 9.

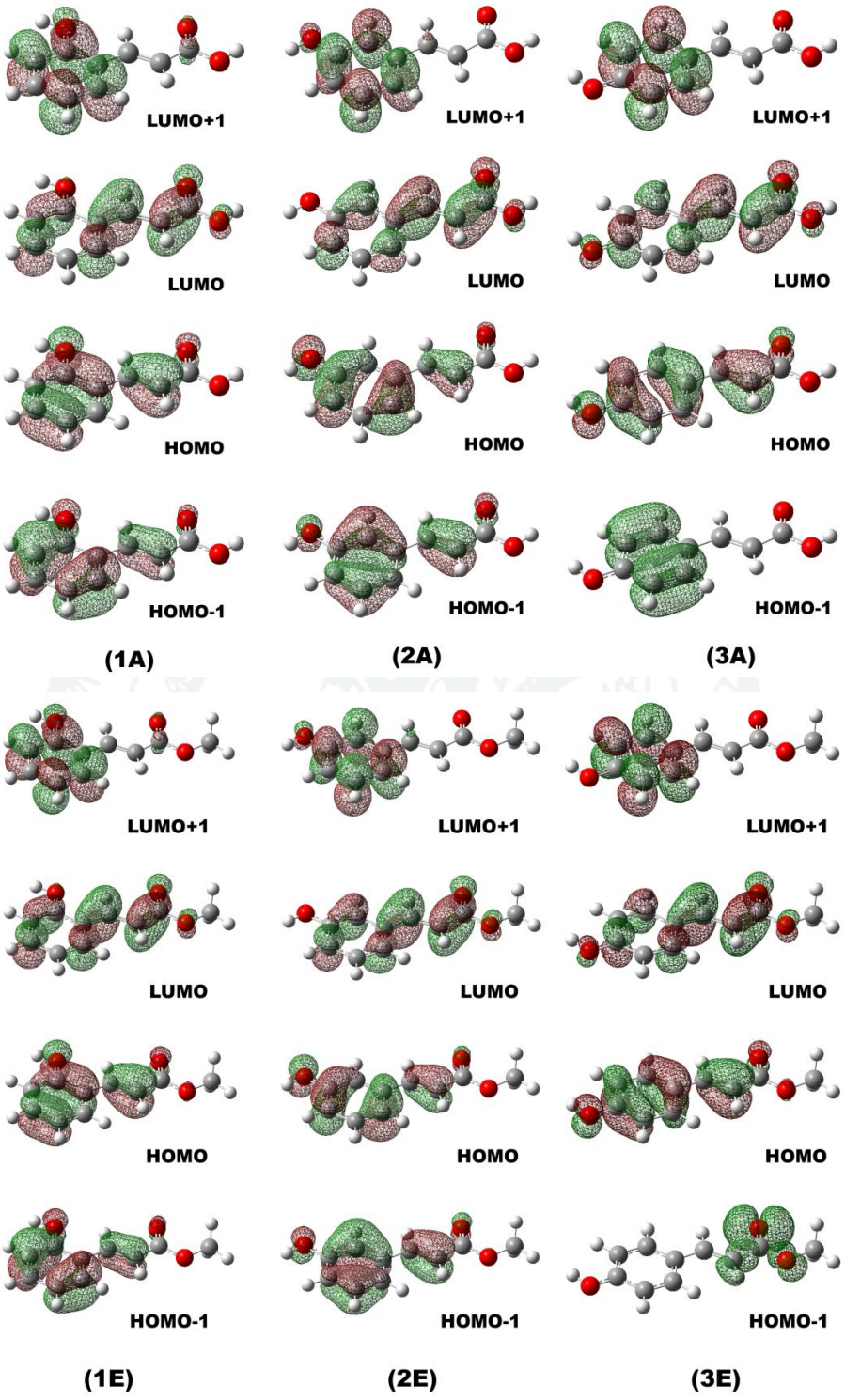

Figure 7 KS orbitals relevant to the low-lying excited states for OH-*ortho*, OH-*meta*, and OH-*para*-substituted cinnamic acids (**1A**–**3A**) and cinnamates (**1E**–**3E**).

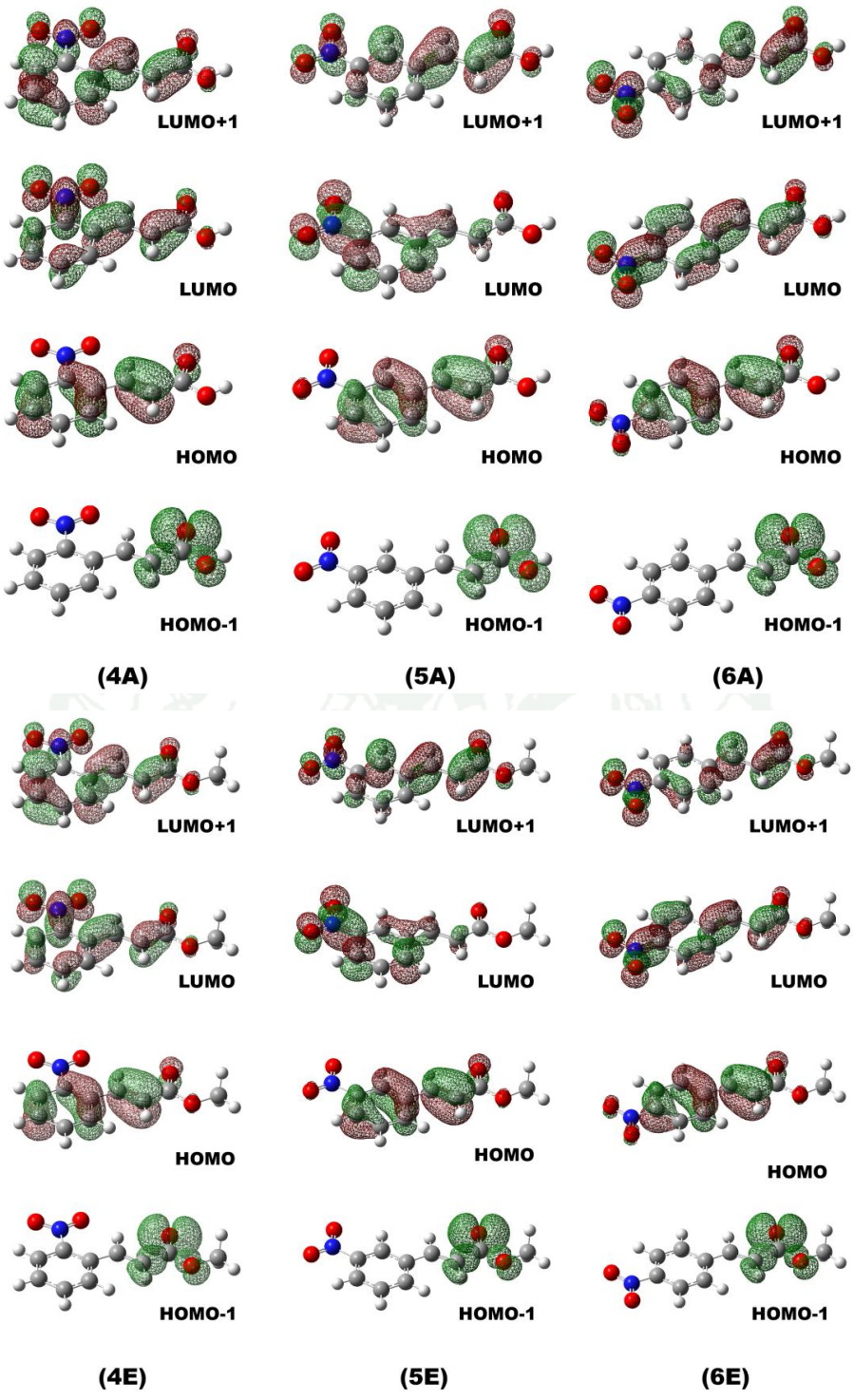

Figure 8 KS orbitals relevant to the low-lying excited states for NO_2-*ortho*, NO_2-*meta*, and NO_2-*para*-substituted cinnamic acids (**4A**–**6A**) and cinnamates (**4E**–**6E**).

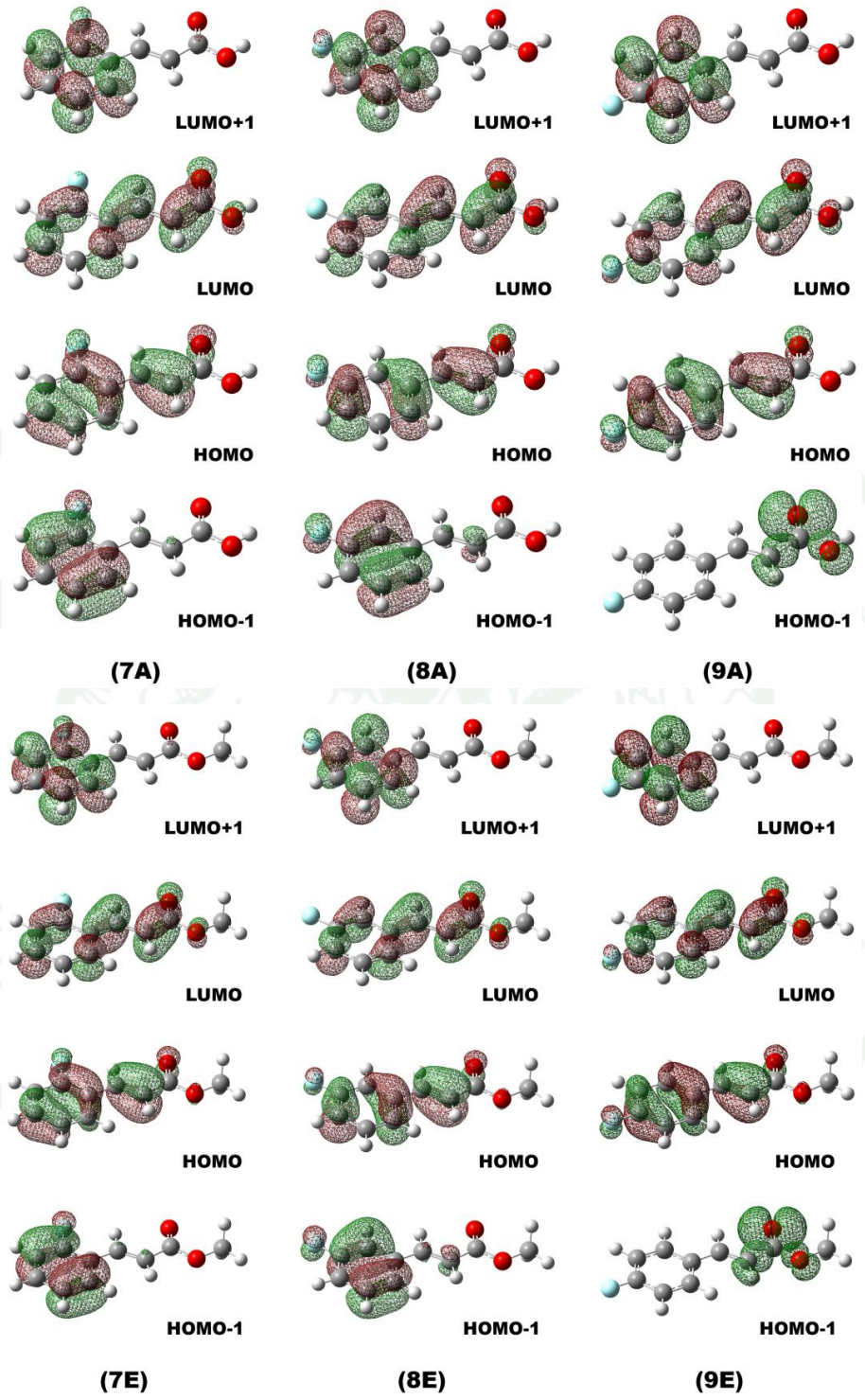

Figure 9 KS orbitals relevant to the low-lying excited states for F-*ortho*, F-*meta* and F-*para*-substituted cinnamic acids (**7A**–**9A**) and cinnamates (**7E**–**9E**).

2.2 Absorption spectra

2.2.1 TD-DFT calculations

The calculated excitation energies (E_{ex}), oscillator strengths (*f*) and composition in terms of KS orbitals (MOs) with the related character of substituted cinnamic acids (**1A**–**9A**) calculated by the TD-B3LYP and TD-CAM-B3LYP methods are summarized in Tables 2 and 4, and those of substituted cinnamates (**1E**–**9E**) are given in Tables 3 and 5. As shown later, TD-B3LYP performs well than TD-CAM-B3LYP in this system and therefore, TD-B3LYP/6-311G(d,p) and TD-CAM-B3LYP/6-311G(d,p) were employed to obtain the energies of the singlet-singlet electronic transitions as well as the oscillator strengths and excitation character of the low-lying excited states. The vertical excitation energies in methanol solution were evaluated within the PCM. The results show that the absorption peaks in methanol solution undergo red shift compared to those in gas phase of both cinnamic acids and cinnamates, significantly. The absorption spectra of all compounds were reasonably reproduced by B3LYP functional in both peak position and intensity.

First, we focus on the TD-DFT absorption wavelengths of the substituted cinnamic acids and cinnamates in gas phase and in methanol solution compared with the experimental results. The experimental spectra were observed in methanol solution. For cinnamic acid derivatives (**1A**–**9A**), the deviations from the experimental values in peak position were within about 15 nm in both, gas phase and in methanol solution, except for *para*-nitro compound (**6A**) and all fluoro compounds (**7A**–**9A**). On the other hand, in cinnamate derivatives (**1E**–**9E**), the deviations from the experimental values in peak position were about 20 nm and 10 nm both in gas phase and in methanol solution, respectively, which is partly attributed to the solvent effect and/or our model neglecting the side chain. Therefore, the excitation energies in solution are in better agreement with the experimental data. However, in TD-B3LYP, the absorption peak of the *para*-nitro substituted cinnamic acid (**6A**) and cinnamate (**6E**) are overestimated (>30 nm) compared to the experimental absorption peak. CAM-

B3LYP functional, a improved hybrid functional with long-range correction (LC), performs well for the excited states of large π-conjugated system. The TD-CAM-B3LYP absorption properties of substituted cinnamic acids and cinnnamates in gas phase and in methanol solution are collected in supporting information. The results show that TD-CAM-B3LYP provides better results than TD-B3LYP for *para*-nitro and fluoro compounds of cinnamic acid (**6A**–**9A**) and cinnamate (**6E**–**9E**), while TD-B3LYP performs well for most of other derivatives. Therefore, we present the assignments and interpretation of the absorption spectra based on the TD-B3LYP results.

The absorption wavelength, hydroxy group substituted at the *ortho*- and *meta*-positions of cinnamic acid (**1A** and **2A**) and cinnamate (**1E** and **2E**) show two distinct absorption bands. **1A** and **1E** compounds have two peaks with large oscillator strength, whereas the spectra of **2A** and **2E** compounds show a single strong peak in the higher energy region, with a shoulder on the lower energy side. The absorption spectra of the *para*-hydroxy group of cinnamic acid (**3A**) and cinnamate (**3E**) consist of a single absorption band, and that of **3A** and **3E** compounds consist of closely separated two peaks, which is in good agreement with the experimental results. The absorption spectra of all hydroxy substitutions of cinnamates are similar in shape to those of the corresponding cinnamic acids. The absorption peaks in *para*-nitro substituted derivatives of cinnamic acid (**6A**) and cinnamate (**6E**) show slightly red shift compared to those in the *ortho*- and *meta*-nitro substituted derivatives of both cinnamic acid (**4A** and **5A**) and cinnamate (**4E** and **5E**). The absorption spectrum of compound **4A** shows a single peak in the higher energy region, and the shoulder on the lower energy side agreed well with the experimental results. While all the experimental spectra of the fluoro group substituted derivatives at the *ortho*-, *meta*- and *para*-positions of cinnamic acids (**7A**, **8A** and **9A**) and cinnamates (**7E**, **8E** and **9E**) show a single absorption band, the TD-DFT absorption spectra of **7A**, **8A**, **7E** and **8E** compounds consist of closely separated two peaks, whereas **9A** and **9E** compounds show a slightly red shift with a single peak. These trends were well reproduced by the present TD-DFT calculations.

Next, we discuss the transition probabilities of substituted cinnamic acids (**1A**–**9A**) and substituted cinnamates (**1E**–**9E**). The shape of absorption spectra or the peak with largest transition probabilities of substituted cinnamic acids is similar to those of cinnamates. Cinnamic acid derivatives with hydroxy substitution at *ortho*- and *meta*-positions have the first peak corresponding to the electronic excitation from HOMO to LUMO (H→L) and the second peak from next HOMO (HOMO-1) to LUMO (H-1→L) transition. The electronic excitation in nitro substituted compound corresponds to the transition from HOMO to LUMO+1 (H→L+1), whereas, those of fluoro substitution is characterized as the transition from HOMO to LUMO (H→L). For *para*-position, the hydroxy, nitro and fluoro substitutions have the same pattern corresponds to the electronic excitation form HOMO to LUMO (H→L). This feature was interpreted by the variation of the KS orbitals due to the different substituted positions.

The KS orbitals relevant for the low-lying excited states of the hydroxy, nitro and fluoro substituted cinnamic acids (**1A**–**9A**) and cinnamates (**1E**–**9E**) at the *ortho*-, *meta*- and *para*-positions are given in Figures 7, 8, and 9, respectively. As shown, the pattern of the orbitals of the cinnamates is similar to that of the cinnamic acids. The HOMO, HOMO-1, LUMO and LUMO+1 are localized on the phenylene vinylene backbone. In the HOMO and HOMO-1, the vinyl double bonds form bonding orbitals and the single bonds linking the phenyl ring with the vinyl double bond are anti-bonding. In the LUMO and LUMO+1, the vinyl double bonds are anti-bonding and the single bonds are bonding. For the substitution, the hydroxy and fluoro groups on the phenyl ring have a small contribution to π-conjugation. Whereas the nitro group has a large contribution in LUMO and LUMO+1, which can also be confirmed by the changes in C–N bond length of the nitro substituted compounds accompanied by excitation.

Table 2 Theoretical absorption energy (E_{ex}, eV/nm), oscillator strength (f), and transition character in terms of KS orbitals in gas phase and in methanol solution for substituted cinnamic acids **(1A**–**9A)** using the TD-B3LYP/6-311G(d,p) method.

	TD-B3LYP/6-311G(d,p)						
	Gas phase			In methanol			*Exp.*
	E_{ex} (eV/nm)	f	Transition character	E_{ex} (eV/nm)	f	Transition character	(nm)
1A	3.96/313 (S_1)	0.270	H→L (63%)	3.73/332 (S_1)	0.307	H→L (67%)	324
	4.34/286 (S_2)	0.000	H-2→L (69%)	4.36/285 (S_2)	0.420	H-1→L (66%)	
	4.54/273 (S_3)	0.357	H-1→L (63%)	4.59/270 (S_3)	0.000	H-2→L (69%)	278
2A	3.91/317 (S_1)	0.080	H→L (65%)	3.74/331 (S_1)	0.109	H→L (68%)	317
	4.38/283 (S_2)	0.000	H-2→L (69%)	4.38/283 (S_2)	0.612	H-1→L (66%)	
	4.54/273 (S_3)	0.526	H-1→L (62%)	4.59/270 (S_3)	0.000	H-2→L (69%)	283
3A	4.20/295 (S_1)	0.666	H→L (70%)	3.98/312 (S_1)	0.786	H→L (70%)	300
	4.44/279 (S_2)	0.000	H-2→L (69%)	4.55/273 (S_2)	0.002	H-1→L (56%)	
	4.60/270 (S_3)	0.023	H→L+1 (50%)	4.69/265 (S_3)	0.000	H-2→L (69%)	
4A	3.53/351 (S_1)	0.000	H-3→L (66%)	3.41/364 (S_1)	0.186	H→L (69%)	
	3.68/337 (S_2)	0.171	H→L (67%)	3.69/336 (S_2)	0.000	H-3→L (67%)	273
	3.85/322 (S_3)	0.000	H-1→L (67%)	4.02/308 (S_3)	0.000	H-2→L (67%)	
	4.12/301 (S_4)	0.000	H-4→L (67%)	4.18/297 (S_4)	0.191	H-1→L (65%)	
	4.40/282 (S_5)	0.178	H-2→L (57%)	4.26/291 (S_5)	0.000	H-5→L (67%)	
	4.76/260 (S_6)	0.264	H→L+1 (57%)	4.60/270 (S_6)	0.377	H→L+1 (64%)	
5A	3.74/332 (S_1)	0.000	H-3→L (64%)	3.53/351 (S_1)	0.026	H→L (69%)	
	3.81/326 (S_2)	0.033	H→L (66%)	3.90/318 (S_2)	0.000	H-3→L (68%)	
	4.20/295 (S_3)	0.000	H-1→L (50%)	4.38/283 (S_3)	0.000	H-5→L (61%)	
	4.24/292 (S_4)	0.000	H-4→L (63%)	4.39/283 (S_4)	0.064	H-1→L (63%)	
	4.56/272 (S_5)	0.268	H→L+1 (51%)	4.41/281 (S_5)	0.000	H-2→L+1 (47%)	274
	4.74/261 (S_6)	0.000	H-1→L+1 (51%)	4.49/276 (S_6)	1.013	H→L+1 (64%)	
	4.77/260 (S_7)	0.651	H→L+1 (43%)	4.71/263 (S_7)	0.000	H-2→L (51%)	
6A	3.63/342 (S_1)	0.000	H-3→L (65%)	3.68/337 (S_1)	0.664	H→L (70%)	
	3.96/313 (S_2)	0.610	H→L (70%)	3.81/325 (S_2)	0.000	H-3→L (67%)	283
	4.00/310 (S_3)	0.000	H-1→L (66%)	3.92/316 (S_3)	0.034	H-1→L (69%)	
7A	4.29/289 (S_1)	0.000	H-2→L (69%)	4.19/296 (S_1)	0.468	H→L (61%)	
	4.30/288 (S_2)	0.324	H→L (56%)	4.40/281 (S_2)	0.293	H-1→L (60%)	265
	4.55/272 (S_3)	0.326	H→L (42%)	4.51/275 (S_3)	0.000	H-2→L (69%)	
8A	4.29/289 (S_1)	0.197	H→L (55%)	4.20/295 (S_1)	0.341	H→L (62%)	
	4.33/287 (S_2)	0.000	H-2→L (69%)	4.46/278 (S_2)	0.411	H→L (34%)	
	4.57/272 (S_3)	0.435	H→L (44%)	4.53/274 (S_3)	0.000	H-2→L (69%)	266
9A	4.38/283 (S_1)	0.000	H-1→L (69%)	4.26/291 (S_1)	0.739	H→L (70%)	
	4.40/282 (S_2)	0.620	H→L (70%)	4.59/270 (S_2)	0.000	H-2→L (69%)	265
	4.66/266 (S_3)	0.012	H-2→L (55%)	4.61/269 (S_3)	0.003	H-1→L (61%)	

Table 3 Theoretical absorption energy (E_{ex}, eV/nm), oscillator strength (f), and transition character in terms of KS orbitals in gas phase and in methanol solution for substituted cinnamates **(1E**–**9E)** using the TD-B3LYP/6-311G(d,p) method.

	TD-B3LYP/6-311G(d,p)						
	Gas phase			In methanol			*Exp.*
	E_{ex} (eV/nm)	f	Transition character	E_{ex} (eV/nm)	f	Transition character	(nm)
1E	3.98/312 (S_1)	0.314	H→L (64%)	3.73/332 (S_1)	0.342	H→L (67%)	332
	4.35/285 (S_2)	0.000	H-2→L (69%)	4.35/285 (S_2)	0.447	H-1→L (66%)	
	4.55/273 (S_3)	0.374	H-1→L (63%)	4.65/267 (S_3)	0.000	H-2→L (69%)	280
2E	3.96/313 (S_1)	0.093	H→L (64%)	3.75/331 (S_1)	0.122	H→L (68%)	325
	4.39/283 (S_2)	0.000	H-2→L (69%)	4.37/284 (S_2)	0.667	H-1→L (66%)	
	4.54/273 (S_3)	0.577	H-1→L (61%)	4.65/267 (S_3)	0.000	H-2→L (69%)	285
3E	4.20/295 (S_1)	0.721	H→L (70%)	3.97/313 (S_1)	0.844	H→L (70%)	314
	4.46/278 (S_2)	0.000	H-1→L (69%)	4.55/273 (S_2)	0.003	H-1→L (55%)	
	4.60/269 (S_3)	0.032	H→L+1 (52%)	4.74/262 (S_3)	0.000	H-2→L (69%)	
4E	3.53/351 (S_1)	0.000	H-3→L (67%)	3.40/365 (S_1)	0.206	H→L (69%)	
	3.65/339 (S_2)	0.188	H→L (67%)	3.69/336 (S_2)	0.000	H-3→L (67%)	281
	3.84/323 (S_3)	0.000	H-1→L (67%)	4.09/303 (S_3)	0.000	H-2→L (67%)	
	4.13/300 (S_4)	0.000	H-5→L (67%)	4.18/297 (S_4)	0.202	H-1→L (64%)	
	4.41/281 (S_5)	0.201	H-2→L (56%)	4.26/291 (S_5)	0.000	H-6→L (68%)	
	4.75/261 (S_6)	0.279	H→L+1 (54%)	4.58/271 (S_6)	0.409	H→L+1 (63%)	
5E	3.74/332 (S_1)	0.000	H-3→L (65%)	3.53/351 (S_1)	0.027	H→L (69%)	
	3.76/330 (S_2)	0.033	H→L (67%)	3.65/339 (S_2)	0.000	H-3→L (68%)	
	4.19/296 (S_3)	0.000	H-1→L (51%)	3.84/323 (S_3)	0.000	H-6→L (67%)	
	4.25/292 (S_4)	0.000	H-5→L (64%)	3.84/323 (S_4)	0.062	H-1→L (62%)	282
	4.56/272 (S_5)	0.306	H→L+1 (53%)	4.47/278 (S_5)	0.000	H-2→L+1 (50%)	
	4.69/265 (S_6)	0.000	H-1→L+1 (51%)	4.47/277 (S_6)	1.096	H→L+1 (63%)	
	4.76/261 (S_7)	0.704	H-2→L (53%)	4.77/260 (S_7)	0.000	H-2→L (51%)	
6E	3.64/341 (S_1)	0.000	H-3→L (65%)	3.66/339 (S_1)	0.708	H→L (70%)	
	3.93/315 (S_2)	0.651	H→L (70%)	3.81/325 (S_2)	0.000	H-3→L (67%)	304
	3.98/311 (S_3)	0.000	H-1→L (67%)	3.92/316 (S_3)	0.033	H-1→L (69%)	
7E	4.30/288 (S_1)	0.000	H-2→L (69%)	4.19/296 (S_1)	0.549	H→L (63%)	
	4.32/287 (S_2)	0.405	H→L (59%)	4.40/282 (S_2)	0.278	H-1→L (61%)	288
	4.57/271 (S_3)	0.307	H-1→L (57%)	4.58/271 (S_3)	0.000	H-2→L (69%)	
8E	4.32/287 (S_1)	0.257	H→L (57%)	4.20/295 (S_1)	0.408	H→L (63%)	284
	4.33/286 (S_2)	0.000	H-2→L (69%)	4.45/279 (S_2)	0.412	H-1→L (60%)	
	4.57/271 (S_3)	0.439	H-1→L (52%)	4.59/270 (S_3)	0.000	H-2→L (69%)	
9E	4.39/282 (S_1)	0.000	H-1→L (69%)	4.24/292 (S_1)	0.803	H→L (70%)	
	4.40/282 (S_2)	0.676	H→L (69%)	4.61/269 (S_2)	0.003	H-1→L (60%)	279
	4.68/265 (S_3)	0.019	H-2→L (53%)	4.65/267 (S_3)	0.000	H-2→L (69%)	

Table 4 Theoretical absorption energy (E_{ex}, eV/nm), oscillator strength (f), and transition character in terms of KS orbitals in gas phase and in methanol solution for substituted cinnamic acids **(1A**–**9A)** using the TD-CAM-B3LYP/6-311G(d,p) method.

	TD-CAM-B3LYP/6-311G(d,p)						
	Gas phase			In methanol			*Exp.*
	E_{ex} (eV/nm)	f	Transition character	E_{ex} (eV/nm)	f	Transition character	(nm)
1A	4.30/288 (S_1)	0.413	H→L (67%)	4.11/302 (S_1)	0.492	H→L (69%)	324
	4.89/254 (S_2)	0.000	H-2→L (64%)	4.75/261 (S_2)	0.250	H-1→L (66%)	
	4.89/254 (S_3)	0.221	H-1→L (63%)	5.09/243 (S_3)	0.000	H-2→L (64%)	278
2A	4.43/280 (S_1)	0.173	H→L (65%)	4.29/289 (S_1)	0.259	H→L (68%)	317
	4.80/258 (S_2)	0.458	H-1→L (62%)	4.68/265 (S_2)	0.493	H-1→L (66%)	283
	4.89/253 (S_3)	0.000	H-2→L (65%)	5.07/244 (S_3)	0.000	H-2→L (65%)	
3A	4.47/277 (S_1)	0.699	H→L (69%)	4.27/290 (S_1)	0.831	H→L (69%)	300
	4.91/252 (S_2)	0.040	H→L+1 (54%)	4.90/253 (S_2)	0.018	H→L+1 (52%)	
	4.95/250 (S_3)	0.000	H-2→L (65%)	5.15/241 (S_3)	0.000	H-2→L (65%)	
4A	3.73/332 (S_1)	0.000	H-3→L (60%)	3.87/321 (S_1)	0.000	H-3→L (62%)	
	4.20/295 (S_2)	0.294	H→L (68%)	3.95/314 (S_2)	0.321	H→L (69%)	273
	4.32/287 (S_3)	0.000	H-5→L (60%)	4.43/280 (S_3)	0.000	H-6→L (61%)	
	4.62/269 (S_4)	0.000	H-2→L (56%)	4.58/271 (S_4)	0.162	H-2→L (63%)	
	4.76/260 (S_5)	0.138	H-1→L (54%)	4.81/258 (S_5)	0.000	H-1→L (53%)	
	5.27/235 (S_6)	0.375	H→L+1 (55%)	5.06/245 (S_6)	0.475	H→L+1 (63%)	
5A	3.89/318 (S_1)	0.000	H-3→L (57%)	4.03/307 (S_1)	0.000	H-3→L (64%)	
	4.39/283 (S_2)	0.000	H-5→L (57%)	4.23/293 (S_2)	0.098	H→L (66%)	
	4.43/280 (S_3)	0.126	H→L (64%)	4.51/275 (S_3)	0.000	H-6→L (64%)	274
	4.81/258 (S_4)	0.000	H-2→L (51%)	4.72/263 (S_4)	0.345	H→L+1 (58%)	
	4.85/256 (S_5)	0.313	H→L+1 (54%)	4.91/252 (S_5)	0.779	H-1v→ (56%)	
	5.26/236 (S_6)	0.657	H-1→L (53%)	5.00/248 (S_6)	0.000	H-2→L (60%)	
6A	3.84/323 (S_1)	0.000	H-3→L (57%)	3.98/311 (S_1)	0.000	H-3→L (61%)	
	4.34/286 (S_2)	0.000	H-5→L (58%)	4.13/300 (S_2)	0.824	H→L (69%)	
	4.37/283 (S_3)	0.741	H→L (69%)	4.42/281 (S_3)	0.034	H-1→L (67%)	282
7A	4.60/270 (S_1)	0.534	H→L (66%)	4.48/277 (S_1)	0.695	H→L (69%)	265
	4.84/256 (S_2)	0.000	H-2→L (64%)	4.84/256 (S_2)	0.081	H-1→L (63%)	
	4.93/251 (S_3)	0.127	H-1→L (60%)	5.03/247 (S_3)	0.000	H-2→L (64%)	
8A	4.67/265 (S_1)	0.486	H→L (67%)	4.55/272 (S_1)	0.654	H→L (69%)	266
	4.86/255 (S_2)	0.000	H-2→L (64%)	4.84/256 (S_2)	0.117	H-1→L (62%)	
	4.89/254 (S_3)	0.164	H-1→L (58%)	5.03/246 (S_3)	0.000	H-2→L (65%)	
9A	4.65/267 (S_1)	0.637	H→L (69%)	4.52/275 (S_1)	0.757	H→L (70%)	269
	4.90/253 (S_2)	0.000	H-2→L (64%)	5.00/248 (S_2)	0.007	H-1→L (52%)	
	5.02/247 (S_3)	0.023	H-1→L (48%)	5.08/244 (S_3)	0.000	H-2→L (65%)	

Table 5 Theoretical absorption energy (E_{ex}, eV/nm), oscillator strength (f), and transition character in terms of KS orbitals in gas phase and in methanol solution for substituted cinnamates **(1E–9E)** using the TD-CAM-B3LYP/6-311G(d,p) method.

	TD-CAM-B3LYP/6-311G(d,p)						
	Gas phase			In methanol			*Exp.*
	E_{ex} (eV/nm)	f	Transition character	E_{ex} (eV/nm)	f	Transition character	(nm)
1E	4.31/288 (S_1)	0.459	H→L (67%)	4.11/302 (S_1)	0.537	H→L (69%)	332
	4.90/253 (S_2)	0.000	H-2→L (63%)	4.75/261 (S_2)	0.262	H-1→L (66%)	
	4.91/253 (S_3)	0.230	H-1→L (63%)	5.14/241 (S_3)	0.000	H-2→L (64%)	280
2E	4.47/278 (S_1)	0.204	H→L (65%)	4.30/289 (S_1)	0.293	H→L (68%)	325
	4.81/258 (S_2)	0.483	H-1→L (61%)	4.68/265 (S_2)	0.520	H-1→L (66%)	285
	4.90/253 (S_3)	0.000	H-2→L (64%)	5.12/242 (S_3)	0.000	H-2→L (65%)	
3E	4.48/277 (S_1)	0.752	H→L (69%)	4.27/291 (S_1)	0.889	H→L (69%)	314
	4.91/252 (S_2)	0.050	H→L+1 (55%)	4.90/253 (S_2)	0.020	H→L+1 (53%)	
	4.96/250 (S_3)	0.000	H-2→L (64%)	5.19/239 (S_3)	0.000	H-2→L (65%)	
4E	3.74/332 (S_1)	0.000	H-3→L (60%)	3.87/321 (S_1)	0.000	H-3→L (62%)	
	4.18/296 (S_2)	0.321	H→L (68%)	3.94/315 (S_2)	0.350	H→L (69%)	281
	4.32/287 (S_3)	0.000	H-6→L (60%)	4.44/280 (S_3)	0.000	H-6→L (61%)	
	4.62/269 (S_4)	0.000	H-1→L (55%)	4.58/271 (S_4)	0.167	H-1→L (63%)	
	4.77/260 (S_5)	0.150	H-2→L (53%)	4.86/255 (S_5)	0.000	H-2→L (53%)	
	5.26/236 (S_6)	0.388	H→L+1 (54%)	5.05/246 (S_6)	0.496	H→L+1 (63%)	
5E	3.89/318 (S_1)	0.000	H-3→L (58%)	4.03/308 (S_1)	0.000	H-4→L (64%)	
	4.39/282 (S_2)	0.000	H-6→L (59%)	4.22/294 (S_2)	0.104	H→L (66%)	
	4.41/281 (S_3)	0.127	H→L (64%)	4.51/275 (S_3)	0.000	H-7→L (64%)	282
	4.81/258 (S_4)	0.000	H-2→L+1 (53%)	4.71/263 (S_4)	0.404	H→L+1 (59%)	
	4.85/256 (S_5)	0.352	H→L+1 (56%)	4.91/253 (S_5)	0.791	H-1→L (57%)	
	5.25/236 (S_6)	0.699	H-1→L (54%)	5.04/246 (S_6)	0.000	H-2→L+1 (60%)	
6E	3.85/322 (S_1)	0.000	H-3→L (58%)	3.98/311 (S_1)	0.000	H-4→L (61%)	
	4.35/285 (S_2)	0.000	H-6→L (59%)	4.12/301 (S_2)	0.872	H→L (69%)	
	4.35/285 (S_3)	0.790	H→L (69%)	4.42/281 (S_3)	0.034	H-1→L (67%)	304
7E	4.60/269 (S_1)	0.592	H→L (67%)	4.48/277 (S_1)	0.757	H→L (69%)	288
	4.85/256 (S_2)	0.000	H-2→L (64%)	4.85/256 (S_2)	0.079	H-1→L (63%)	
	4.95/250 (S_3)	0.126	H-1→L (60%)	5.07/244 (S_3)	0.000	H-2→L (64%)	
8E	4.68/265 (S_1)	0.562	H→L (68%)	4.54/273 (S_1)	0.719	H→L (70%)	284
	4.87/255 (S_2)	0.000	H-2→L (64%)	4.85/256 (S_2)	0.114	H-1→L (62%)	
	4.91/253 (S_3)	0.146	H-1→L (58%)	5.08/244 (S_3)	0.000	H-2→L (64%)	
9E	4.66/266 (S_1)	0.688	H→L (69%)	4.51/275 (S_1)	0.817	H→L (70%)	279
	4.91/252 (S_2)	0.000	H-2→L (64%)	5.01/248 (S_2)	0.008	H-1→L (51%)	
	5.03/247 (S_3)	0.031	H→L+1 (49%)	5.13/242 (S_3)	0.000	H-2→L (64%)	

2.2.2 SAC-CI calculations

Global hybrid (B3LYP) and range-separated hybrid (CAM-B3LYP) were adopted for the calculations, however, there were some deviations from experiment in the results and the calculated spectra were not satisfactory for the definitive assignments and the detailed discussion on the difference among the different derivatives. Thus, further theoretical work based on accurate wave function theory is necessary to understand the details of photophysical properties and to provide reliable information for molecular design. The symmetry-adapted cluster-configuration interaction (SAC-CI) method has been utilized to more accurately calculate theoretical spectroscopy of many π-conjugated systems and has also been applied to the photochemistry of biological systems.

First, we discuss the absorption spectra calculated using the SAC-CI methods in the gas phase and in methanol solution for **1A**–**9A** and **1E**–**9E** compared with the experimental absorption spectra in methanol solution (Tables 6 and 7, Figures 10 and 11). In general, the absorption spectra of all compounds were reproduced reasonably well by the SAC-CI method in both peak position and intensity. The excitation energies in solution are in better agreement with the experimental data, although the PCM is not satisfactory for protic solvents. The SAC-CI spectra show that the two π–π* transitions in the *para*-substituted compounds have relatively small splitting between two peaks compared with those in the *ortho*- and *meta*-substituted compounds.

To calculate the solvent effect with the SAC-CI method, the PCM-SAC-CI method was developed recently (Cammi *et al.*, 2010; Fukuda *et al.*, 2011). However, the method for calculating large systems is still under development; therefore, we investigated the excitation energies and oscillator strengths while including the solvent effect with the help of the PCM-TD-DFT calculations. In this study, the solvent correction for the $i \rightarrow a$ transition was estimated from PCM-TD-CAM-B3LYP calculations as:

$$\Delta E^{SAC-CI}_{i\rightarrow a,(solv)} = \Delta E^{SAC-CI}_{i\rightarrow a,(vac)} + \Delta\Delta E^{TD-CAM-B3LYP}_{i\rightarrow a,(solv)} \quad (1)$$

and

$$f^{SAC-CI}_{i\rightarrow a,(solv)} = f^{SAC-CI}_{i\rightarrow a,(vac)} + \frac{\Delta E^{SAC-CI}_{i\rightarrow a,(vac)}}{\Delta E^{TD-CAM-B3LYP}_{i\rightarrow a,(vac)}} \Delta f^{TD-CAM-B3LYP}_{i\rightarrow a,(solv)} \quad (2)$$

where $\Delta E^{SAC-CI}_{i\rightarrow a,(vac)}$ is the excitation energy in vacuum calculated by SAC-CI, $\Delta\Delta E^{TD-CAM-B3LYP}_{i\rightarrow a,(solv)}$ is the solvent effect on the excitation energy obtained by TD-CAM-B3LYP, $f^{SAC-CI}_{i\rightarrow a,(vac)}$ is the oscillator strength in vacuum obtained by SAC-CI, $\Delta E^{TD-CAM-B3LYP}_{i\rightarrow a,(vac)}$ is the excitation energy in vacuum found by TD-CAM-B3LYP, and $\Delta f^{TD-CAM-B3LYP}_{i\rightarrow a,(solv)}$ is the difference between oscillator strength in vacuum and solution calculated by TD-CAM-B3LYP. The TD-DFT results for evaluating solvent effect with the CAM-B3LYP/6-311G(d,p) method for these compounds in gas phase and in methanol solution.

The experimental spectra of *ortho*-hydroxy cinnamic acid (**1A**) and cinnamate (**1E**) show two distinct absorption bands. The SAC-CI spectra also have two peaks with large oscillator strengths. These peaks are attributed to the combination of the H→L and H–1→L (next HOMO to LUMO) transitions. The absorption spectrum of **1E**, for example, has its lowest peak centered at 332 nm (3.73 eV). Accordingly, the calculated value is 323 nm (3.84 eV) for the gas phase and 341 nm (3.63 eV) in solution. The second peak was observed at 280 nm (4.43 eV) in comparison with the calculated peak at 285 nm (4.35 eV) in solution. The solvent effects of these states are range from –0.20 to –0.15 eV. On the higher energy side, a weak shoulder is observed and this shoulder is attributed to the nπ* transition. The calculated oscillator strength of this transition in the planar structure is nearly zero and intensity borrowing occurs via vibronic coupling. The solvent effect of this state gives a blue shift of the peak. The dipole moment of the nπ* state is smaller than that of the ground state (Tables 6 and 7) and the blue shift therefore occurs in the polar solvent.

The *meta*-hydroxy derivatives (**2E**, **2A**) have a single strong absorption band with asymmetric shoulders. The SAC-CI calculation also gives two ππ* transitions

with a single strong peak and a shoulder on the lower-energy side and one nπ* transition. Unlike the *ortho* derivative, the small oscillator strength of the lower ππ* peak is attributed to the cancellation of the transition moment of the H→L and H−1→L components with almost the same weight. The oscillator strength of the lower peak reduces drastically in methanol solution. The SAC-CI calculations reproduced the experimental values satisfactorily: two ππ* transitions were calculated at 3.83 and 4.42 eV in solution, which are comparable with the observed values of 3.82 and 4.35 eV, respectively.

The absorption spectra of the *para*-hydroxy compounds (**3E**, **3A**) consist of a single broad absorption band in contrast to the *ortho* and *meta* derivatives. The SAC-CI calculations predicted two close peaks for these *para*-derivatives and reproduced the experimental feature. The transition characters of these states are also different from the *ortho* and *meta* derivatives: two ππ* transitions are the combinations of H→L and H→L+2 transitions. This is similar to the trend in the absorption spectra of the methoxy cinnamates, as reported in our previous work . The spectra including the solvent effect differ from the experimental results. Note that the transition characters of these states by TD-CAM-B3LYP are different from those by SAC-CI. We ascribed the deviation from experiment in solution to this difference in the theoretical results. The absorption spectra of all hydroxy cinnamic acids (**1A**–**3A**) are similar in shape to the corresponding cinnamates (**1E**–**3E**).

Next, we turn to absorption spectra of nitro cinnamic acids (**4A**–**6A**) and cinnamates (**4E**–**6E**). The molecular geometry and its effect on the absorption spectra of nitro derivatives with respect to the angle of the NO_2 group are discussed in detail in the Appendix. For these molecules, the σ-electron-withdrawing and the π-electron-donating character of the nitro group is of interest. The shoulder absorption at ca. 310 nm of *ortho*-(**4A**) and *para*-(**6A**) cinnamic acids disappeared after the compound was esterified into cinnamate, whereas the shoulder absorption of the *meta*-nitro compounds (**5E**, **5A**) remained. The strong ππ* transition of these derivatives is located above 280 nm in the higher UVB region. In the nitro derivatives, five low-

lying excited states were found; namely two ππ* and three nπ* transitions. The calculated spectra of the *ortho* and *meta* compounds show a single strong absorption band in the higher energy region with a shoulder on the lower-energy side that agree well with the experimental spectra. For example, in **4A**, the strong absorption peak was calculated at 4.44 eV in solution, which is compared with the observed value of 4.41 eV. On the other hand, the spectra of *para* compounds (**6E**, **6A**) show a single absorption band observed at 4.40 and 4.08 eV, respectively, and the peak of **6E** is much lower than those of **4E** and **5E**. The lower ππ* transition of **4E** is almost not observed; only weak shoulder overlaps. The *ortho*-nitro compound is not planar at both nitro group and propenyl group in the S_0 state. The absorption of the lower ππ* transition at non-planar structure is weaker than that at planar structure as shown in Appendix, which might be responsible for the single absorption peak nature of **4E** considering the thermal distribution of various conformation.

Finally, we focus on the absorption spectra of the fluoro derivatives of cinnamic acids (**7A**–**9A**) and cinnamates (**7E**–**9E**). Fluoro cinnamates show a single absorption band with a maximum at ca. 280 nm, while those of fluoro cinnamic acids are at ca. 270 nm. The strong peak with large oscillator strength is attributed to the H→L transitions. Compared with the hydroxy and nitro derivatives, the separation of the two ππ* transitions of the fluoro derivatives is narrow and the SAC-CI spectra reproduce this feature. The trend of absorption spectra in different substitution positions was also reproduced; the transition energies of the strong absorption peak for **7E**, **8E**, and **9E** were calculated at 4.44, 4.46, and 4.47 eV, which are compared with the observed values at 4.31, 4.37, and 4.44 eV, respectively. The absorption spectra of all fluoro cinnamic acids (**7A**–**9A**) are similar to those of corresponding cinnamates (**7E**–**9E**).

Table 6 Excitation energies (E_{ex}), absorption wavelengths (λ_{abs}), oscillator strengths (f), and dipole moments (μ) in the gas phase and in methanol for cinnamic acids (**1A**–**9A**) calculated using the direct SAC-CI method.

	SAC-CI/D95(d)								*Exp.*
	State	E_{ex} (eV)	λ_{abs} (nm)	f	Excitation character	μ (D)[a]	$E_{ex(solv)}$[b]	$f_{(solv)}$[b]	(nm)
1A	*XA′*					(3.54)			
	1*A′*	3.88	320	0.281	H→L (38%), H-1→L (16%)	4.37	3.69	0.210	324
	2*A′*	4.51	275	0.236	H-1→L (36%), H→L (21%)	3.71	4.37	0.210	278
	1*A″*	4.82	257	0.000	H-3→L (31%), H-3→L+8 (13%)	0.11	5.03	0.000	
2A	*XA′*					(3.65)			
	1*A′*	4.01	309	0.084	H→L (29%), H-1→L (21%)	2.35	3.87	0.006	317
	2*A′*	4.52	274	0.426	H→L (31%), H-1→L (29%)	4.99	4.40	0.393	283
	1*A″*	4.82	257	0.000	H-3→L (36%), H-3→L+8 (14%)	0.11	5.00	0.000	
3A	*XA′*					(2.93)			
	1*A′*	4.16	298	0.335	H→L (36%), H→L+1 (22%)	4.61	3.96	0.212	300
	2*A′*	4.38	283	0.344	H→L+1 (27%), H→L (25%)	4.55	4.37	0.363	
	1*A″*	4.87	255	0.000	H-3→L (36%), H-3→L+11 (14%)	0.11	5.07	0.000	
4A	*XA′*					(5.79)			
	1*A′*	4.06	305	0.154	H→L (33%), H-1→L (15%)	3.16	3.81	0.128	
	1*A″*	4.39	282	0.000	H-4→L (31%), H-4→L+1 (18%)	0.08	4.58	0.000	
	2*A′*	4.64	267	0.351	H-1→L (26%), H→L (24%)	4.46	4.45	0.327	273
5A	*XA′*					(4.90)			
	1*A′*	4.15	299	0.079	H→L (30%), H-1→L (16%)	2.25	3.94	0.105	
	1*A″*	4.52	274	0.000	H-4→L+1 (27%), H-4→L (25%)	0.08	4.71	0.000	
	2*A′*	4.60	270	0.249	H→L+1 (27%), H-1→L (26%)	3.78	4.47	0.219	274
6A	*XA′*					(3.43)			
	1*A′*	4.12	301	0.033	H-1→L (36%), H→L+2 (17%)	1.45	3.95	0.000	
	2*A′*	4.33	286	0.767	H→L (61%), H-1→L (10%)	6.83	3.92	0.021	
	1*A″*	4.35	285	0.000	H-4→L (31%), H-4→L+1 (19%)	0.09	4.09	0.685	282
7A	*XA′*					(3.29)			
	1*A′*	4.23	293	0.244	H→L (31%), H-1→L (24%)	3.90	4.11	0.097	
	1*A″*	4.51	275	0.000	H-3→L (43%), H-3→L+2 (24%)	0.09	4.69	0.000	
	2*A′*	4.53	274	0.266	H-1→L (28%), H→L (26%)	3.93	4.44	0.308	265
8A	*XA′*					(2.44)			
	1*A′*	4.32	287	0.043	H-1→L (34%), H→L+1 (24%)	1.62	4.27	0.084	
	1*A″*	4.53	274	0.000	H-3→L (46%), H-3→L+2 (25%)	0.09	4.70	0.000	
	2*A′*	4.56	272	0.552	H→L (48%), H→L+1 (13%)	5.65	4.44	0.388	266
9A	*XA′*					(1.28)			
	1*A′*	4.38	283	0.238	H→L (29%), H→L+1 (25%)	3.78	4.37	0.252	
	1*A″*	4.56	272	0.000	H-3→L (44%), H-3→L+2 (23%)	0.09	4.74	0.000	
	2*A′*	4.58	271	0.406	H→L (32%), H→L+1 (22%)	4.83	4.45	0.287	269

[a] Values in parentheses show the dipole moment of the ground state (*XA'*).
[b] Solvent effect is calculated by PCM-TD-CAM-B3LYP in methanol solution.

Table 7 Excitation energies (E_{ex}), absorption wavelengths (λ_{abs}), oscillator strengths (f), and dipole moments (μ) in the gas phase and in methanol for methyl cinnamates (**1E**–**9E**) calculated using the direct SAC-CI method.

	SACCI/D95(d)								*Exp.*
	State	E_{ex} (eV)	λ_{abs} (nm)	f	Excitation character	μ (D)[a]	$E_{ex(solv)}$[b]	$f_{(solv)}$[b]	(nm)
1E	*XA′*					(2.99)			
	1*A′*	3.84	323	0.267	H→L (34%), H-1→L (16%)	4.28	3.63	0.198	332
	2*A′*	4.50	275	0.273	H-1→L (33%), H→L (22%)	4.00	4.35	0.244	280
	1*A″*	4.79	259	0.000	H-3→L (32%), H-3→L+10 (12%)	0.13	5.03	0.000	
2E	*XA′*					(3.30)			
	1*A′*	4.00	310	0.082	H→L (28%), H-1→L (23%)	2.32	3.83	0.002	325
	2*A′*	4.55	273	0.431	H→L (58%), H-1→L (48%)	5.00	4.42	0.396	285
	1*A″*	4.75	261	0.000	H-3→L (37%), H-3→L+10 (14%)	0.13	4.97	0.000	
3E	*XA′*					(2.31)			
	1*A′*	4.15	299	0.287	H→L (33%), H→L+2 (23%)	4.27	3.93	0.160	314
	2*A′*	4.37	284	0.407	H→L (28%), H→L+2 (27%)	4.96	4.35	0.433	
	1*A″*	4.83	257	0.000	H-3→L (36%), H-3→L+14 (14%)	0.12	5.06	0.000	
4E	*XA′*					(5.88)			
	1*A′*	4.01	309	0.166	H→L (35%), H-1→L (15%)	3.30	3.77	0.137	
	1*A″*	4.21	295	0.000	H-3→L (31%), H-3→L+1 (18%)	0.11	4.32	0.000	
	2*A′*	4.63	268	0.351	H-1→L (26%), H→L+1 (23%)	4.47	4.44	0.334	281
5E	*XA′*					(5.40)			
	1*A′*	4.12	301	0.080	H→L (31%), H-1→L (16%)	2.26	3.93	0.101	
	1*A″*	4.36	284	0.000	H-4→L+1 (26%), H-4→L (22%)	0.10	4.48	0.000	
	2*A′*	4.61	269	0.262	H→L+1 (46%), H-1→L (43%)	3.87	4.47	0.213	282
6E	*XA′*					(4.20)			
	1*A′*	4.27	290	0.062	H-1→L (36%), H→L+1 (18%)	1.95	4.06	0.048	
	1*A″*	4.33	286	0.000	H-4→L (29%), H-4→L+1 (17%)	0.11	4.53	0.000	
	2*A′*	4.39	282	0.762	H→L (78%), H-1→L (17%)	6.77	4.15	0.679	304
7E	*XA′*					(3.09)			
	1*A′*	4.23	293	0.242	H→L (30%), H-1→L (25%)	3.88	4.13	0.282	
	1*A″*	4.37	284	0.000	H-3→L (28%), H-3→L+2 (28%)	0.11	4.59	0.000	
	2*A′*	4.56	272	0.307	H→L (28%), H-1→L (28%)	4.21	4.44	0.143	288
8E	*XA′*					(2.54)			
	1*A′*	4.33	286	0.038	H-1→L (34%), H→L+1 (25%)	1.51	4.27	0.066	
	1*A″*	4.38	283	0.000	H-3→L (42%), H-3→L+2 (23%)	0.10	4.59	0.000	
	2*A′*	4.60	269	0.626	H→L (70%), H→L+1 (17%)	5.99	4.46	0.472	284
9E	*XA′*					(1.27)			
	1*A′*	4.38	283	0.171	H→L+1 (28%), H→L (25%)	3.21	4.36	0.191	
	1*A″*	4.45	278	0.000	H-3→L (43%), H-3→L+2 (23%)	0.11	4.67	0.000	
	2*A′*	4.61	269	0.542	H→L (37%), H→L+1 (19%)	5.57	4.47	0.414	279

[a] Values in parentheses show the dipole moment of the ground state (*XA′*).
[b] Solvent effect is calculated by PCM-TD-CAM-B3LYP in methanol solution.

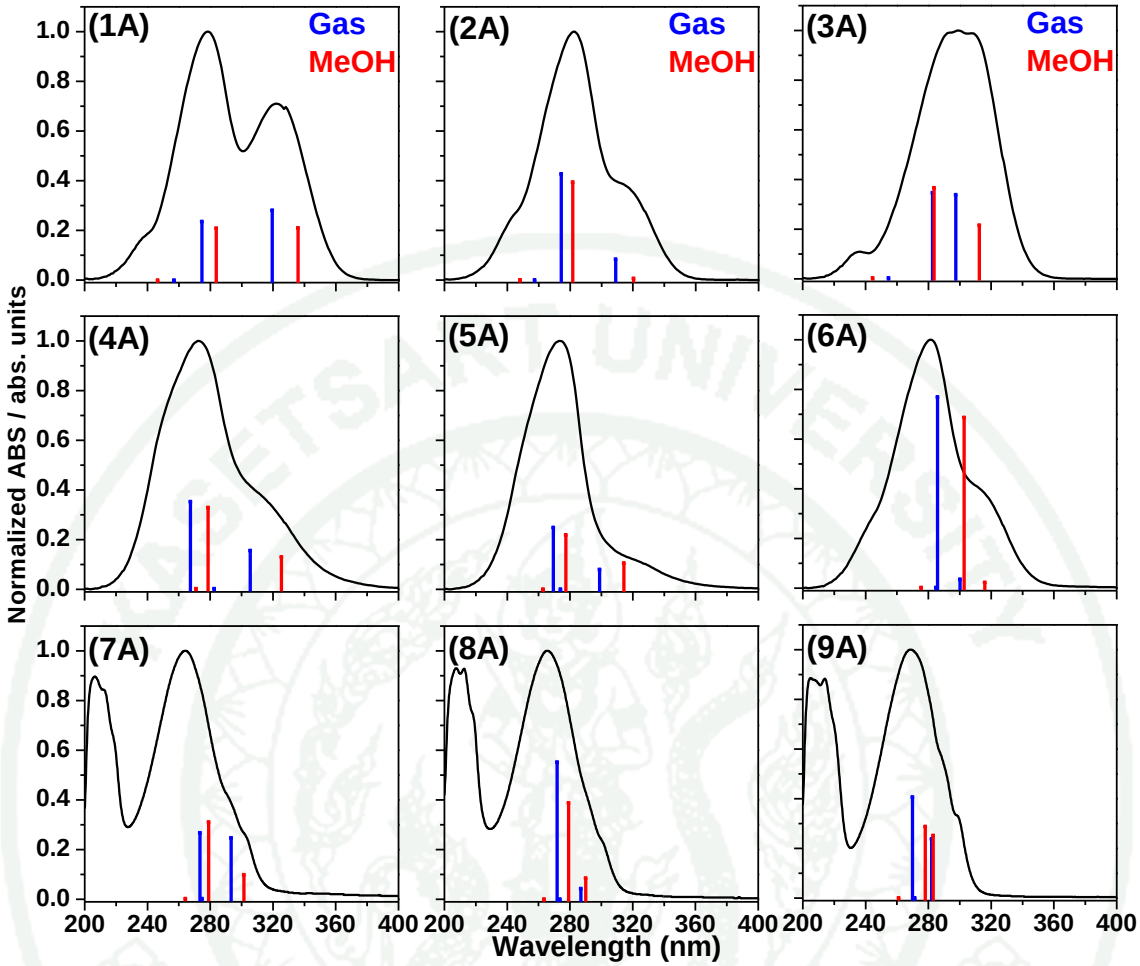

Figure 10 Absorption spectra of hydroxy (**1A**–**3A**), nitro (**4A**–**6A**), and fluoro (**7A**–**9A**) cinnamic acids substituted at the *ortho*, *meta*, and *para* positions calculated using the direct SAC-CI method in the gas phase (blue) and in methanol solution (red) compared with the experimental spectra.

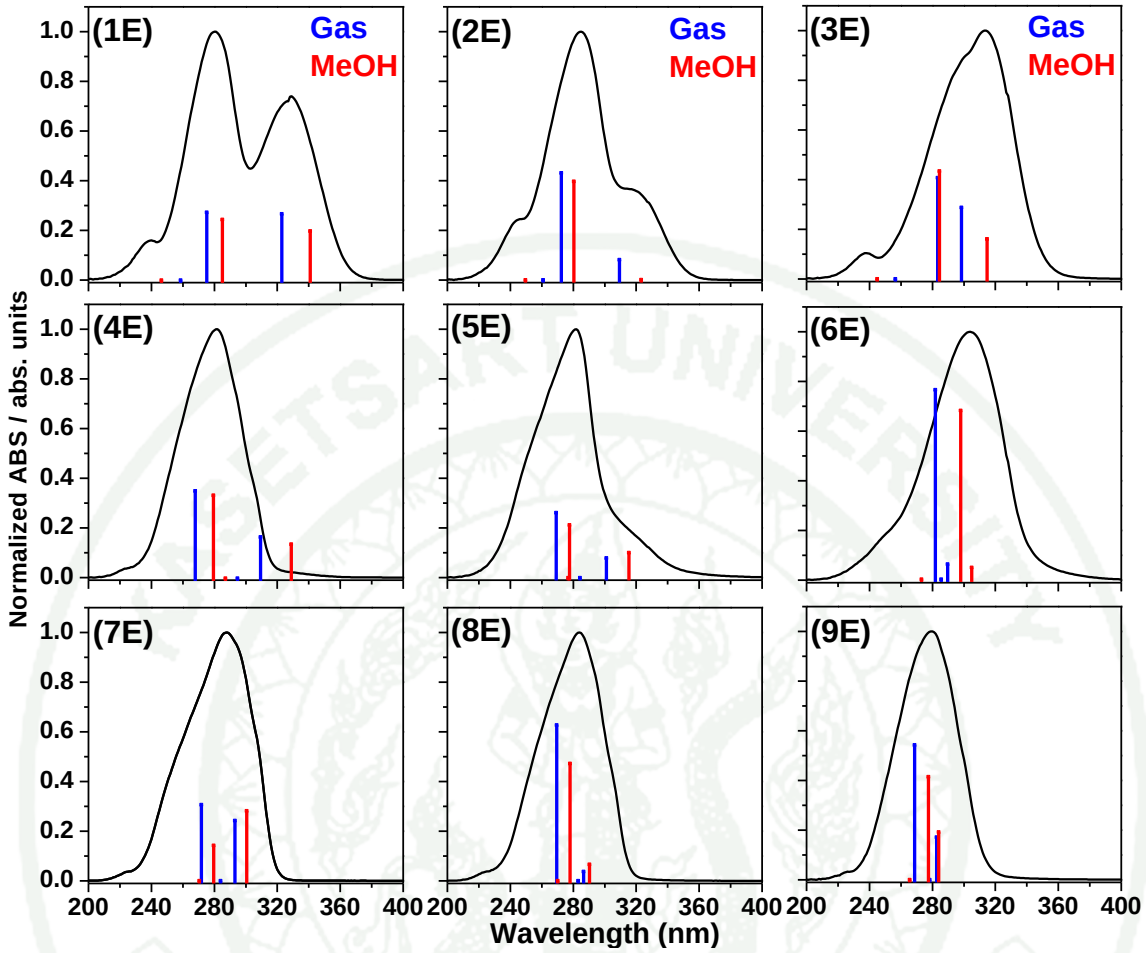

Figure 11 Absorption spectra of hydroxy (**1E**–**3E**), nitro (**4E**–**6E**), and fluoro (**7E**–**9E**) methyl cinnamates substituted at the *ortho*, *meta*, and *para* positions calculated using the direct SAC-CI method in the gas phase (blue) and in methanol solution (red) compared with the experimental spectra.

In addition, we compare the dipole moments of the ground and excited states to interpret the solvent effect on absorption spectra qualitatively. They are given in Tables 6 and 7 and Figures 8 and 9 for cinnamic acids (**1A**–**9A**) and methyl cinnamates (**1E**–**9E**), respectively. For all the compounds studied here, the calculated dipole moments (μ) of the excited states are much larger in the A' state and smaller in the A'' state than those in the ground (XA') state. In the A'' state, a lone pair electron is promoted to the distributed π* orbital, which reduces the dipole moment, while in the A' state, charge polarization is enhanced by the ππ* transition. These are the origin of the solvent effect in which the absorption peaks of the ππ* states show a red shift. In contrast those of the nπ* state show a blue shift in methanol solution compared with those in the gas phase for both cinnamic acids and methyl cinnamates.

2.2.3 Comparison between SAC-CI and TD-DFT calculations

The comparison between SAC-CI and TD-DFT results is given in Tables 8 and 9 for all the derivatives. The TD-DFT values are due to the previous calculations based on the global hybrid (B3LYP) and range-separated hybrid (CAM-B3LYP) functional. The agreement between SAC-CI and experiment is better than that of TD-DFT on average. For some derivatives, the shape of theoretical spectrum and the ππ* peak splitting are very different between SAC-CI and TD-DFT (B3LYP); for example, **3E** (peak splitting), **4E**, **8E**, and **9E** (spectrum shape). Note that the agreement with experiment for B3LYP is better than that of CAM-B3LYP for these molecules. This indicates that the calculations with accurate DFT functionals theory are necessary for the reliable analysis and assignment of the absorption spectra in the present case.

Table 8 Absorption wavelengths (nm) in the gas phase and in methanol solution for substituted cinnamic acids (**1A**–**9A**) using TD-B3LYP, TD-CAM-B3LYP, and SAC-CI compared with the experimental values.

	Gas phase						In methanol						*Exp.*
	B3LYP		CAM-B3LYP		SAC-CI		B3LYP		CAM-B3LYP		SAC-CI		MeOH
	λ_{abs}	$\lvert\Delta E\rvert$	λ_{abs}	$\lvert\Delta E\rvert$	λ_{abs}	$\lvert\Delta E\rvert$	λ_{abs}	$\lvert\Delta E\rvert$	λ_{abs}	$\lvert\Delta E\rvert$	λ_{abs}	$\lvert\Delta E\rvert$	
1A	313	11	288	36	320	4	332	8	302	22	336	12	324
	273	5	254	24	275	3	285	7	261	17	284	6	278
2A	317	0	280	37	309	8	331	14	289	28	320	3	317
	273	10	258	25	274	9	283	0	265	18	282	1	283
3A	295	5	277	23	298	2	312	12	290	10	313	13	300
4A	260	13	295	22	267	6	270	3	314	41	279	6	273
5A	260	14	280	6	270	4	276	2	293	19	277	3	274
6A	313	31	283	1	286	4	337	55	300	18	303	21	282
7A	288	23	270	5	274	9	296	31	277	12	279	14	265
8A	272	6	265	1	272	6	278	12	272	6	279	13	266
9A	282	13	267	2	271	2	291	22	275	6	279	10	269

Table 9 Absorption wavelengths (nm) in the gas phase and in methanol solution for substituted methyl cinnamates **(1E**–**9E)** using TD-B3LYP, TD-CAM-B3LYP, and SAC-CI compared with the experimental values.

	Gas phase						In methanol						*Exp.*
	B3LYP		CAM-B3LYP		SAC-CI		B3LYP		CAM-B3LYP		SAC-CI		MeOH
	λ_{abs}	$\lvert\Delta E\rvert$	λ_{abs}	$\lvert\Delta E\rvert$	λ_{abs}	$\lvert\Delta E\rvert$	λ_{abs}	$\lvert\Delta E\rvert$	λ_{abs}	$\lvert\Delta E\rvert$	λ_{abs}	$\lvert\Delta E\rvert$	
1E	312	20	288	44	323	9	332	0	302	30	341	9	332
	273	7	253	27	275	5	285	5	261	19	285	5	280
2E	313	12	278	47	310	15	331	6	289	36	323	2	325
	273	12	258	27	273	12	284	1	265	20	281	4	285
3E	295	19	277	37	299	15	313	1	291	23	315	1	314
4E	261	20	296	15	268	13	271	10	315	34	279	2	281
5E	261	21	281	1	269	13	277	5	294	12	277	5	282
6E	315	11	285	19	282	22	339	35	301	3	298	6	304
7E	287	1	269	19	272	16	296	8	277	11	279	9	288
8E	271	13	265	19	269	15	279	5	273	11	278	6	284
9E	282	3	266	13	269	10	292	13	275	4	278	1	279

The experimental and SAC-CI absorption energies of the hydroxy, nitro, and fluoro cinnamates are compared in Figure 12. The experimental peak positions are shown as black vertical lines and the SAC-CI values are shown as red vertical lines for only the ππ* excited states. The SAC-CI values are those obtained in methanol solution. In general, the agreement between experiment and SAC-CI is satisfactory for both the peak position and the energy separation of the ππ* excited states. The energy difference $\Delta\Delta E$(ππ*) of the lower and higher ππ* excited states is large in the *ortho* derivatives; $\Delta\Delta E$(ππ*, *ortho*) > $\Delta\Delta E$(ππ*, *meta*) > $\Delta\Delta E$(ππ*, *para*). The trends in energy difference in different substitutions are also clear, $\Delta\Delta E$(ππ*, hydroxy) > $\Delta\Delta E$(ππ*, nitro) > $\Delta\Delta E$(ππ*, fluoro). These trends are in good agreement with experimental observations. The hydroxy derivatives have clearly separated absorption peaks and cover the UVB (280–320 nm) and UVA (320–400 nm) regions.

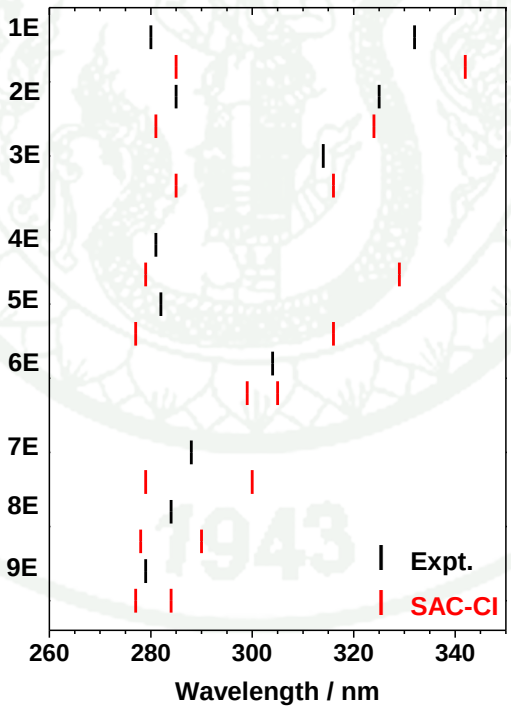

Figure 12 Comparison of the experimental (black bar) and SAC-CI (red bar) absorption energies for hydroxy (**1E**–**3E**), nitro (**4E**–**6E**), and fluoro (**7E**–**9E**) methyl cinnamates in methanol solution. In SAC-CI, only the ππ* excited states are shown.

1.3 Potential energy curves (PECs)

The angle of the nitro group relative to the cinnamate unit θ (C_1=C_2–N_{19}=O_{21}) affects the optical properties as it affects the π-conjugation. In particular, the *ortho*-nitro derivatives have non-planar structures in the S_0 state because of steric effects. Therefore, the ground state potential energy curves (S_0 PECs) along the angle θ of the nitro group with respect to the phenyl ring were calculated using the B3LYP/6-31G(d) method. *Ortho*-(**4E**), *meta*-(**5E**), and *para*-(**6E**) nitro methyl cinnamates were examined for the angle θ (C_1=C_2–N_{19}=O_{21}). The S_0 PECs were partially optimized at fixed angles (θ = 0° to 180° in steps of 15°) with all the other coordinates optimized as shown in Figure 13.

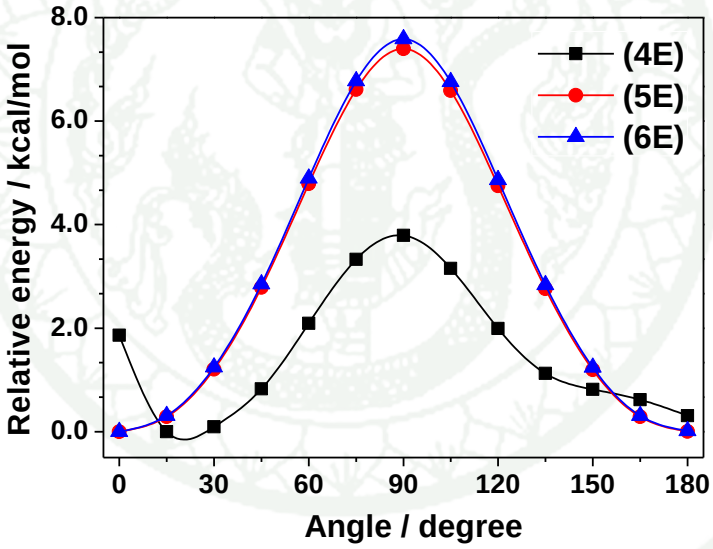

Figure 13 Ground-state PECs along the angle (C_1=C_2–N_{19}=O_{21}) of NO_2 to the molecular plane for the nitro methyl cinnamates **(4E**–**6E)** calculated using the B3LYP/6-31G(d) method.

The most stable conformation was located at θ = 0° for **5E** and **6E** and θ = ~15° for **4E**. At θ = 90°, the calculated energy barriers relative to the most stable conformation for **4E**, **5E**, and **6E** were 3.79, 7.40, and 7.59 kcal/mol, respectively. Note that the propenyl unit is also not coplanar to the benzene unit in **4E**. The low

rotational energy barrier of about 1.0 kcal/mol in the range of θ = 0°–30° for **5E** and **6E** and θ = 10°–45° for **4E** indicates that a certain range of non-planar conformations contributes to the absorption spectra at room temperature. With these structures, the excitation energies were calculated using the SAC-CI/D95(d) method to examine their dependence on the angle.

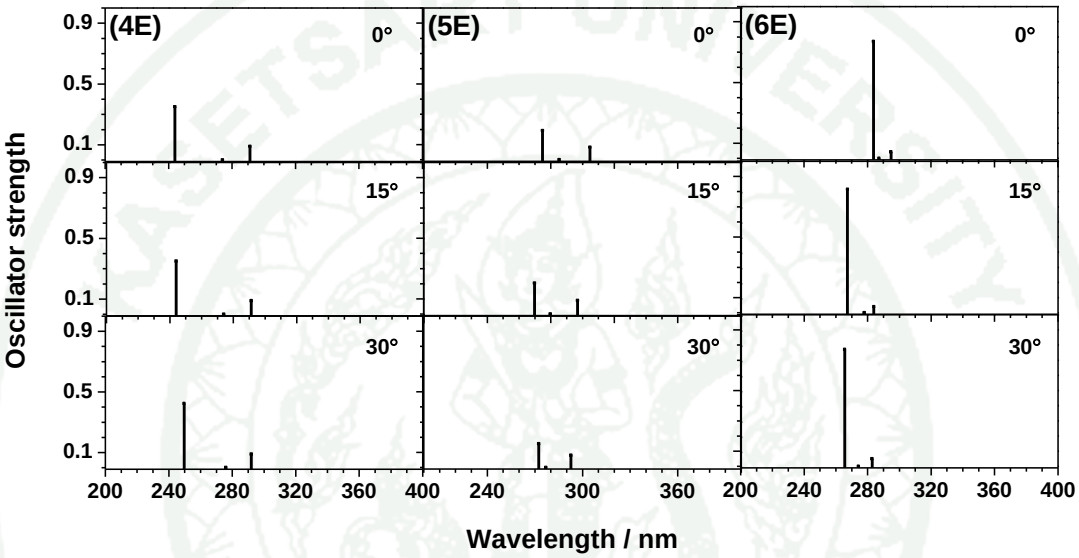

Figure 14 SAC-CI absorption spectra for the nitro methyl cinnamates **(4E**–**6E)** at angle (C_1=C_2–N_{19}=O_{21}) of θ = 0°, 15° and 30° calculated using the SAC-CI/D95(d) method.

The calculated spectra for θ = 0°, 15°, and 30° of **4E**, **5E**, and **6E** are shown in Figure 14. The trend of the absorption peaks for these compounds for these angles do not change significantly. In the *ortho* derivative (**4E**), the peaks shows a blue shift at θ = 15° relative to the planar structure, while this shift is relaxed at θ = 30°. The ratio of the peak intensity between the first and second ππ* transitions change with regard to the angle, which is related to the single absorption peak nature of **4E**. On the other hand, the peaks of the *meta*-(**5E**) and *para*-(**6E**) derivatives show small shifts.

1.4 Emission spectra

The emission spectra of the substituted cinnamic acids (**1A**–**9A**) and cinnamates (**1E**–**9E**) were obtained in acetonitrile solution. When observing the emission spectra, the absorbance at the excitation wavelength was kept constant (0.1) at the maximum absorption wavelength for all the sample solutions; for example, **1E** excited at 275 nm (the second peak) and **2E** at 276 nm. This condition represents to the absorption of light in the UVB region. For **1E** and **2E**, the emission spectra with the excitation are displayed at lower peak (322 and 312 nm). For UVB absorbers, the strong emission is not a desirable property. The emission spectra of **1A**–**9A** in aerobic condition and in N_2 gas are compared in Figure 15, while those of **1E**–**9E** are in Figure 16. Note that the emission of **2E** is much stronger than that of nitro- and fluoro-derivatives, and therefore the observed condition for **2E** is different from other derivatives.

Emissions were clearly detected in some cinnamic acids and cinnamates. The effect of the substituent position is different among hydroxy, nitro, and fluoro derivatives. For example, in hydroxy derivatives, *meta*-hydroxy derivative (**2E**) shows considerable emission compared with the *para* derivative (**3E**). This is related to the lifetime of the excited states and more in detail, the energy barrier to the conical intersection leading to nonradiative decay, as discussed in the next section. In the presence of oxygen in the solution (black line in Figures 15 and 16), no strong emissions from cinnamic acids and cinnamates with fluoro or nitro substituents were observed. To see the effect of the oxygen quenching, the emission under N_2 gas was also examined. The emission intensities of some cinnamic acids and cinnamates increased under N_2 gas significantly (red line in Figures 15 and 16). This means **4E** and **5E** (and **8A** and **9A**) are significantly quenched and **3E** in part, while other compounds are not quenched so much. Despite the existence of an electron-withdrawing group in esters **6E**, **7E**, and **8E**, for example, the emissions of those compounds were almost not quenched by oxygen. These results indicate that the triplet excited state is generated in some derivatives with an electron-withdrawing group, however, it depends on the position of substitution. Namely, after the

excitations to the S_1 or S_2 states, the relaxation to the T_2 state occurs in the molecules which show drastic changes in emission under oxygen quenching (Photoisomerization). The relative position of the singlet and triplet excited states and the nature of the PECs of singlet excited states may also be important. In the derivatives with an electron-donating group such as *para*-hydroxy derivatives, the relaxation seems to take place via a singlet state as also observed in the previous work (Lewis *et al.*, 1989). Interestingly, for *meta*-derivatives (**2E** and **2A**), the emission in aerobic condition is stronger than that in N_2 gas. The emission or relaxation via triplet state also depends on the lifetime of the excited species. The further time-resolved analysis is necessary for the understanding the relaxation in the excited states, in particular for the derivatives where the triplet state is involved in the relaxation process.

The emission energies of the substituted cinnamic acid and methyl cinnamate derivatives were also calculated using the SAC-CI/D95(d) method at their CIS excited state ($\pi\pi^*$, S_1)-optimized structures. The calculated emission energies in methanol, oscillator strengths (f), radiative lifetimes (τ), and dipole moments (μ) of the cinnamic acids and methyl cinnamates are summarized in Tables 10 and 11, respectively. The SAC-CI emission peaks for the *para* position of all compounds show the highest oscillator strengths, in the range of 0.579–0.832. These oscillator strengths do not directly correlate to the emission strength because nonadiabatic decay competes with emission, particularly for *para* derivatives. The transition probabilities for emissions of substituted cinnamic acids *and* methyl cinnamates have been observed with the peak maximum at $1A'$ corresponding to the H→L transition. Note that *ortho*-nitro derivatives (**4E** and **4A**) are also planar in the S_1 state.

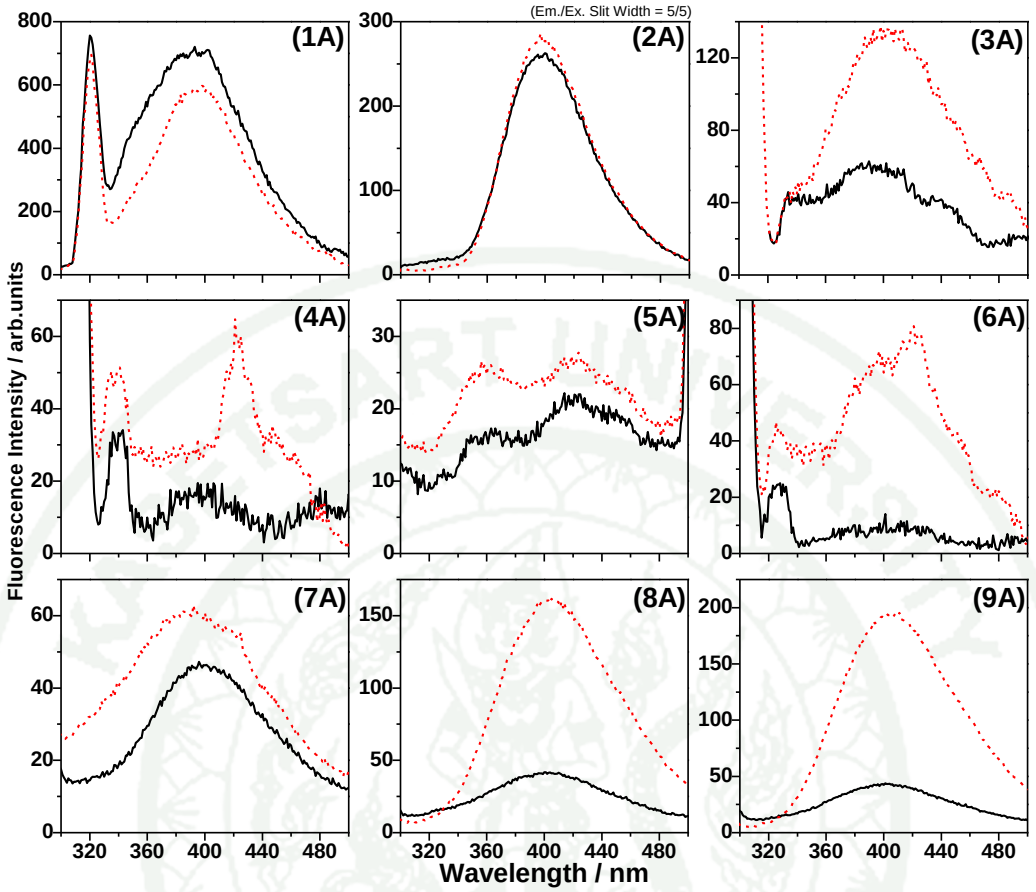

Figure 15 Emission spectra of hydroxy (**1A**–**3A**), nitro (**4A**–**6A**), and fluoro (**7A**–**9A**) cinnamic acids substituted at the *ortho*, *meta*, and *para* positions in the presence of oxygen (black line) and under nitrogen (red line). The observed condition is different for **2E**.

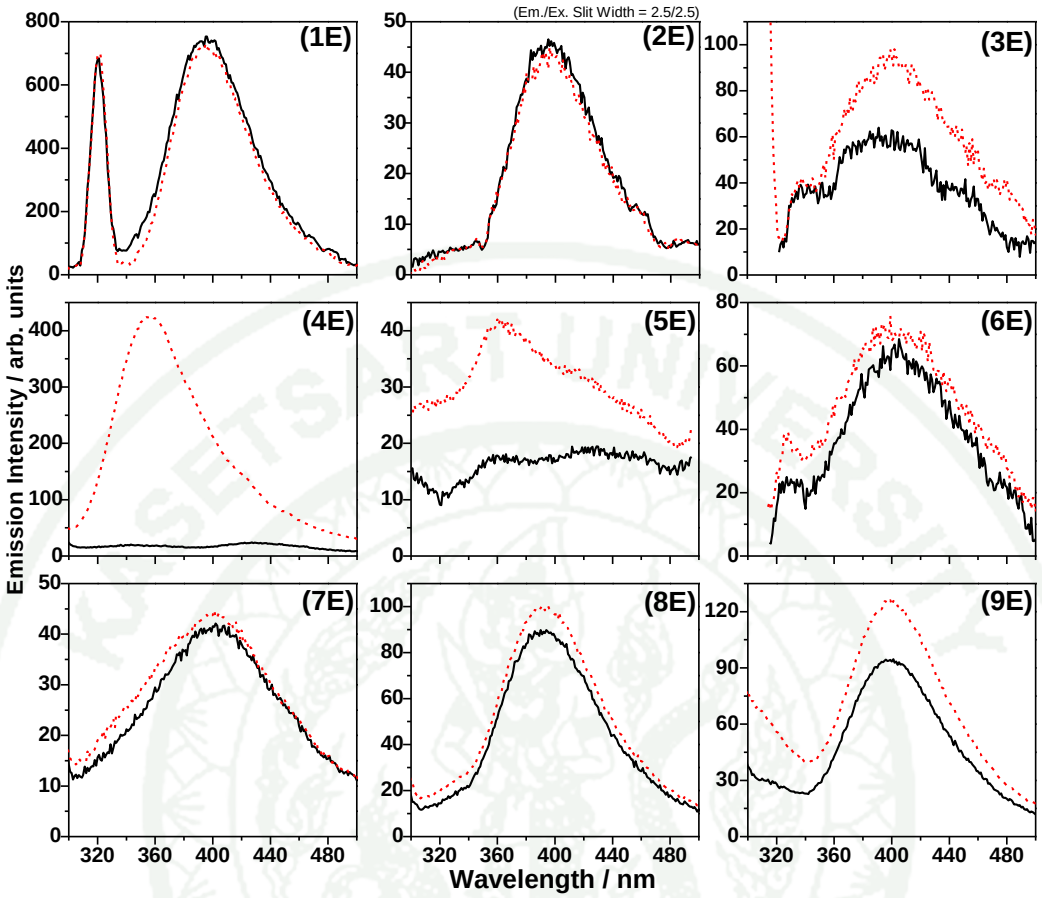

Figure 16 Emission spectra of hydroxy (**1E**–**3E**), nitro (**4E**–**6E**), and fluoro (**7E**–**9E**) cinnamates substituted at the *ortho*, *meta*, and *para* positions in the presence of oxygen (black line) and under nitrogen (red line).

The radiative lifetime is relevant to the discussion of relaxation. The fluorescence transition energies and oscillator strengths were used to calculate the radiative lifetime by using the Einstein transition probabilities in the following formula (Litani-Barzilai *et al.*, 2004):

$$\tau = \frac{c^3}{2E_{Flu}^2 f} \qquad (3)$$

where c is the velocity of light, E_{Flu} is the fluorescence transition energy, and f is the oscillator strength.

Table 10 Excitation energies (E_{ex}), emission wavelengths (λ_{em}), oscillator strengths (f), radiative lifetimes (τ), and dipole moments (μ) for substituted cinnamic acids (**1A**–**9A**) calculated using the direct SAC-CI method.

	SAC-CI/D95(d)						
	State	E_{ex} (eV)	λ_{em} (nm)	f	τ (ns)	Transition character	μ (D)[a]
1A	1*A*′	3.51	353	0.437	4.28	H→L (50%)	5.73 (4.63)
2A	1*A*′	3.68	337	0.255	6.69	H→L (46%)	4.27 (4.19)
3A	1*A*′	3.62	343	0.597	2.95	H→L (67%)	6.60 (3.88)
4A	1*A*′	3.76	330	0.377	4.33	H→L (48%)	5.14 (7.99)
5A	1*A*′	3.74	332	0.255	6.49	H→L (44%)	4.24 (5.29)
6A	1*A*′	4.00	310	0.840	1.72	H→L (76%)	7.45 (5.60)
7A	1*A*′	3.76	330	0.525	3.11	H→L (48%)	6.07 (4.26)
8A	1*A*′	3.96	313	0.472	3.12	H→L (50%)	5.61 (2.84)
9A	1*A*′	3.83	323	0.570	2.75	H→L (58%)	6.26 (1.66)

[a] Values in parentheses show the dipole moment of the ground state (*XA*′).

Table 11 Excitation energies (E_{ex}), emission wavelengths (λ_{em}), oscillator strengths (f), radiative lifetimes (τ), and dipole moments (μ) for substituted methyl cinnamates (**1E**–**9E**) calculated using the direct SAC-CI method.

	SAC-CI/D95(d)						
	State	E_{ex} (eV)	λ_{em} (nm)	f	τ (ns)	Transition character	μ (D)[a]
1E	1*A*′	3.46	358	0.434	4.44	H→L (45%)	5.75 (3.94)
2E	1*A*′	3.66	338	0.276	6.23	H→L (45%)	4.65 (3.78)
3E	1*A*′	3.62	342	0.598	2.94	H→L (65%)	6.60 (3.10)
4E	1*A*′	3.74	332	0.380	4.34	H→L (51%)	5.18(8.11)
5E	1*A*′	3.70	335	0.221	7.59	H→L (43%)	3.97 (5.85)
6E	1*A*′	3.85	322	0.832	1.87	H→L (74%)	7.55 (4.75)
7E	1*A*′	3.79	327	0.536	2.99	H→L (48%)	6.10 (3.92)
8E	1*A*′	3.99	311	0.482	3.01	H→L (49%)	5.64 (2.90)
9E	1*A*′	3.87	321	0.579	2.66	H→L (56%)	6.29 (1.38)

[a] Values in parentheses show the dipole moment of the ground state (*XA*′).

The predicted radiative lifetimes of the present molecules are collected in Tables 10 and 11. The direct comparison of the calculated f and τ with the experimental emission intensity is not straightforward due to some possible relaxation

processes. Long radiative lifetimes were calculated for the *meta* derivatives; for example, those for *meta*-hydroxy (**2E**) and *meta*-nitro (**5E**) methyl cinnamates were 6.23 and 7.59 ns, respectively. The radiative lifetimes of the *para* compounds are slightly shorter than those of the other compounds. For the hydroxy substituent, the predicted radiative lifetimes are in the order of the *meta*-, *ortho*-, and *para*-substituted compounds. These results are similar to the trend in fluorescence lifetimes of the methoxy cinnamates, as reported in the previous experimental work (Karpkird *et al.*, 2009).

1.5 Photostability

Photostability is a desirable property for various applications of photofunctional materials or compounds such as for sunscreen. The UV absorbers used in cosmetics must be photochemically inert. If they are not, chemical bonds may be rearranged, leading to decomposition; the absorbance of the resulting compounds might be diminished or even lost (Rodil *et al.*, 2009). The photostability of each compound was examined by the relative absorbance at the maximum absorption wavelength of the compound. The photostability (*S*) was evaluated as:

$$S = I_{\text{irr}} / I_{\text{unirr}} \quad (4)$$

where I_{irr} and I_{unirr} denote absorbance of irradiated and unirradiated samples, respectively, observed at the maximum absorption wavelength of each compound. The photostability was examined after 5, 10, and 30 min of irradiation and is displayed in Figure 17. The photoabsorption of *trans* and *cis* isomers are assumed to be similar as shown for methoxy cinnmates. In view of photostability, the *trans–cis* isomerization does not matter because the interchange between these isomers occurs and those two isomers work as a suitable UVB/UVA absorber. For more detailed analysis of photostability, the measurements of the decomposed products and *cis* isomer is done

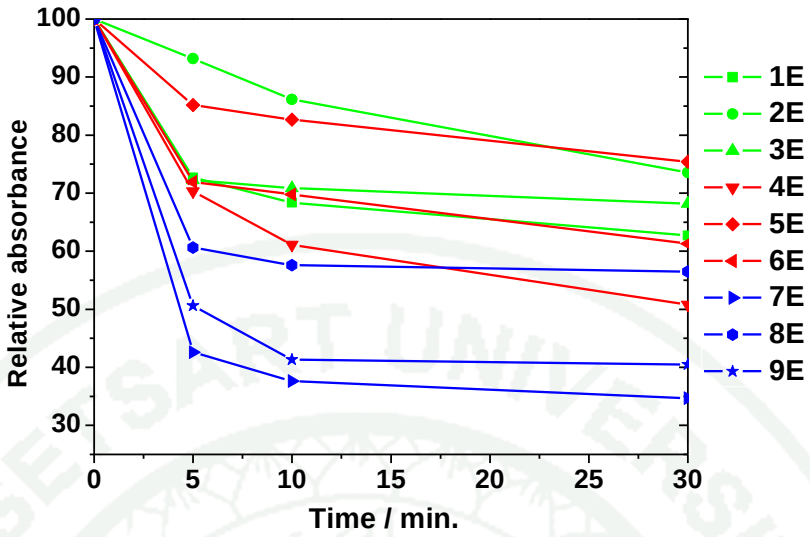

Figure 17 Photostability of 1×10^{-5} M cinnamate derivatives (**1E**–**9E**) in methanol solution. The decrease in absorbance of each compound was monitored at its maximum absorption as indicated.

Among all cinnamates with hydroxy, nitro, and fluoro substituents, *meta*-substituted derivatives showed better photostability than the corresponding *para*- and *ortho*-substituted derivatives. In particular, *meta*-hydroxy cinnamate (**2E**) and *meta*-nitro cinnamate (**5E)** showed significant photostability. Generally, the derivatives containing the hydroxy group were more photostable than cinnamates containing nitro and fluoro groups. However, this photostability should be carefully evaluated for the desired performance as an UVB absorber, because *meta* derivatives show strong emission and decay to the ground state by emission. Thus, the decomposition in the course of nonradiative decay would be small in *meta* derivatives and the apparent photostability of these compounds is better than others. For example, **2E** shows strong emission and **5E** has less absorption in the UVB and UVA regions. The fluoro cinnamates (**7E**–**9E**) show less photostability than hydroxy and nitro substituents. The photostability of halo substituted cinnamates were reported as photosensitive compounds in visible wavelength. Consequently, these materials can be used for optical device applications. Thus, *para*-hydroxy cinnamate (**3E**) would be an excellent UVB absorber with respect to photostability and photoabsorption. These results might be also useful for optically addressable devices.

Detailed analysis of hydroxycinnamate at *ortho* (**1E**), *meta* (**2E**), and *para* (**3E**) positions before and after light irradiation was done using high performance liquid chromatography (HPLC) as shown in Figure 18. Analysis during the degradation product was done at 25°C using a CLIPEUS 18 column (partical size 5μm, 150x3.0 mm I.D.; Higgins Analytical, Inc). The mobile phase used was methanol:water (90/10 v/v) at a flow rate of 0.5 ml/min. The UV detector was set at the maximum absorption for each compound. The 1000 p.p.m. stock solution was diluted 100 fold with pure methanol before injection. The sample injection volume was 10 μl. The sample solution was irradiated with a broadband UVB lamp (Daavlin, OH). As the results, the HPLC revealed a new peak and therefore indicated an accumulation of some decomposed products. These results qualitatively agree with the above UV irradiation experiment.

Moreover, the possibility of *trans*-*ortho*-hydroxy cinnamic acid is occurred via transformation to *cis*-isomers by irradiation of UV light and might cyclize to produce coumarin. The identification of the mixture obtained after photoirradiation for *ortho*-hydroxy cinnamic acid (**1A**) was done by HPLC, HPLC-MS and NMR as shown in Figures 19, 20, and 21, respectively. Collection of standard *ortho*-hydroxy cinnamic acid (**1A**) and its degradation product was done at 25°C using a CLIPEUS 18 column (partical size 5μm, 150x3.0 mm I.D.; Higgins Analytical, Inc). The mobile phase used was methanol:water (90/10 v/v) with trifluoroacetic acid (TFA) (0.01 v/v) at a flow rate of 0.2 ml/min. The UV detector was set at the 278 and 324 nm. The 1000 p.p.m. stock solution was diluted 100 times with pure methanol before injection. The sample injection volume was 10 μl for each compound. Positive-ion mass spectra were recorded corresponding to the each peak form HPLC chromatogram.

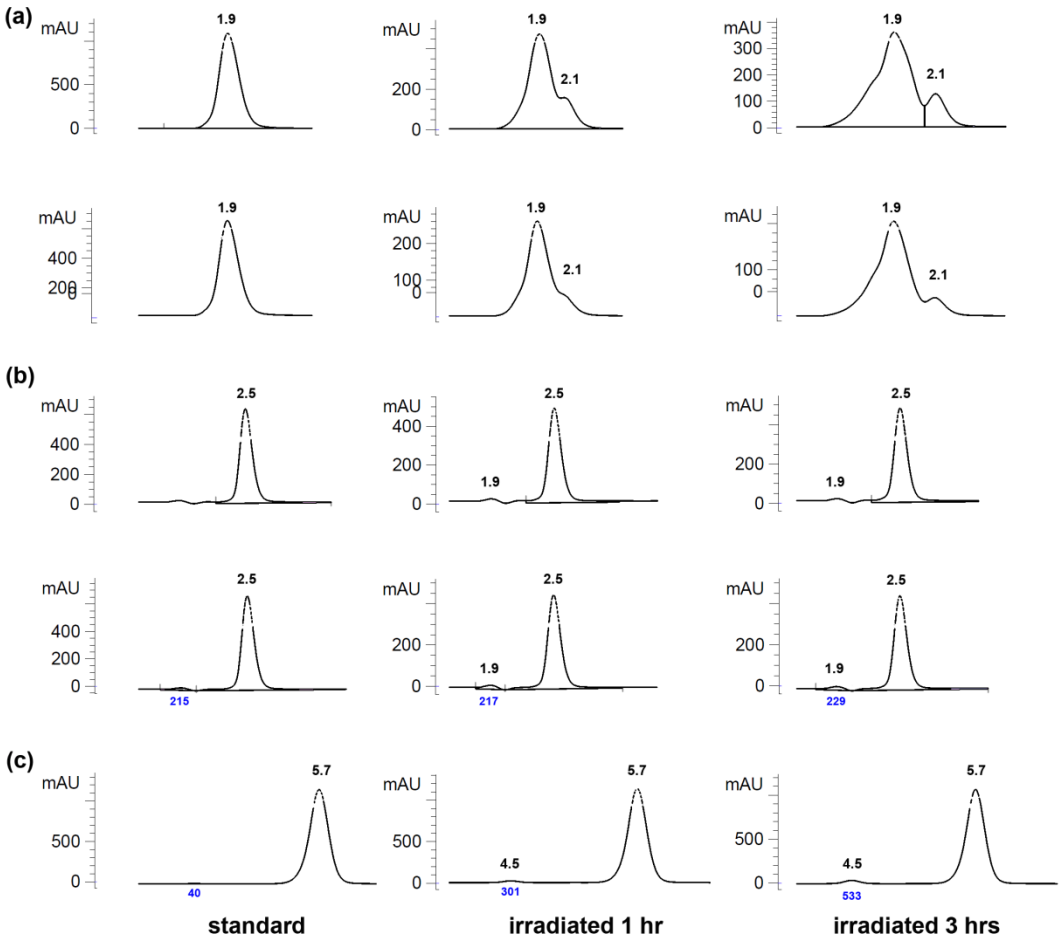

Figure 18 Chromatograms of (a) *ortho*-(**1E**) (b) *meta*-(**2E**) and (c) *para*-(**3E**)-hydroxy cinnamate before and after light irradiated at1 hr and 3 hrs. The HPLC was done at 25°C using a CLIPEUS 18 column. The mobile phase used was methanol:water (90:10 v/v) at the flow rate of 0.5 mL min^{-1}. The UV detector was set at 280 (above) and 332 (below) nm for **1E**, 285 (above) and 325 (below) nm for **2E** and 314 nm for **3E**. The sample injection volume was 10 μL. Peak area of side product is shown in blue color.

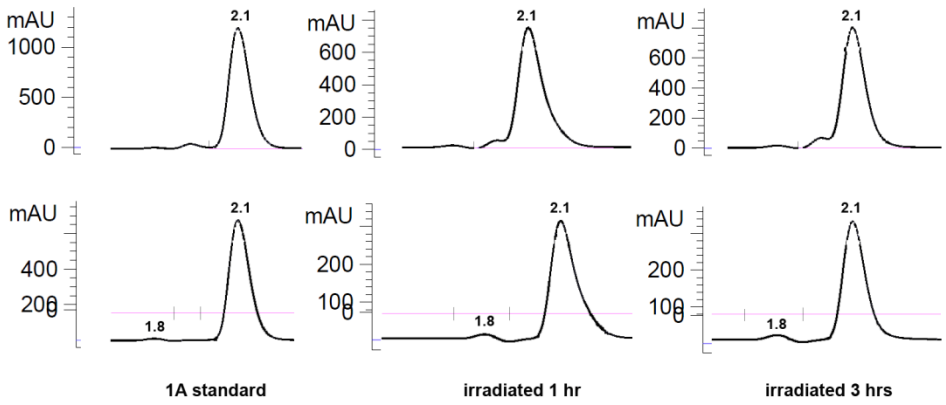

Figure 19 Chromatograms of standard *ortho*-hydroxycinnamic acid (**1A**) before and after light irradiated at1 hr and 3 hrs. The HPLC was done at 25°C using a CLIPEUS 18 column. The mobile phase used was methanol:water (90:10 v/v) at the flow rate of 0.5 mL min^{-1}. The UV detector was set at 278 (above) and 324 (below) nm. The sample injection volume was 10 µL.

HPLC chromatogram, mass spectra and NMR spectra of the light-exposed cinnamic acid (**1A**) confirmed that **1A** degraded into new product when exposed to sunlight. Although it has been known the possibility of *trans-ortho*-hydroxycinnamic acid is occurred via transformation to the *cis*-isomers on irradiation of UV light and might cyclize to produce coumarin. As the results, Figure 19 show the HPLC chromatograms of **1A** as the UV detector at 324 nm revealed a new peak at retention time 1.9 min and therefore indicated an accumulation of a new product. Moreover, mass spectra of decomposed product are showed in Figure 20. Both spectra gave a protonated molecular peak at m/z of 147.3 and 103.4. The similarity between the two mass spectra confirmed that both compounds were isomerization. It should be mentioned here that all other peaks in the spectra correspond to the cluster ions of the mobile phase. NMR data revealed a *trans*-isomer for the standard **1A** and *cis*-isomer at the same position for the isolated photo-degradation product. NMR spectra of light exposed **1A** indicated the presence of small signal of *cis*-isomer at 5.82 ppm after irradiated at 30 and 60 min as shown in Figure 21.

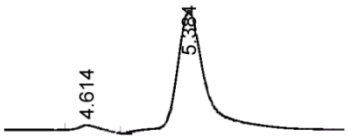

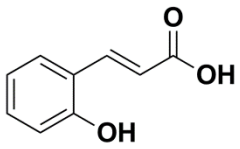

Chemical Formula: $C_9H_8O_3$
Exact Mass: 164.05
Molecular Weight: 164.16
m/z: 164.05 (100.0%), 165.05 (9.9%), 166.05 (1.0%)
Elemental Analysis: C, 65.85; H, 4.91; O, 29.24

At retention time of 4.6

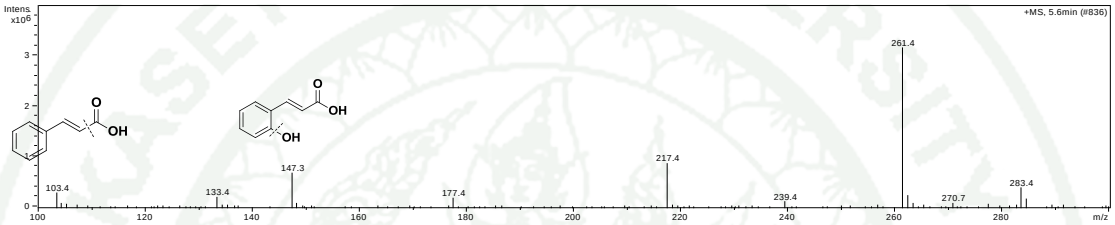

At retention time of 5.4

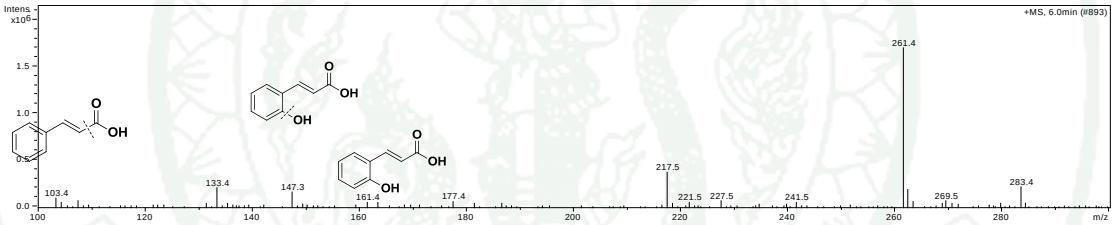

Mobile Phase (Methanol:Water 90:10 v/v) + TFA 0.01 v/v

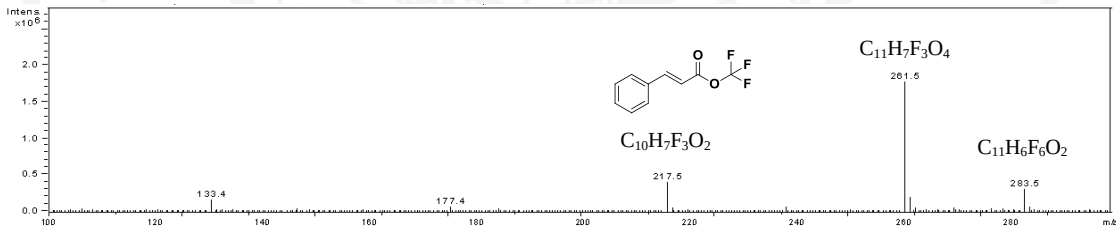

Figure 20 Mass spectra of the peaks from HPLC chromatogram for *ortho*-hydroxycinnamic acid (**1A**). The HPLC was done at 25°C using a CLIPEUS 18 column. The mobile phase used was methanol:water (90:10 v/v) with trifluoroacetic acid (TFA) 0.01 v/v at the flow rate of 0.2 mL min^{-1}. The sample injection volume was 10 μL.

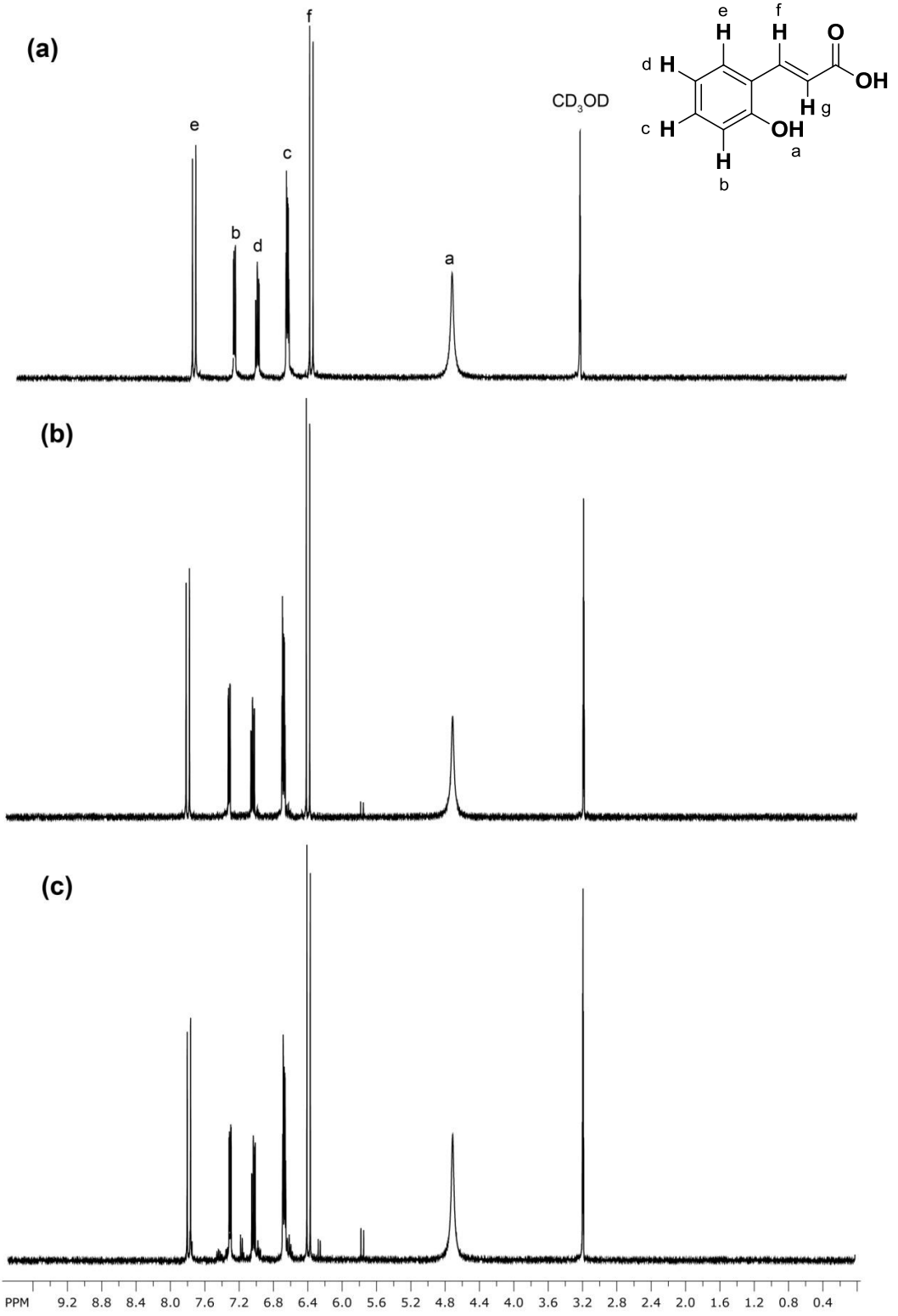

Figure 21 ^{1}H NMR (400 MHz) of *ortho*-hydroxy cinnamic acid **(1A)** (a) before, (b) after light irradiated at 30 min and (c) 120 min. (deuterated methanol as solvent).

1.6 Photoisomerization

The relaxation processes in the excited states are important for UV blocking molecules. One possible relaxation is a nonradiative decay via the conical intersection or the nπ* state (de Groot *et al.*, 2008; Shimada *et al.*, 2012). The emission or radiative decay competes with the nonradiative decay to the ground state. We focus here on the former relaxation pathway via the conical intersection. As discussed above, theoretical radiative lifetime is dependent on the substituent and also its position. This means that the ratio of the radiative to nonradiative decay varies among the compounds. For example, the radiative decay of *ortho* and *meta* compounds is slower than that of *para* compounds in the theoretical results.

Hydroxy cinnamates show somewhat better UVB blocking performance than nitro and fluoro compounds with regard to absorption and photostability. The emission strength is very different among three hydroxy derivatives. Thus, we concentrate here on the nonradiative relaxation of hydroxy derivatives and examined the relevant *cis–trans* isomerization at the propenyl double bond. The S_1 and S_2 PECs along the torsion angle $\omega(C_3–C_7=C_9–C_{11})$ were calculated for the hydroxy methyl cinnamates (**1E**–**3E**). Many internal coordinates would also contribute to the relaxation process. The PECs were calculated by CIS(D)/6-31G(d)//CIS/6-31G(d) calculations using the partial optimization for torsion angles (ω=0°–40° and 140°–180°) with all the other coordinates being optimized. For this purpose, the CASSCF calculations are desirable; however, we failed to converge the complete active space self-consistent field (CASSCF) calculations for the variation of this coordinate. The present CIS(D)//CIS calculations afford to qualitative picture. The calculated S_1 and S_2 PECs are shown in Figure 22. The vertical absorption energy levels of the S_1, S_2 and T_2 states are also shown in the figure except for the T_1 state which is located much below (about 3.5 eV). From the oxygen-quenching experiment, the relaxation predominantly occurs via a singlet S_1 excited state for hydroxy cinnamates. The energy barrier (ω=180-140°) to the conical intersection, which we can evaluate properly by the present method, is an important factor in the relaxation process.

In all cases, the *trans* structures (ω= 180°) are more stable than the *cis* structures (ω= 0°), as also seen in the previous reports (Promkatkaew *et al.*, 2009). We consider here the photoexcitation and subsequent relaxation from the *trans* structure. After photoexcitation, the cinnamates in the S_1 state lead to the conical intersection with torsion at the propenyl double bond. For the *ortho* compound (**1E**), the S_1 PEC is almost flat with very low energy barrier to conical intersection, which may also lead to radiative decay with fluorescence. No energy barrier was found for the *para* compound (**3E**) and nonradiative decay would occur via conical intersection. For *meta* compound (**2E**), the S_1 PEC has a large energy barrier so that the nonradiative decay is strongly prohibited and it leads to a strong emission. These results qualitatively match with the emission spectra in Figures 15 and 16. These results also agree with the recent studies of the hydroxy and methoxy derivatives (Promkatkaew *et al.*, 2009; Shimada *et al.*, 2012). Since the present CIS(D) calculations remain in qualitative picture, more detailed theoretical analysis is necessary for this relaxation dynamics.

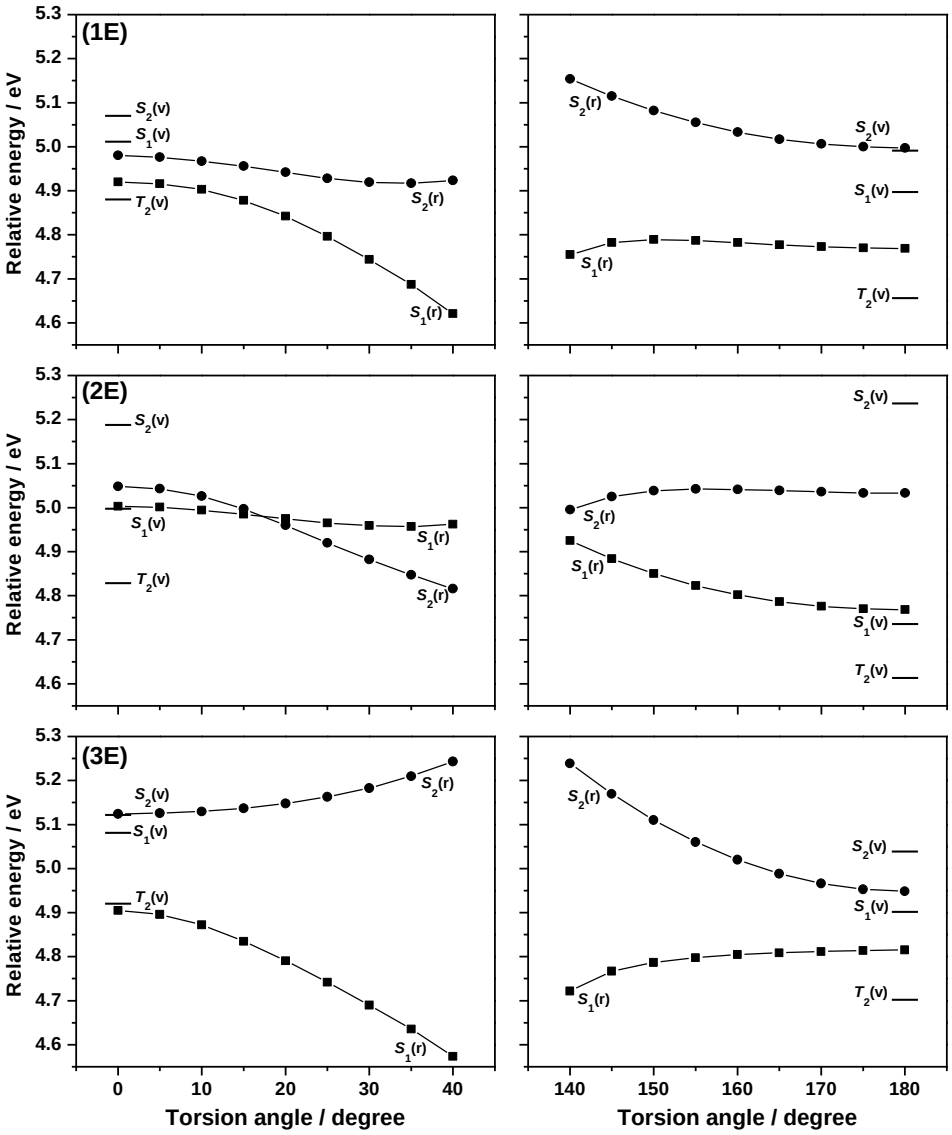

Figure 22 Excited state PECs for the hydroxy methyl cinnamates (**1E**–**3E**). The PECs of S_1(r) and S_2(r) were obtained by CIS(D)/6-31G(d)//CIS/6-31G(d) with fixed the torsion angle ω (C_3–C_7=C_9–C_{11}). The energy levels of S_1(v), S_2(v) and T_2(v) were obtained by CIS(D)/6-31G(d). All energies are relative to the ground state of *trans*-isomer (ω = 180°).

In summary, the *para*-hydroxy compound (**3E**) shows superior UVB blocking performance with respect to the relaxation process to *ortho*-(**1E**) and *meta*-(**2E**) compounds. It also has the best performance among the derivatives studied here, considering its absorption and photostability. Based on the absorption spectra compared in Figure 23, *para*-methoxy compound shows similar or slightly better UVB absorbing performance than *para*-hydroxy compound regarded that both compounds have similar photostability and photoemission property (Karpkird *et al.*, 2009; Monhaphol *et al.*, 2007).

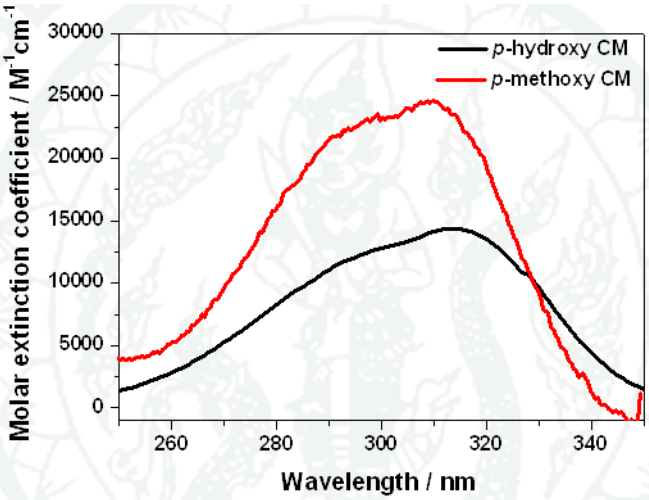

Figure 23 A comparison of the experimental absorption spectra in methanol between *para*-hydroxy-(**3E**) and *para*-methoxy cinnamates.

2. Investigation on the inclusion complexes between methoxycinnamic acid and cyclodextrin by performing quantum chemical calculations

2.1 Quantum chemical calculations

2.1.1 Methoxycinnamic acid modified cyclodextrins

The ground-state geometries of methoxycinnamic acid (*p*CA, 245CA, and 246CA), cyclodextrins (α-, β-, and γ-CDs), and methoxycinnamic acid modified cyclodextrins **[1]** *p*CA-αCD, **[2]** *p*CA-βCD, **[3]** 245CA-βCD, **[4]** 246CA-βCD, and **[5]** 246CA-γCD were optimized by using M06-2X/6-31G(d,p) level of theory without any symmetry restrain in both gas phase and water. CDs were modified by functionalization of their primary hydroxyl rims with various methoxycinnamoyl moieties. To investigate CA modified CDs, two orientations are considered where the aromatic ring of CA is located internal and external binding conformations. We called the "inside" and "outside" orientations. Moreover, to better understand the complexation, we have studied two different inclusion processes with the host/guest ratios being 1:2 and 2:2.

First, we look at the inside and outside orientations and focus on the *cis–trans* structure of the torsion angle θ (C_1–C_7=C_8–C_9) for CA when located inside and outside of the cavity of CDs. The torsion angle θ was investigated as shown in Table 12 and Figure 24. It was found that all complexes in both the inside and outside orientations show *trans*-structure with the torsion angle θ = 160–170° in both gas phase and water, except for the inside orientation of complex **[1]** show *cis*-structure with the torsion angle $\theta \sim -4.32°$. This indicating that complex **[1]** *p*CA could insert into the cavity of the smallest αCD as *cis*-structures. No significant change in torsion angle could be recognized between gas phase and water.

Table 12 Torsion angles θ of C_1–C_7=C_8–C_9 (degree) of methoxycinnamic acid when bound to cyclodextrins in both gas phase and water.

Complex	Gas Phase		Water (PCM)	
	inside	outside	inside	outside
[1] *p*CA-αCD	-4.32	-164.67	-4.32	-165.26
[2] *p*CA-βCD	-172.37	-163.67	-170.96	-165.06
[3] 245CA-βCD	-168.11	-173.51	-168.90	-174.60
[4] 246CA-βCD	-167.73	-168.94	-167.49	-167.30
[5] 246CA-γCD	171.72	-159.30	171.16	-163.31

Then, we have compared the lowest interaction energies of five complexes between the methoxycinnamic acid modified cyclodextrins for the inside and outside orientations. Liu and Guo indicated the most important driving forces in the inclusion complexes are electrostatic, van der Waals and hydrophobic interactions, hydrogen bonding and release of conformational strain. (Liu and Guo, 2002) The complex stability depends on molecular size and shape complementation but also on the external medium and environmental conditions.

In Table 13, the lowest interaction energies of five complexes for the inside and outside orientations in both gas phase and water are displayed. Complexes **[1]**, **[2]**, and **[5]** have the lowest interaction energies at the outside orientation, whereas complexes **[3]** and **[4]** have the lowest interaction energies at the inside orientation in both gas phase and water. Therefore, complexes **[1]**, **[2]**, and **[5]** are more favorable located outside the CDs cavity, while complexes **[3]** and **[4]** are stable when located inside the CDs cavity. The optimized structures for CA inside CDs are shown in Figure 24. Interestingly, the energy differences between inside and outside orientations for complex **[1]** are 10.33 kcal/mol (gas phase) and 7.05 kcal/mol (water). This confirms that complex **[1]** is stable at the outside orientation.

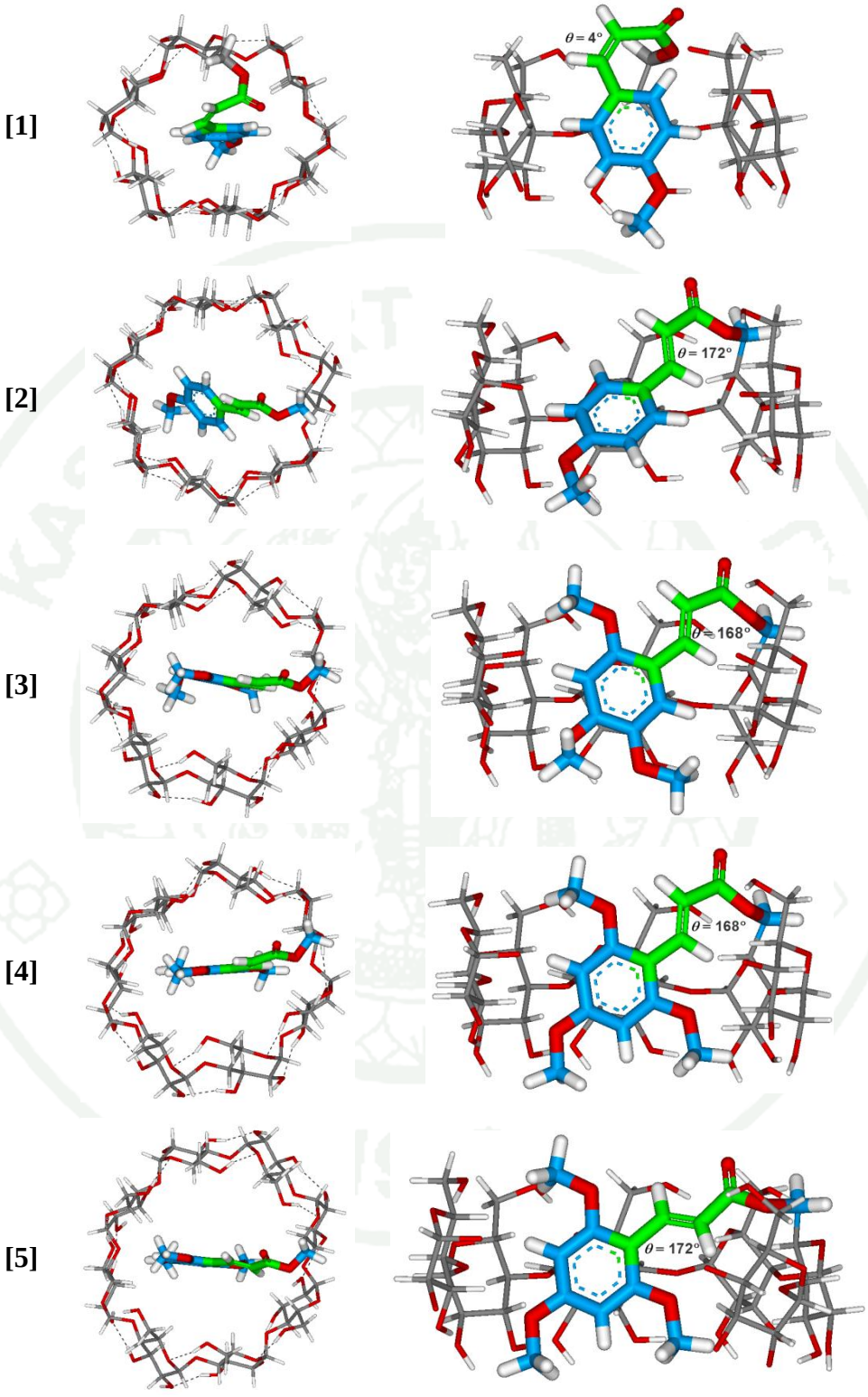

Figure 24 The optimized geometries of the methoxycinnamic acid modified inside cyclodextrins calculated at the M06-2X/6-31G(d,p) level.

Table 13 Interaction energies of methoxycinnamic acid located inside and outside cyclodextrin in both gas phase and water.

Complex	Gas Phase ΔE (kcal/mol)	Water (PCM) ΔE (kcal/mol)
[1] *p*CA-αCD	10.33	7.05
[2] *p*CA-βCD	5.64	2.91
[3] 245CA-βCD	-2.11	0.06
[4] 246CA-βCD	-5.93	-4.57
[5] 246CA-γCD	8.01	4.12

To better understand the complexation, we have studied two different inclusion processes with the host/guest ratios being 1:2 and 2:2 for the βCD modified with different CA of complexes **[2]** *p*CA-βCD, **[3]** 245CA-βCD, and **[4]** 246CA-βCD as shown in Table 14 and Figure 25. As the result, it was speculated that CA was located inside the CD cavities with more hydrophobicity environment for complexes **[3]** 245CA-βCD and **[4]** 246CA-βCD corresponding to the more negative binding (ΔE_b) energies. Therefore, the *ortho*-, *meta*- and *para*-trimethoxycinnamic acid (245CA) and *ortho*-, and *para*-trimethoxycinnamic acid (246CA) compounds are more stable in the medium β-CDs. Whereas, the smallest *para*-monomethoxycinnamic acid (*p*CA) compound could not fit within the cavity of medium β-CDs.

Table 14 Binding (ΔE_b) energies (kcal/mol) between methoxycinnamic acid and cyclodextrins with the ratios being 2:1 and 2:2 in both gas phase and water.

Complex	CA/CD (2:1)		CA/CD (2:2)	
	Gas Phase	Water	Gas Phase	Water
[2] *p*CA-βCD	-25.88	-20.56	-59.79	-51.25
[3] 245CA-βCD	-44.91	-28.86	-71.39	-50.82
[4] 246CA-βCD	-50.35	-34.57	-72.80	-53.60

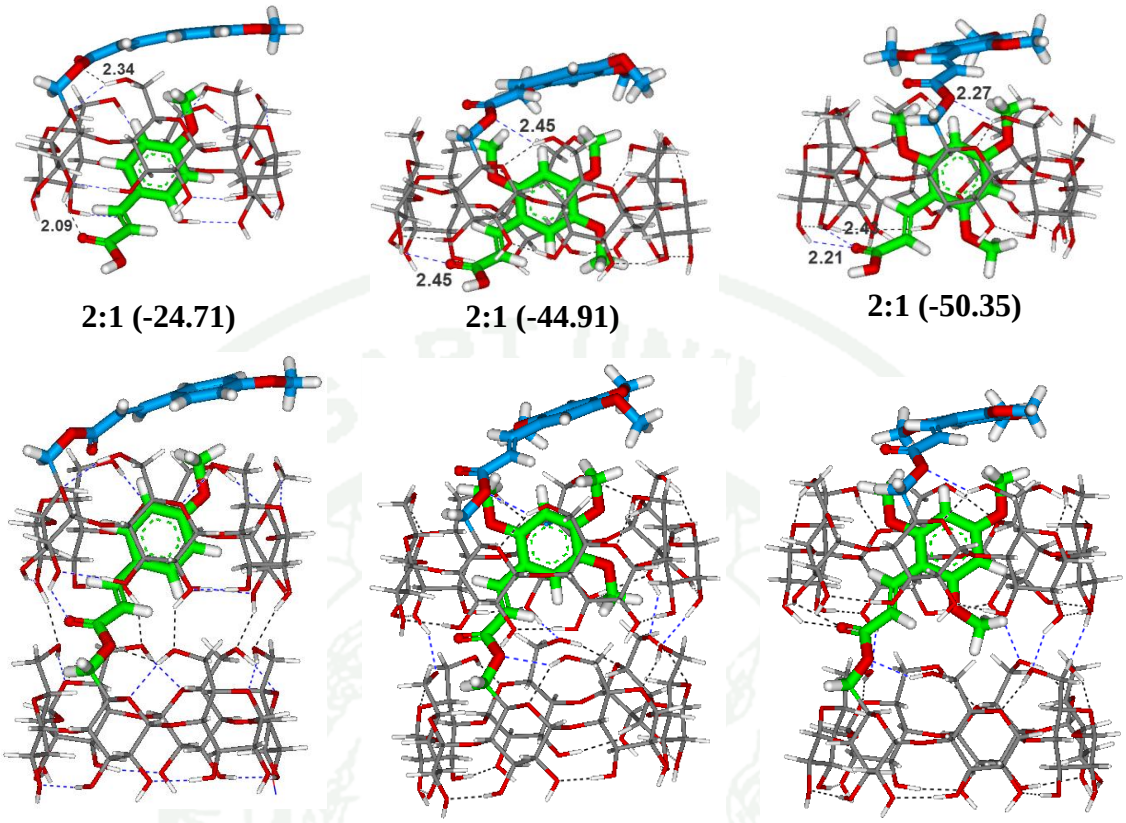

Figure 25 The optimized geometries representation of the inclusion complex of methoxycinnamic acid modified cyclodextrins calculated at the M06-2X/6-31G(d,p) level. The dotted lines denote possible hydrogen bonds with $d_{H\cdots O}$ < 2.5 Å. The red color stands for oxygen, blue for hydrogen, and gray for carbon. The values in the parenthesis are the binding energies (kcal/mol) of the inclusion complex.

Several intermolecular H-bonds in the complex between the host and guest are formed as shown by the dotted lines in Figure 25. Here, the hydrogen bond defined as a C–H···O distance is less than 2.5 Å. Although the C–H···O hydrogen bond is weak, it is believed to play an important role besides the van der Waal force and the hydrophobic interaction in the host-guest complexation. The results calculated indicated that the higher stability of the inclusion complex, the more intermolecular H-

bonds are formed between the host and guest according to the calculated ΔE_b value. For the CA modified CDs, we considered β-CD with different methoxycinnamic acid. As the result, we found that the trimethoxycinnamic acids (246CA and 245CA) show the most energetically favorable geometries than that of the monomethoxycinnamic acid (*p*CA).

2.1.2 Methoxycinnamic acid included cyclodextrins

These inclusion complexes do not contain any covalent bond between host and guest molecules and their stability depends on molecular size and shape complementation but also on the external medium and environmental conditions. The most important driving forces in the inclusion complexes are electrostatic, van der Waals and hydrophobic interactions, hydrogen bonding and release of conformational strain (Liu and Guo, 2002).

These calculations show that for all five complexes the methoxycinnamic acid molecules are located inside the cavity. Two orientations of the methoxycinnamic acid guest molecule were considered. For simplicity, when the aromatic ring is inserted first into CDs, we call this the "head orientation", if the carboxylic (COOH) group is located near the narrow rim and when COOH group is inserted firstly this orientations is called "tail orientation" corresponding to the COOH group located near the wider rim of the CDs (Figure 26).

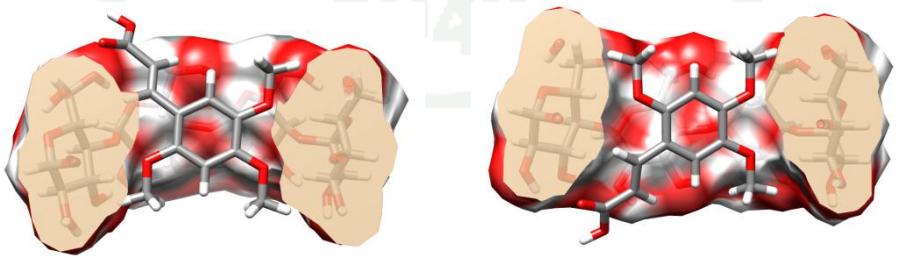

head orientation **tail orientation**

Figure 26 Structures of the M06-2X/6-31G(d,p) energy minima obtained for complex **[3]** 245CA-βCD: head and tail orientations.

Upon examining the optimized geometry of inclusion complex, we notice that the CA molecule is located in the cavity of CD according to the head and tail orientations. The phenyl moiety of methoxycinnamic acid is staying inside the cavity of CD. Notable intermolecular hydrogen bonds between hydroxyl group of CD and carboxylic group of cinnamic acid have been observed. The results are shown in Table 15 with the binding (ΔE_{b}) and deformation(ΔE_{d}) energies between methoxycinnamic acid and cyclodextrins in gas phase and in water, respectively.

Table 15 Binding (ΔE_{b}) and deformation (ΔE_{d}) energies (kcal/mol) between methoxycinnamic acid and cyclodextrins in gas phase and water.

Complex	Gas Phase				Water			
	ΔE_{b}	ΔE_{d}	$\Delta E_{\mathrm{d}}(\mathrm{CD})$	$\Delta E_{\mathrm{d}}(\mathrm{CA})$	ΔE_{b}	ΔE_{d}	$\Delta E_{\mathrm{d}}(\mathrm{CD})$	$\Delta E_{\mathrm{d}}(\mathrm{CA})$
				head orientation				
[1] *p*CA-αCD	-20.65	-26.80	1.60	4.54	-18.04	-23.72	1.50	4.18
[2] *p*CA-βCD	-21.42	-35.11	1.73	11.95	-17.57	-30.40	2.36	10.47
[3] 245CA-βCD	-24.07	-37.46	4.01	9.38	-15.11	-26.16	4.37	6.67
[4] 246CA-βCD	-18.35	-29.57	4.73	6.49	-13.30	-25.78	5.01	7.47
[5] 246CA-λCD	-21.01	-28.13	2.56	4.56	-16.53	-20.22	1.95	1.74
				tail orientation				
[1] *p*CA-αCD	-27.38	-35.82	2.57	5.87	-19.75	-26.65	2.05	4.85
[2] *p*CA-βCD	-30.69	-40.19	1.02	8.48	-22.07	-29.18	0.40	6.72
[3] 245CA-βCD	-37.96	-52.61	2.35	12.30	-25.58	-37.18	1.80	9.80
[4] 246CA-βCD	-37.23	-52.83	4.88	10.72	-24.49	-37.45	3.81	9.14
[5] 246CA-λCD	-35.41	-50.22	4.69	10.12	-24.17	-35.45	3.75	7.53

It is significant that the value of binding energies is higher than that of deformation energy for the same complex in both gas phase and water. ΔE_{b} and ΔE_{d} the initial and final distances between the centroids of CA and CD are summarized in Table 15. The DFT method was used in the geometry optimization. The final energy calculations was performed using the M06-2X/6-31G(d,p) method. Further calculations were performed to include the solvation effect of water using the

polarizable continuum model (PCM). It was found that the binding energies in water are higher than those in gas phase.

2.2 Molecular docking and molecular dynamics simulations

Molecular docking was chosen for obtaining the best binding interaction of 245CA to βCDs. We carried out Docking by using MOE-dock system. The geometries of methoxycinnamic acid and cyclodextrins were fully optimized using M06-2X/6-31G(d,p) methods. The binding energies of the ligand and CDs were analyzed. As the results, the there are 25 docked structures of inclusion complexes of **[3]** 245CA-βCD. Most of the docking structures are located at the wider rim of CDs. Hydrogen bond interactions between methoxycinnamic acid and OH groups of CDs are found. Moreover, we were fully optimized all 25 structures by using the M06-2X/6-31G(d,p) method in both gas phase and water. We found that the most stable complex is tail orientation from QM calculations for complex **[3]** 245CA-βCD. Three lowest binding energies and the optimized geometries for docked compound are shown in Table 16 and Figure 27.

We carried out docking by using MOE-dock system. We found the 25 docked structures for inclusion complexes of **[3]** 245CA-βCD. As the results, most of the docking structures are located at the wider rim of CDs by forming the hydrogen bond interactions between methoxycinnamic acid and OH groups of CDs. Moreover, we were fully optimized all 25 structures by using the M06-2X/6-31G(d,p) method in both gas phase and water as shown in Table 16.

Table 16 Binding (ΔE_b) energies (kcal/mol) for molecular docking of complex **[3]** 245CA-βCD.

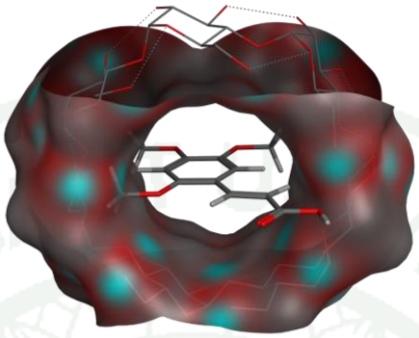

[3] 245CA-βCD		Gas phase		Water	
		ΔE_b	Relative en.	ΔE_b	Relative en.
Orientation	**head**	-24.07	13.89	-15.11	10.47
	tail	-37.96	0.00	-25.58	0.00
Docking	**1**	-17.03	20.93	-14.97	10.61
	2	-14.44	23.52	-10.64	14.94
	3	-22.27	15.68	-20.43	5.15
	4	-23.18	14.78	-17.41	8.17
	5	-28.85	9.11	-21.42	4.16
	6	-18.91	19.05	-16.68	8.90
	7	-20.60	17.36	-17.19	8.39
	8	-26.69	11.27	-23.23	2.35
	9	-18.97	18.99	-16.25	9.33
	10	-27.65	10.31	-23.92	1.66
	11	-22.17	15.79	-17.38	8.20
	12	-26.33	11.63	-21.64	3.94
	13	-23.26	14.69	-19.88	5.70
	14	-26.09	11.87	-21.95	3.63
	15	-17.72	20.24	-15.25	10.33
	16	-25.42	12.53	-20.68	4.90
	17	-23.67	14.29	-19.51	6.07
	18	-26.57	11.39	-24.78	0.80
	19	-23.34	14.61	-19.59	5.99
	20	-17.88	20.08	-16.02	9.56
	21	-21.83	16.12	-18.58	7.00
	22	-26.34	11.62	-21.50	4.08
	23	-26.97	10.99	-24.32	1.26
	24	-31.41	6.54	-21.59	3.99
	25	-31.48	6.47	-20.60	4.98

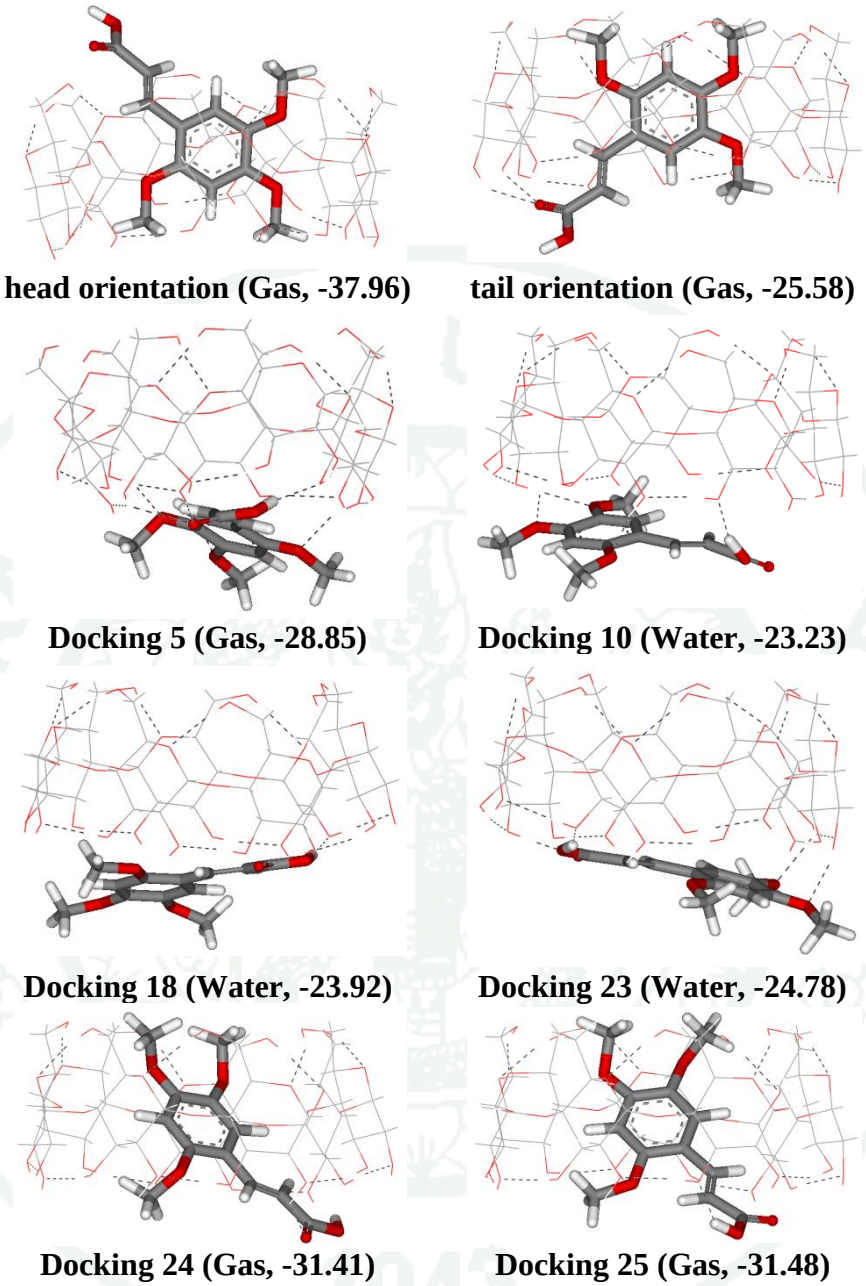

Figure 27 The selected optimized geometries of the inclusion complex of methoxycinnamic acid modified cyclodextrin for three lowest binding energies (kcal/mol) in gas phase: Docking 5, 24, and 25 and in water: Docking 10, 18, and 23 using M06-2X/6-31G(d,p) method. The values in the parenthesis are the binding energies. The dotted lines denote possible hydrogen bonds with $d_{H\cdots O} < 2.5$ Å.

To obtain accuracy and reliability of the binding mode information of the inclusion process between CA and CDs at the molecular level, we carried out MD simulations for the binary system of complex **[3]** 245CA-βCD in water. The trajectories of the insertion angles, rotation of the non-polar parts of the guest inside the host and other geometrical features give detailed information on the dynamics of the complexes. The "head" and "tail" orientations were investigated and taken from M06-2X/6-31G(d,p) calculations.

In Figures 28, 29, and 30, Amber program has been applied for molecular dynamics simulations of complex [3] 245CA-βCD. Root mean square displacement (RMSD) from MD simulations is shown in Figure 29. After heating, all systems have reached equilibrium. Lower fluctuation was found in head and tail orientation both cyclodextrin and methoxycinnamic acid.

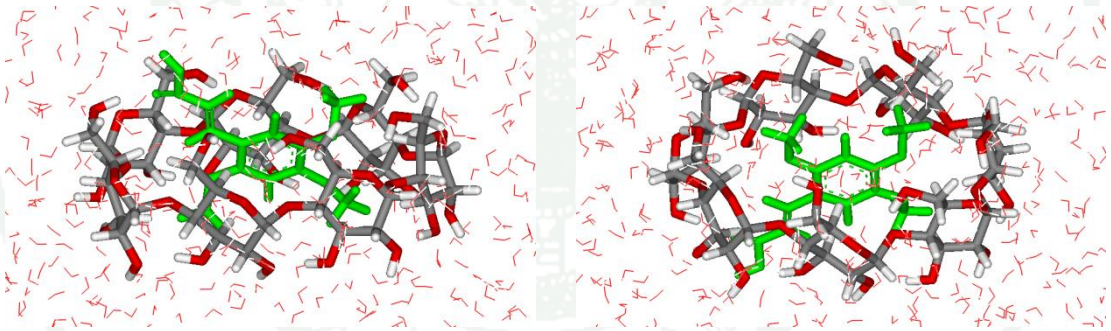

head orientation **tail orientation**

Figure 28 After minimization for forming complex **[3]** 245CA-βCD of head and tail orientations.

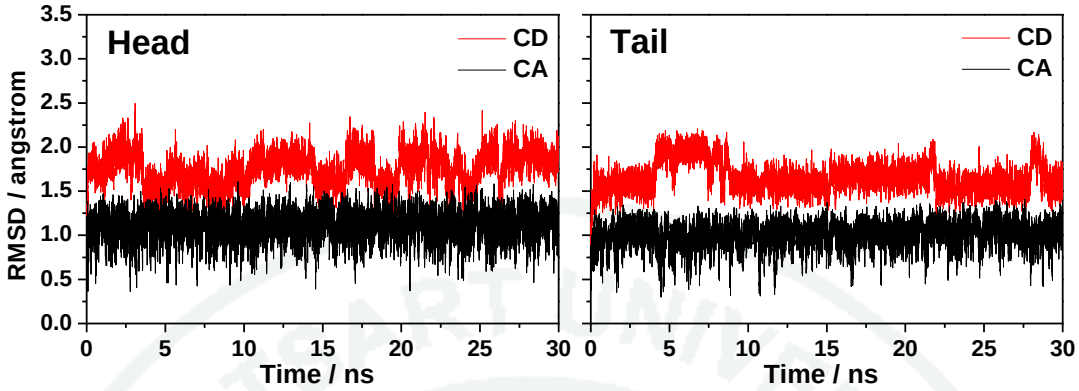

Figure 29 Root mean square displacement (RMSD) for CA and CD complex for the head and tail orientations of complex **[3]** 245CA-βCD.

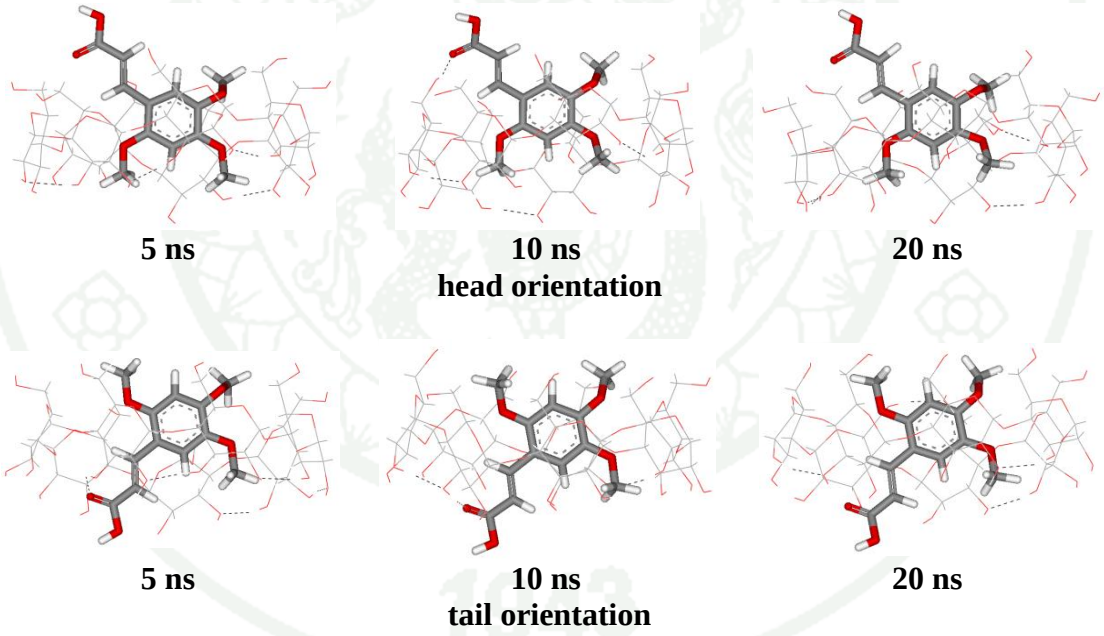

Figure 30 Snapshots of the inclusion process for forming complex **[3]** 245CA-βCD of the head and tail orientations. Water molecules were not included for clarity. The dotted lines denote possible hydrogen bonds with $d_{H\cdots O} < 2.5$ Å.

2.3 UV−Vis spectra

To reveal the host-guest interactions that are relevant to UVB blocking, the UV absorption spectra were performed using TD-DFT calculations at the same M06-2X/6-31G(d,p) level of theory in their optimized structures in gas phase and in solution. The solvent effect of all complexes was calculated using the polarizable continuum model (PCM) with DMSO in order to compare with the experimental data. The UV absorption wavelength of the methoxycinnamic acid derivatives, cyclodextrin derivatives and inclusion complexes with four orientations are displayed in Tables 17 and 18.

Table 17 Excitation energies (E_{ex}), absorption wavelengths (λ_{abs}), and oscillator strengths (f) in the gas phase and in DMSO for methoxyinnamic acid and cyclodextrins calculated using the TD-M06-2X/6-31G(d,p) method compared with the experimental data.

Compound		State	Gas Phase			DMSO (PCM)			*Exp.**
			E_{ex} (eV)	λ_{abs} (nm)	f	E_{ex} (eV)	λ_{abs} (nm)	f	(nm)
Guest	*p*CA	S_1	4.61	269	0.789	4.41	281	0.917	320
	245CA	S_1	4.05	306	0.521	3.86	321	0.629	350
		S_2	4.97	250	0.213	4.85	256	0.226	290
	246CA	S_1	4.50	276	0.724	4.26	291	0.842	320
Host	αCD	S_1	8.18	152	0.000	8.27	150	0.003	
	βCD	S_1	8.17	152	0.001	8.26	150	0.004	
	γCD	S_1	8.16	152	0.002	8.26	150	0.005	

*Data from (Karpkird and Wanichweacharungruang, 2010)

The absorption properties of the CA and CDs are displayed in Table 17. The TD-DFT absorption spectra of *p*CA and 246CA compounds show only one strong absorption peak with the highest oscillator strength (*f*), while compound 245CA has one strong absorption peak at the lower region and one shoulder at the higher region. The UV−Vis calculations show the same trend with the experimental data but the wavelength difference is larger than 30 nm (in DMSO) and 40 nm (in gas phase). No significant absorption in the UV−Vis region is observed for CDs.

Table 18 Excitation energies (E_{ex}), absorption wavelengths (λ_{abs}), and oscillator strengths (f) in the gas phase and in DMSO for host-guest inclusion complexes calculated using the TD-M06-2X/6-31G(d,p) method compared with the experimental data .

Complex		State	Gas Phase			DMSO (PCM)			*Exp.**
			E_{ex} (eV)	λ_{abs} (nm)	f	E_{ex} (eV)	λ_{abs} (nm)	f	(nm)
[1]	(a) inside	S_1	4.94	251	0.189	4.87	255	0.349	
	(b) outside	S_1	4.51	275	0.671	4.38	283	0.795	
	(c) head	S_1	4.71	263	0.399	4.53	273	0.538	
	(d) tail	S_1	4.31	288	0.464	4.30	289	0.582	320
[2]	(a) inside	S_1	4.69	264	0.254	4.51	275	0.612	
	(b) outside	S_1	4.41	281	0.729	4.29	289	0.869	
	(c) head	S_1	4.50	276	0.539	4.35	285	0.683	
	(d) tail	S_1	4.16	298	0.591	4.14	299	0.732	320
[3]	(a) inside	S_1	4.12	301	0.335	3.98	311	0.419	
		S_3	4.97	249	0.148	4.83	257	0.041	
	(b) outside	S_1	3.96	313	0.546	3.83	324	0.654	
		S_2	4.89	254	0.202	4.83	257	0.211	
	(c) head	S_1	4.25	292	0.281	4.07	305	0.354	
		S_2	4.89	253	0.013	4.94	251	0.068	
	(d) tail	S_1	3.72	334	0.348	3.71	335	0.440	350
		S_2	4.70	264	0.126	4.71	263	0.147	290
[4]	(a) inside	S_1	4.43	280	0.486	4.23	293	0.620	
	(b) outside	S_1	4.35	285	0.756	4.19	296	0.889	
	(c) head	S_1	4.60	269	0.405	4.43	280	0.503	
	(d) tail	S_1	4.17	297	0.450	4.12	301	0.575	325
[5]	(a) inside	S_1	4.28	289	0.568	4.08	304	0.718	
	(b) outside	S_1	4.28	289	0.679	4.18	297	0.815	
	(c) head	S_1	4.51	275	0.532	4.35	285	0.650	
	(d) tail	S_1	4.18	296	0.480	4.12	301	0.608	320

*Data from (Karpkird and Wanichweacharungruang, 2010)

Furthermore, we have investigated the UV–Vis absorption properties of CDs modified by CA and CD/CA inclusion complexes with four orientations: inside, outside, head, and tail orientations (Table 18). The experimental absorption spectrum of the CDs modified by CA for five complexes were similar to their parent CA. The UVB (280-320 nm) absorption was observed in complexes **[1]**, **[2]**, **[4]**, and **[5]** while both UVA (320-400) and UVB absorptions were detected in complex **[3]**

corresponding to the 245CA (Karpkird and Wanichweacharungruang, 2010). For the TD-DFT calculations, it was found that all complexes with four orientations show the similar absorption wavelength trend with the experimental data. CDs have no significant absorption in UV−Vis region, after inclusion of CA to form inclusion complex, a serial of strong absorption bands have been observed.

Among four orientations, tail orientation shows the best TD-DFT absorption wavelength compared with the experimental data for all complexes. Interestingly, the calculated spectra of complex **[3]** 245CA-βCD were observed in both UVB and UVA region at 264 and 334 nm (gas phase) and 263 and 335 nm (DMSO) corresponding to 290 and 350 nm (experimental peak). In addition, the UV−Vis absorption in gas phase and DMSO solution are similar in (d) tail orientation but blue shifted in the (a) inside, (b) outside, and (c) head orientations as show Table 18. This indicates that the tail orientations for five complexes show the stable orientations in both gas phase and DMSO. Therefore, the calculated UV−Vis results show clearly that the tail orientation of inclusion complex between CA and CD is most stable orientations and can absorb in both UVB and UVA regions which is similar to the parent CA.

3. Skin sensitization prediction using quantum chemical calculations: A theoretical model for the S_NAr Domain

We were firstly interested in assessing whether chemicals used in a particular application (consumer vs pharmaceutical for example) are more likely to display differences in reactivity alerts. For example it might be expected that drugs will be more carefully screened for reactive features (i.e. potentially leading to drug drug interaction (Kalgutkar and Soglia, 2005)) than chemicals used in manufacturing or consumer products due to the high systemic concentration generally achieved (Stumpf, 2006). Compounds in the oral drug dataset compiled are expected to achieve higher systemic exposure than topically applied drug dataset. The LLNA dataset differs from the former two as it contains primarily non-drug like compounds used in consumer products. Indeed, Figure 29 shows that the three different datasets are not dramatically different in terms of the non-reactive functionalities present (NR = 35%, 45% and 41% for oral drugs, topical drugs and consumer chemicals respectively). This might have been expected that the latter set was artificially enriched with sensitizers as many known sensitizers from other assays have been used to validate the LLNA assay. This confirms that the presence of a reactive structural alert in a molecule should not simply be taken as meaning that the compound is high risk.

Analysis of the compiled LLNA measurements broken down by reaction domain does reveal significance differences. The mean pEC3 (quantitative measures only) broken down by reaction domain clearly shows that certain chemical domains are more likely to lead to severe skin sensitization than others (Figure 32). It is notable that the least represented type of compound in Figure 31 are those of the S_NAr domain, and these can be shown to lead to the highest sensitization of all the chemical classes on average. S_N2, Acyl and MA are shown to display a comparable risk, with SB being the least problematic on average. It is also worth noting that chemicals classed as containing no reactive functionality also show sensitization potential. This however is overestimated since most NR compounds do not have quantitative pEC3 measures (i.e. class based only). Attempts to further identify trends with simple molecule properties were unsuccessful but perhaps not unsurprising given reports by others (Roberts *et al.*,

2011). This alternatively may be due to the relative small datasets and rather limited chemical diversity.

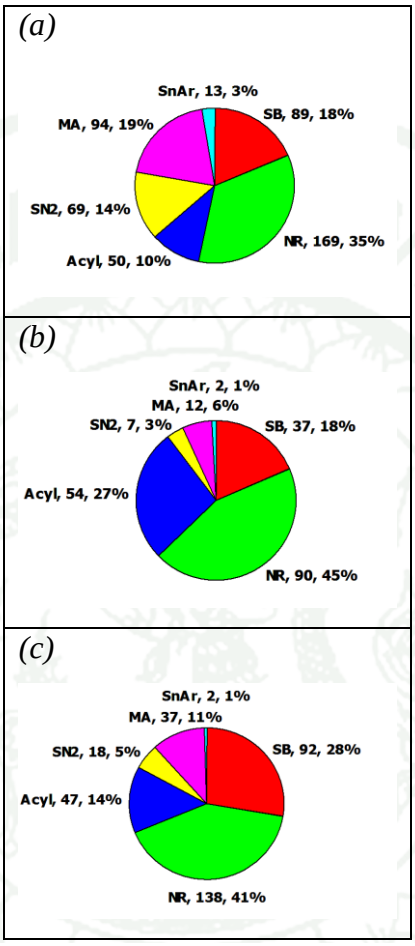

Figure 31 Pie chart showing distribution (a) Topical oral drugs (b) Top-200 reported oral drugs and (c) all compounds reported with data from LLNA assays.

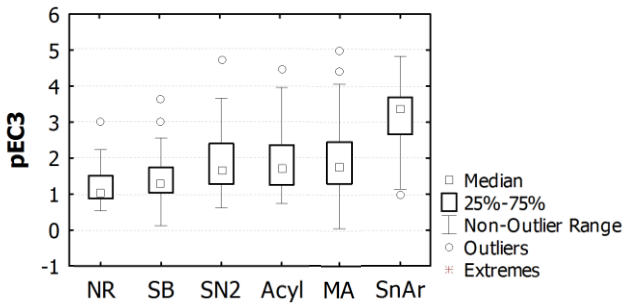

Figure 32 ANOVA correlation of pEC3 values for mechanisms: SB, S_NAr, S_N2, Acyl, MA, and non-sensitizer (NR).

Figure 29 and Figure 30 clearly show the need for additional methods, on top of the reaction domain scheme, help to discriminate sensitizers from non-sensitizers more effectively. It is also notable that the S_NAr domain poses a particularly significant threat of all the reaction classes. Nevertheless, such compounds make up 13% of oral drugs, 2% of topical drugs and 2% of all compounds tested in the LLNA assay. In the next section we discuss a purely theoretical QC based method suitable for use in the ranking of chemicals.

QC model of skin sensitization

The general addition-elimination reactions of chemicals from the S_NAr domain are summarized in Figure 33. The displacement of halogen or pseudohalogen group can proceed in either one or two steps as shown. Addition of the nucleophile to the aromatic ring leads to a resonance-stabilized carbanion, which is the transition state for the S_N2 process, and a stable intermediate for the S_N1 process. The nature of the leaving group, and the stabilizing effect of the ring substituents control the barrier height (Roberts *et al.*, 2011). The first step in the process is expected to be the rate determining step due to the unfavorable loss of aromaticity. The complete reaction profiles for the 23 chemicals studied here are reported in Table 19.

There are divided into two sets: the first set is that corresponding to the generation of a reactive species, the second involving the reaction of that species with DNA. In this analysis, the displacement of halogen or pseudohalogen was considered to proceed in two steps: addition of the nucleophile ($:Nu^-$) forms a resonance-stabilized carbanion with a new C–Nu bond, produces an intermediate with a negative charge delocalization in the ring, and elimination of the leaving group from this intermediate. Step [1] is rate-determining since the aromaticity of the benzene ring is lost. Moreover, it is assumed that this step holds also for the biological nucleophiles involved in sensitization. In Step [2], loss of the leaving group re-forms the aromatic ring. This step is fast because the aromaticity of the benzene ring is restored.

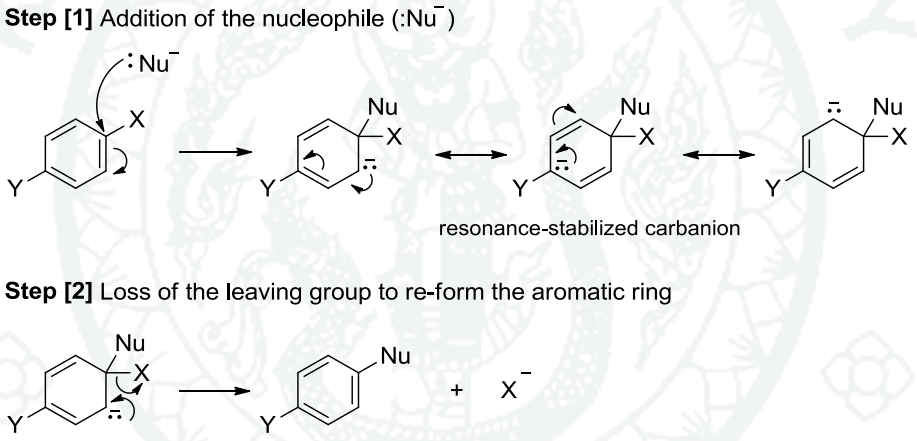

Figure 33 The general addition-elimination reaction of chemicals from the S_NAr domain.

Table 19 The predicted QC reaction profile of the S_NAr domain and the comparable QMM prediction (Roberts *et al.*, 2011).

Structure		X	Class	pEC3	Relative energy (kcal/mol)						Homo-Lumo E	clogP	QMM
					Isolated Reactant	TS1	Inter	TS2	Product	Isolated Product			
1	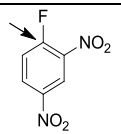	F	Extreme	3.76	4.80	4.27	-14.04	-3.67	-12.29	-11.85	3.99	1.81	3.77
2	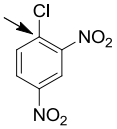	Cl	Extreme	3.42	5.25	5.84	-11.84	15.97	-42.36	-39.76	3.85	2.33	3.42
3	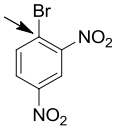	Br	Extreme	3.46	5.66	4.41	-	-	-41.75	-31.76	3.81	2.50	3.34
4	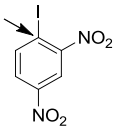	I	Strong	3.24	3.24	5.99	-	-	-48.60	-50.31	4.02	2.81	3.12
5	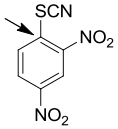	SCN	Extreme	3.68	5.26	4.90	-12.29	-12.28	-37.02	-33.44	3.70	2.13	3.70
6	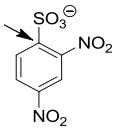	SO_3	Moderate	2.12	2.17	8.91	-9.37	9.13	-1.35	98.75	3.74	0.97	2.13

Table 19 (Continued).

Structure		X	Class	pEC3	Relative energy (kcal/mol)						Homo-Lumo E	clogP	QMM
					Isolated Reactant	TS1	Inter	TS2	Product	Isolated Product			
7	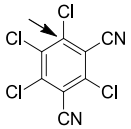	Cl	Extreme	4.88	5.37	5.37	-	-	-37.35	-34.52	4.38	3.88	5.15
	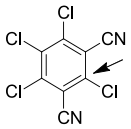					4.36			-37.92	-35.00			
	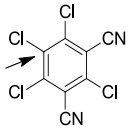					12.29			-37.25	-34.45			
8	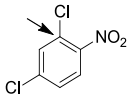	Cl	Weak	0.98	4.13	9.93	-	-	-41.74	-39.68	4.11	3.07	1.23
9	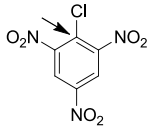	Cl	Extreme	3.69	8.99	1.88	-27.36	-26.12	-41.52	-36.99	3.55	2.20	6.49
10	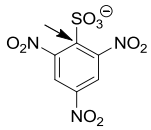	SO_3	Strong	2.99	3.32	5.89	-24.55	1.56	0.44	103.98	3.70	0.85	5.20

Table 19 (Continued).

Structure		X	Class	pEC3	Relative energy (kcal/mol)						Homo-Lumo E	clogP	QMM
					Isolated Reactant	TS1	Inter	TS2	Product	Isolated Product			
11	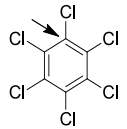	Cl	NR	NR	4.28	15.29	-	-	-36.67	-34.61	5.41	5.68	7.58
12	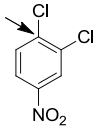	Cl	NR	NR	3.07	11.12	-	-	-39.48	-36.98	4.08	3.07	6.54
13	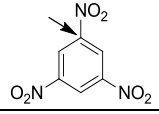	NO_2	NR	NR	5.52	10.77	-	-	-23.06	-18.46	3.69	1.58	6.22
14	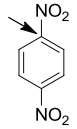	NO_2	NR	NR	3.64	7.31	-0.67	0.90	-21.71	-18.57	3.59	1.71	5.63
15	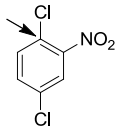	Cl	NR	NR	4.41	10.59	-	-	-40.59	-39.08	4.09	3.07	5.45
16	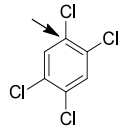	Cl	NR	NR	2.86	19.03	-	-	-38.76	-37.47	5.61	4.44	4.98

Table 19 (Continued).

Structure		X	Class	pEC3	Relative energy (kcal/mol)						Homo-Lumo E	clogP	QMM
					Isolated Reactant	TS1	Inter	TS2	Product	Isolated Product			
17	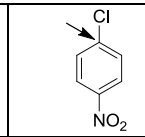	Cl	NR	NR	2.11	13.06	-	-	-38.31	-37.15	4.19	2.45	4.85
18	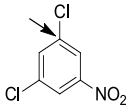	Cl	NR	NR	3.07	18.96	-	-	-37.63	-36.37	4.06	3.07	4.53
19	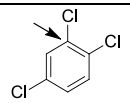	Cl	NR	NR	2.51	20.43	-	-	-38.57	-37.39	5.81	3.82	4.38
20	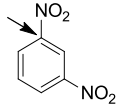	NO_2	NR	NR	3.93	18.03	-	-	-19.71	-16.31	3.97	1.71	4.39
21	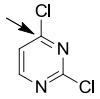	Cl	Strong	2.33	3.16	8.69	-	-	-38.34	-37.43	5.18	2.20	3.29
22	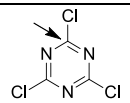	Cl	Extreme	3.31	4.93	2.35	-	-	-42.88	-39.48	4.75	3.53	10.48
23	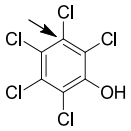	Cl	NR	NR	3.82	16.83	-	-	-36.41	-34.68	5.54	4.68	6.98

Should the reactivity of the sensitizing chemicals be under kinetic control we would expect the RDS to correlate well with the experimental pEC3. Alternately, should the process depend on the overall thermodynamics, we would expect the exothemicity of the products to be important. The complete profiles of chemicals 1-6 are shown pictorially in Figure 34 as well as the 3 possible products for 7. It can be seen for those chemicals with halogen or pseudo halogen leaving groups and common core (i.e. 2,4-dinitrobenzene), that the profile can vary substantially. Firstly, it can be seen that the more effective leaving groups, Br- (3) and I- (4), display S_N2 character and results in highly exothermic products. In contrast, chemicals 1,2,5 and 6 results in S_N1 based processes. For chemicals 1 and 6 it can be seen that the products are much lower in energy than the corresponding intermediate or reactant configuration, and that the 2nd step is rate determining for the full addition-elimination process. Chemical 2 also displays a higher barrier for the second step. Nevertheless, it is possible that the intermediate can also give rise to the sensitization response and not the elimination product.

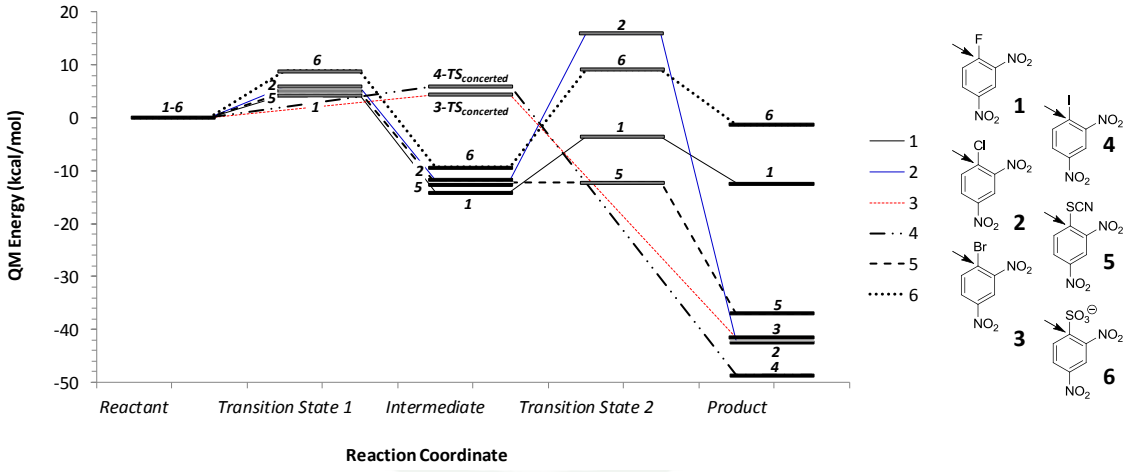

Figure 34 The reaction profiles obtained for chemicals 1–6. Chemicals 1, 2, 5 and 6 show an S_N1 based profile while it follows a S_N2 profile for 3 and 4.

For the 2,4-dinitrobenzene compounds, analysis of the correlation between the quantitative pEC3 value and the computed barrier to intermediate/product shows a rather strong correlation (r^2=0.93) (Figure 34). Plotting the rate determining step to

product formation (i.e. for S_N1 it can be the second transition state) does not improve the correlation suggesting that the chemical sensitization may involve formation of a relatively stable carbanion intermediate in some cases (see Figure 2). Analysis of a more diverse set of chemicals that contain the same Cl leaving group, shows a moderate correlation between the pEC3 and the barrier of (r^2=0.58). More importantly, the line of best fit for both relationships in Figure 34 are remarkably similar suggesting that a single QC descriptor is needed to explain the sensitization potential, irrespective of ring substituents or leaving group.

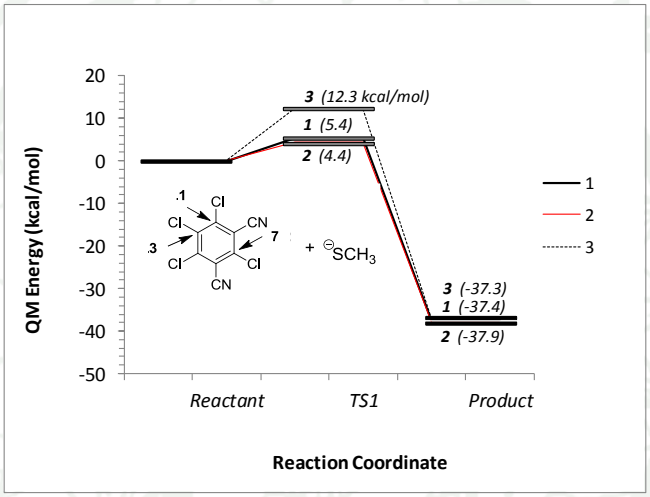

Figure 35 The reaction profiles for 3 different products obtained for chemical 7.

Chemical 7 appears to be an outlier. To try to understand this we investigated the reaction profile in more detail and considered the two other distinct addition-elimination positions (Figure 35). It is found that the other positions of attack not initially considered were considerably higher in energy suggesting this was not the cause of 7 being an outlier. Further analysis showed that of all the chemicals studied here, only 11, 16 and 23 have higher clogP values. The latter 3 chemicals have much higher barriers to reaction rendering them weak to non-sensitizers. Thus it is possible that the additional lipophilicity of 7, with its low barrier to reaction, may make the formation initial protein-sensitizer even more favorable. The increased association due to hydrophobic forces coupled with the low barrier results in more extreme sensitization than expected from the barrier alone. The r^2 of observed for the pEC3 vs

QC barrier for chemicals with Cl leaving groups increases from 0.58 to 0.74. While it would be desirable to include an additional term in such a model to account for lipophilicity, the lack of sufficient data to confirm the hypothesis and fit a reliable, 2 parameter QSAR equation, means that the use of a QC based descriptor alone is more appropriate. In addition, we cannot rule out whether other factors contribute, including; (a) the use here of an inappropriate mechanism or nucleophile in our QC model (b) that molecular recognition may be important for this chemical or (c) the difference is due to experimental error.

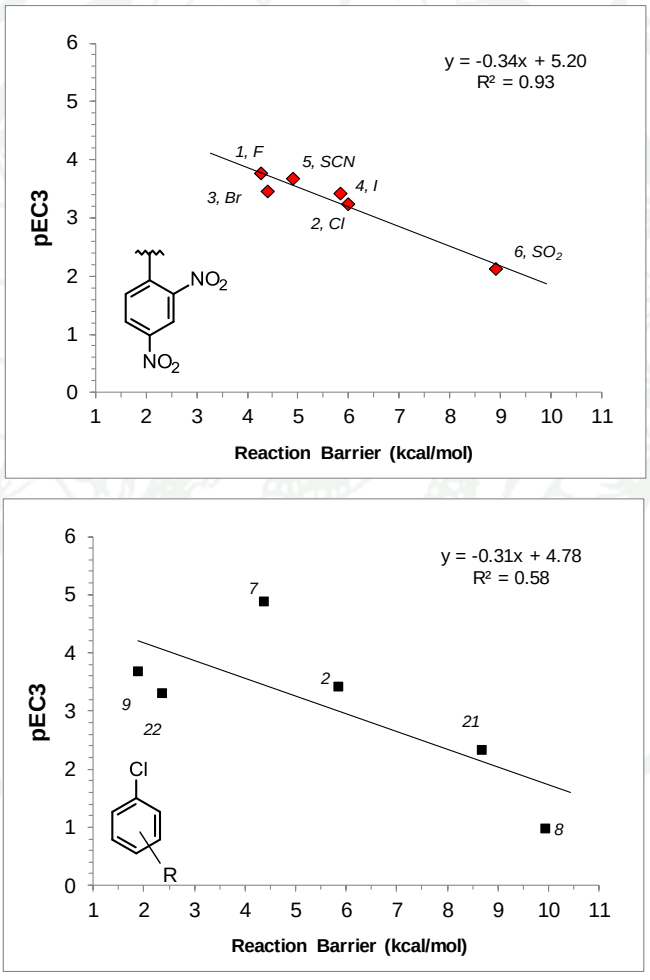

Figure 36 Plot of the pEC3 vs the predicted barrier to reaction for chemicals with a common di-nitro-phenyl core with different halogen or pseudo halogen leaving groups (above) and a more diverse set of chemicals with a common chloro leaving group (below).

In figure 36 we plot the predicted QC barrier to formation of the stable product or intermediate vs the pEC3 (or class) for all 23 chemicals investigated here. We find that the correlation of pEC3 vs the barrier for the 12 chemicals with quantitative pEC3s is reasonably strong (r^2=0.63). Barriers to reaction below ~10 kcal/mol indicate a sensitizer and the absolute value can be related directly to the strength of sensitization. Chemical 7 still appears to be an outlier as discussed above, being more potent than predicted, which may be due to its higher than average clogP. This would be consistent with reports for other domains (Roberts *et al.*, 2006b). Removing this outlier would result in an r^2=0.74. The least potent sensitizer has a predicted barrier of 9.93 kcal/mol. We find that we can use this cut-off to categorize the sensitizers from non-sensitizers with 100% accuracy (N=12), with just 1 non-sensitizer (N=11) being miss-predicted as a sensitizer (9%). For quantitative measurements, we find that there is a high correlation between the experimental pEC3 and the calculated barrier to formation of the low energy product or intermediate. The non-sensitizer miss predicted is chemical 14. Analysis of the data shows that 14 has a rather unstable, low energy product compared to the others chemicals (1, 6, 10, and 20 have lower), Interestingly, this was also an outlier in the QMM model of Roberts *et al.* (Roberts *et al.*, 2011). In their case instead of using the experimental σ of ortho Cl, they used the meta value as it gave a better fit. We however suggest that this was perhaps inappropriate as the calculated QC barriers also suggest that it is an outlier and not an issue with the substituent parameter selection process. This is possibly due to factors beyond the consideration of this rather simple QC model or the QMM model as discussed above.

The S_NAr QMM model by Roberts *et al.* (Roberts *et al.*, 2011) consisted of a QSAR equation that took into account both the electron withdrawing effect of the ring substituents and the strength of the leaving group. Their 2 descriptor model was very effective in discriminating between chemical sensitizers and non-sensitizers as can be seen in Figure 36. For the 12 chemicals with quantitative pEC3 values an r^2 with the QMM of 0.41 is observed. Using a cut-off of ~1, 100% of the sensitizers are correctly classified but 5 of the non-sensitizers would also be misclassified (i.e. 45%). This suggests the 2 descriptor QMM is somewhat inferior to the 1 descriptor QC model

developed here. Nevertheless, a notable advantage of the QMM approach is that estimations take minutes to hours, assuming substituent parameters are available. In contrast, simulations will take ~1 day per compound per computer (i.e. Intel i7) to obtain the complete reaction profile.

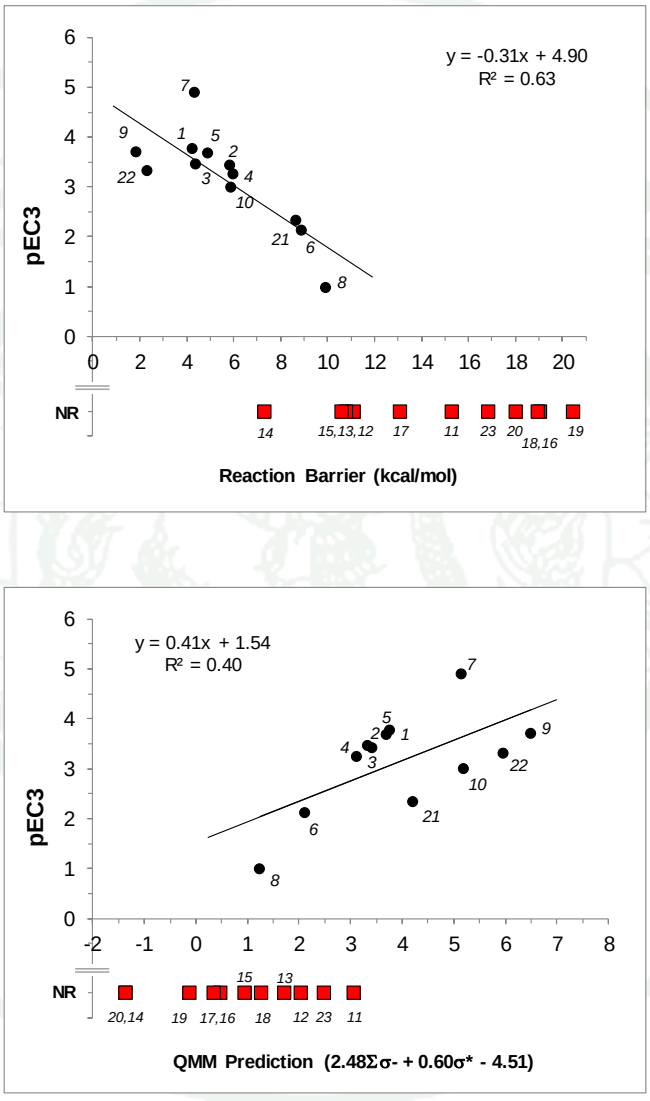

Figure 37 Plot of the pEC3 vs the predicted barrier for all chemicals investigated in this study (top). Also shown for the purpose of comparison are the QSAR model results derived from the work of Roberts *et al.*

The recent study by Enoch and Roberts (Enoch and Roberts, 2013) on the MA reaction domain most closely resembles this one and it is worth comparing and contrasting the approaches used. The authors in the former study approximated the barrier by calculating the energy of the intermediate, minus the isolated energies of the component reactants (i.e. Michael acceptor and SCH_3), which we term E_{int}. This assumes that the barrier heights are directly proportional to the intermediates, which may not work well for reactions where no stable intermediate exists. The authors found that the correlation between the approximated barrier and the pEC3 for 26 compound (4 outliers removed) was sizeable at r^2=0.43. Addition of a single additional descriptor (Solvent accessible surface area) and removal of an additional outlier led to a much better correlation (r^2=0.79). In the case of the S_NAr domain (only 6 chemicals react via an S_N2 process), using the E_{int} measure leads to a rather poor correlation with the pEC3 (r^2=0.08, N=6 chemicals 1, 2, 5, 6, 9, 10). This can be rationalized from Figure 37 where it is apparent that the barrier heights do not necessarily correlate well with either the intermediate or product energy. Also worth noting is the fact that the correlation of the HOMO-LUMO energy with pEC3 for all 12 quantitative pEC3 measurements is also weak (r^2=0.02) suggesting it is also not a good surrogate for the barrier height for the S_NAr domain.

CONCLUSIONS

1. Photophysical properties and photochemistry of substituted cinnamic acids and cinnamates, based on TD-DFT and SAC-CI investigations

The photophysical properties and photochemistry of these compounds were also studied theoretically using the direct SAC-CI method. The photoisomerization pathway in the S_1 state leading to nonradiative decay to the ground state was also examined using the CIS(D)//CIS calculations. A series of cinnamic acids (**1A**–**9A**) and cinnamates (**1E**–**9E**) with monohydroxy-, nitro- and fluoro-substituents were synthesized to explore better performance in UVB blocking. The absorption and emission spectra of these compounds were observed and the photostability examined.

The characteristics of the absorption spectra in the UVB region were reasonably reproduced in both peak position and intensity by the SAC-CI calculations, and the transition character of these 18 derivatives is analyzed in detail. The hydroxy derivatives have broad absorption bands in the UVA and UVB regions. The agreement of the SAC-CI results with the experimental values is better than the TD-DFT calculations. The shape of theoretical spectrum and the peak splitting are also different between SAC-CI and TD-DFT for some derivatives. This indicates that the accurate calculations based on wave function theory are necessary for the reliable analysis and assignments of the absorption spectrum in the present case. The emission spectra with oxygen quenching suggest that the emission or relaxation of some derivatives with an electron-withdrawing group (nitro and fluoro derivatives) occurs via a triplet state, particularly for **4E**, **8A**, and **9A**, whereas those with an electron-donating group (hydroxy derivatives) occur via a singlet excited state. However, this is not the general trend and depends on the substitution position or derivatives, for example, **6E**, **7E** and **8E**. The emission energies and oscillator strengths from the local minimum in the planar structure were also calculated for all compounds. The radiative lifetimes derived from these values varied strongly with regard to the substitution position in the phenyl ring; the *para* derivatives have relatively short lifetimes. Based on the examination of the photoabsorption after irradiation, the hydroxy derivatives show

excellent photostability compared with that of the nitro and fluoro derivatives. We also examined the S_1 and S_2 PECs of the hydroxy derivatives along the torsion angle at the phenylene double bond, which lead to the conical intersection. Derivatives substituted at the *meta* position has an energy barrier to the conical intersection in S_1 and therefore show relatively strong fluorescence, whereas those at the *para* position show weak fluorescence without an energy barrier, leading to nonradiative decay.

Among the derivatives studied in the present work, *para*-hydroxy derivative is an excellent UV absorber because of their broad absorption in the UVB/UVA regions, less emission, and photostability compared with other derivatives. This compound shows similar UVB blocking performance as *para*-methoxy derivative in the previous work (Karpkird *et al.*, 2009; Monhaphol *et al.*, 2007). Interestingly, fluoro-cinnmates show the less photostability. These results might be useful for optically addressable devices. The present work provides useful information on the performance of proper UVB blocking compounds and the possibility of photoactive molecules in the UV–Vis wavelength domain.

2. Investigation on the inclusion complexes between methoxycinnamic acid and cyclodextrin by performing quantum chemical calculations

In summary, we have performed a combined quantum chemical calculations, molecular docking, and molecular dynamics simulations study on the host-guest inclusion of methoxycinnamic acids and cyclodextrin derivatives. The calculated results reveal that CA and CDs can form inclusion complexes in both the gas phase and water. The structures and thermodynamic stabilities were studies the host-guest complexes between CDs and CA. These inclusion complexes do not contain any covalent bond between host and guest molecules and their stability depends on molecular size and shape complementation but also on the external medium and environmental conditions.

DFT and TD-DFT results show clearly that the tail orientation of CA inserted into the cavity of CD is more favorable than the head orientation. The calculated

UV−Vis spectra show clearly that the tail orientation of inclusion complex between CA and CD is most stable orientations and can absorb in both UVB and UVA regions which is similar to the parent CA.

3. Skin sensitization prediction using quantum chemical calculations: A theoretical model for the S_NAr Domain

In this chapter, we have reported the use of a QC based approach using a model SCH_3 nucleophile to predict the kinetics and thermodynamic parameters associated with the addition-elimination reaction profile for a set of 23 chemicals of the S_NAr domain. We find that calculating the full reaction profile for chemicals of the S_NAr domain is important since, as highlighted in Figure 3, the reactions can proceed by both S_N1 and S_N2 processes depending on the activating substituents and the nature of the leaving group. It is therefore not reliable to approximate the barrier with either the HOMO-LUMO energy, or indeed the energy of the high energy intermediate since in many cases it will not exist (i.e. for S_N2 based processes).

We find that the use of a single computed descriptor, namely the barrier to formation of the stable product or intermediate can help us to separate sensitizer and non-sensitizer. Barriers to reaction below 10 kcal/mol indicate a sensitizer and the absolute value can be related directly to the strength of sensitization. The use of a cut-off of ~10 kcal/mol allows us to categorize 100% (N=12) of the sensitizers from the non-sensitizers (N=11), with just one non-sensitizer being miss-predicted as a weak sensitizer (9%). For quantitative measurements, we find that there is a high correlation between the experimental pEC3 and the calculated barrier to formation of the low energy product or intermediate. We find an r^2=0.64 for all 23 chemicals, compared to r^2=0.41 for the comparable QSAR based approach reported elsewhere (Roberts *et al.*, 2011). One main outlier can be rationalized by consideration of the thermodynamics. In this case it has a low barrier but forms a rather unstable product suggesting the reaction is not necessarily under kinetic control.

Physical chemistry approaches such as QSARs (Aptula *et al.*, 2005; Aptula and Roberts, 2006; Roberts *et al.*, 2006a; b; Roberts *et al.*, 2009) based on physico-chemical parameters and substituent constants, or QC (Enoch and Roberts, 2013) calculations, have proved to be useful in helping discriminating sensitizers from non-sensitizers. We note that the precision of QC model simulations and the physical insight and understanding that can be garnered from them could prove useful for skin sensitization assessment, especially when combined in the so–called weight of evidence approach. QC methods are not 100% accurate since we are only using surrogate nucleophiles for a complex biological process, however, we postulate that the experimental identification of the most prevalent nucleophiles or indeed the precise proteins that cause skin sensitization would provide an additional means to help to improve the performance of such atomic simulations.

LITERATURE CITED

Allen, C.F.H. and F.W. Spangler. 1943. Ethyl benzalmalonate. **Org. Syn. Coll.** 3:377-380.

Anderson, S.E., P.D. Siegel and B.J. Meade. 2011. The LLNA: a brief review of recent advances and limitations. **J. Allergy Clin. Immunol.** 2011:1-10.

Aptula, A.O., G. Patlewicz and D.W. Roberts. 2005. Skin sensitization: reaction mechanistic applicability domains for structure-activity relationships. **Chem. Res. Toxicol.** 18(9):1420-1426.

_____, and D.W. Roberts. 2006. Mechanistic applicability domains for nonanimal-based prediction of toxicological end points: general principles and application to reactive toxicity. **Chem. Res. Toxicol.** 19(8):1097-1105.

Attoui Yahia, O. and D.E. Khatmi. 2009. Theoretical study of the inclusion processes of venlafaxine with β-cyclodextrin. **J. Mol. Struct. - THEOCHEM** 912(1–3):38-43.

Bader, J.S. and B.J. Berne. 1996. Solvation energies and electronic spectra in polar, polarizable media: Simulation tests of dielectric continuum theory. **J. Chem. Phys.** 104(4):1293-1308.

Becke, A.D. 1988. Density-functional exchange-energy approximation with correct asymptotic behavior. **Phys. Rev. A** 38(6):3098-3100.

Brewster, M.E. and T. Loftsson. 2007. Cyclodextrins as pharmaceutical solubilizers. **Adv. Drug Delivery Rev.** 59(7):645-666.

Buschmann, H.J. and E. Schollmeyer. 2002. Applications of cyclodextrins in cosmetic products: a review. **J. Cosmet. Sci.** 53(3):185-191.

Cammi, R., R. Fukuda, M. Ehara and H. Nakatsuji. 2010. Symmetry-adapted cluster and symmetry-adapted cluster-configuration interaction method in the polarizable continuum model: Theory of the solvent effect on the electronic excitation of molecules in solution. **J. Chem. Phys.** 133(2):024104-024124.

Case, D.A., T.A. Darden, I. T.E. Cheatham, C.L. Simmerling, J. Wang, R.E. Duke, R. Luo, R.C. Walker, W. Zhang, K.M. Merz, B. Roberts, S. Hayik, A. Roitberg, G. Seabra, J. Swails, A.W. Goetz, I. Kolossváry, K.F. Wong, F. Paesani, J. Vanicek, R.M. Wolf, J. Liu, X. Wu, S.R. Brozell, T. Steinbrecher, H. Gohlke, Q. Cai, X. Ye, J. Wang, M.-J. Hsieh, G. Cui, D.R. Roe, D.H. Mathews, M.G. Seetin, R. Salomon-Ferrer, C. Sagui, V. Babin, T. Luchko, S. Gusarov, A. Kovalenko and P.A. Kollman. 2012. **AMBER12,** University of California, San Francisco.

Centini, M., M. Maggiore, M. Casolaro, M. Andreassi, R. Maffei Facino and C. Anselmi. 2007. Cyclodextrins as cosmetic delivery systems. **J. Incl. Phenom.** 57(1-4):109-112.

Cezard, C., X. Trivelli, F. Aubry, F. Djedaini-Pilard and F.-Y. Dupradeau. 2011. Molecular dynamics studies of native and substituted cyclodextrins in different media: 1. Charge derivation and force field performances. **Phys. Chem. Chem. Phys.** 13(33):15103-15121.

Chakraborty, A., S. Kar and N. Guchhait. 2006. Photoinduced intramolecular charge transfer (ICT) reaction in *trans*-methyl *p*-(dimethylamino) cinnamate: A combined fluorescence measurement and quantum chemical calculations. **Chem. Phys.** 320(2–3):75-83.

Changenet-Barret, P., A. Espagne, S. Charier, J.-B. Baudin, L. Jullien, P. Plaza, K.J. Hellingwerf and M.M. Martin. 2004. Early molecular events in the photoactive yellow protein: role of the chromophore photophysics. **Photochem. Photobiol. Sci.** 3(8):823-829.

Chawla, H.M. and S. Mrig. 2009. Simultaneous quantitative estimation of oxybenzone and 2-ethylhexyl-4-methoxycinnamate in sunscreen formulations by second order derivative spectrophotometry. **J. Anal. Chem.** 64(6):585-592.

Chen, G. and M. Jiang. 2011. Cyclodextrin-based inclusion complexation bridging supramolecular chemistry and macromolecular self-assembly. **Chem. Soc. Rev.** 40(5):2254-2266.

Coulston, R.J., H. Onagi, S.F. Lincoln and C.J. Easton. 2006. Harnessing the energy of molecular recognition in a nanomachine having a photochemical on/off switch. **J. Am. Chem. Soc.** 128(46):14750-14751.

Davis, M.E. and M.E. Brewster. 2004. Cyclodextrin-based pharmaceutics: past, present and future. **Nat. Rev. Drug Discov.** 3(12):1023-1035.

de Groot, M., E.V. Gromov, H. Koppel and W.J. Buma. 2008. High-resolution spectroscopy of methyl 4-hydroxycinnamate and its hydrogen-bonded water complex. **J. Phys. Chem. B** 112(14):4427-4434.

De, P., M. Baltas and F. Bedos-Belval. 2011. Cinnamic acid derivatives as anticancer agents - a review. **Curr. Med. Chem.** 18(11):1672-1703.

Du, X., W. Lu, N. Ding, H. Dai, X. Teng and H. Deng. 2006. Spectral properties and supramolecular inclusion complexes of β-cyclodextrin with flexible amphiphilic and rigid compounds. **J. Photochem. Photobiol. A: Chem.** 177(1):76-82.

Dunning, T.H. and P.J. Hay. 1976. T. H. Dunning Jr. and P. J. Hay, pp. 1-28. *In* H. F. Schaefer III eds. **Modern Theoretical Chemistry**, Vol. 3, Plenum, New York.

Ehara, M., J. Hasegawa and H. Nakatsuji. 2005.**S**AC-CI method applied to molecular spectroscopy, pp. 1099-1141. *In* C. E. Dykstra, G. Frenking, K. S. Kim, and G. E. Scuseria eds. **Theory and applications of computational chemistry: the first 40 years, a volume of technical and historical perspectives**, Elsevier: Oxford, U.K.

Enoch, S.J., J.C. Madden and M.T.D. Cronin. 2008. Identification of mechanisms of toxic action for skin sensitisation using a SMARTS pattern based approach. **SAR QSAR Environ. Res.** 19(5-6):555-578.

_____, and D.W. Roberts. 2013. Predicting skin sensitization potency for michael acceptors in the LLNA using quantum mechanics calculations. **Chem. Res. Toxicol.** 26(5):767-774.

Fabian, J. 2001. Electronic excitation of sulfur-organic compounds - performance of time-dependent density functional theory. **Theor. Chem. Acc.** 106(3):199-217.

Fenyvesi, É., K. Otta, I. Kolbe, C. Novák and J. Szejtli. 2004. Cyclodextrin complexes of UV filters. **J. Incl. Phenom.** 48(3-4):117-123.

Frisch, M.J., G.W. Trucks, H.B. Schlegel, G.E. Scuseria, M.A. Robb, J.R. Cheeseman, G. Scalmani, V. Barone, B. Mennucci, G.A. Petersson, H. Nakatsuji, M. Caricato, X. Li, H.P. Hratchian, A.F. Izmaylov, J. Bloino, G. Zheng, J.L. Sonnenberg, M. Hada, M. Ehara, K. Toyota, R. Fukuda, J. Hasegawa, M. Ishida, T. Nakajima, Y. Honda, O. Kitao, H. Nakai, T. Vreven, J.A. Montgomery, J.E. Peralta, F. Ogliaro, M. Bearpark, J.J. Heyd, E. Brothers, K.N. Kudin, V.N. Staroverov, R. Kobayashi, J. Normand, K. Raghavachari, A. Rendell, J.C. Burant, S.S. Iyengar, J. Tomasi, M. Cossi, N. Rega, J.M. Millam, M. Klene, J.E. Knox, J.B. Cross, V. Bakken, C. Adamo, J. Jaramillo, R. Gomperts, R.E. Stratmann, O. Yazyev, A.J. Austin, R. Cammi, C. Pomelli, J.W. Ochterski, R.L. Martin, K. Morokuma, V.G. Zakrzewski, G.A. Voth, P. Salvador, J.J. Dannenberg, S. Dapprich, A.D. Daniels, Farkas, J.B. Foresman, J.V. Ortiz, J. Cioslowski and D.J. Fox. 2009. **Gaussian 09, Revision B.01.** Gaussian, Inc., Pittsburgh PA.

Fu, Y., L. Liu and Q.-X. Guo. 2002. A theoretical study on the inclusion complexation of cyclodextrins with inorganic cations and anions. **J. Incl. Phenom.** 43(3-4):223-229.

Fukuda, R., M. Ehara, H. Nakatsuji and R. Cammi. 2011. Nonequilibrium solvation for vertical photoemission and photoabsorption processes using the symmetry-adapted cluster-configuration interaction method in the polarizable continuum model. **J. Chem. Phys.** 134(10):104109-104111.

Fukuda, R. and H. Nakatsuji. 2008. Formulation and implementation of direct algorithm for the symmetry-adapted cluster and symmetry-adapted cluster-configuration interaction method. **J. Chem. Phys.** 128(9):094105-094114.

Furuki, T., F. Hosokawa, M. Sakurai, Y. Inoue and R. Chujo. 1993. Microscopic medium effects on a chemical reaction. A theoretical study of decarboxylation catalyzed by cyclodextrins as an enzyme model. **J. Am. Chem. Soc.** 115(7):2903-2911.

Gaspar, L.R. and P.M.B.G. Maia Campos. 2006. Evaluation of the photostability of different UV filter combinations in a sunscreen. **Int. J. Pharm.** 307(2):123-128.

Gerberick, F., M. Aleksic, D. Basketter, S. Casati, A.T. Karlberg, P. Kern, I. Kimber, J.P. Lepoittevin, A. Natsch, J.M. Ovigne, C. Rovida, H. Sakaguchi and T. Schultz. 2008. Chemical reactivity measurement and the predicitve identification of skin sensitisers. The report and recommendations of ECVAM Workshop 64. **Altern. Lab. Anim.** 36(2):215-242.

Gromov, E.V., I. Burghardt, H. Köppel and L.S. Cederbaum. 2005. Impact of sulfur vs oxygen on the low-lying excited states of *trans-p*-coumaric acid and *trans-p*-coumaric thio acid. **J. Phys. Chem. A** 109(20):4623-4631.

Hammond, G.S. 1955. A correlation of reaction rates. **J. Am. Chem. Soc.** 77(2):334-338.

Hansch, C. and T. Fujita. 1964. p-σ-π analysis. A method for the correlation of biological activity and chemical structure. **J. Am. Chem. Soc.** 86(8):1616-1626.

Hehre, W.J., R. Ditchfield and J.A. Pople. 1972. Self-consistent molecular orbital methods. XII. Further extensions of gaussian-type basis sets for use in molecular orbital studies of organic molecules. **J. Chem. Phys.** 56(5):2257-2261.

Hellingwerf, K.J., J. Hendriks and T. Gensch. 2003. Photoactive yellow protein, a new type of photoreceptor protein: Will this “yellow lab” bring us where we want to go? **J. Phys. Chem. A** 107(8):1082-1094.

Huong, S.P., V. Andrieu, J.-P. Reynier, E. Rocher and J.-D. Fourneron. 2007. The photoisomerization of the sunscreen ethylhexyl *p*-methoxy cinnamate and its influence on the sun protection factor. **J. Photochem. Photobiol. A: Chem.** 186(1):65-70.

Ishigami, T., K. Nakazato, M. Uehara and T. Endo. 1979. Marked dependence of multiplicity in direct *Z,E* photoisomerization of a series of methyl cinnamtes on their *para*-substituents. **Tetrahedron Lett.** 20(10):863-866.

Jacquemin, D., V.r. Wathelet, E.A. Perpète and C. Adamo. 2009. Extensive TD-DFT benchmark: Singlet-excited states of organic molecules. **J. Chem. Theory Comput.** 5(9):2420-2435.

Jorgensen, W.L., J. Chandrasekhar, J.D. Madura, R.W. Impey and M.L. Klein. 1983. Comparison of simple potential functions for simulating liquid water. **J. Chem. Phys.** 79(2):926-935.

Kalgutkar, A.S. and J.R. Soglia. 2005. Minimising the potential for metabolic activation in drug discovery. **Expert Opin. Drug Metab. Toxicol.** 1(1):91-142.

Karpkird, T. and S. Wanichweacharungruang. 2010. Synthesis and photostability of methoxycinnamic acid modified cyclodextrins. **J. Photochem. Photobiol. A: Chem.** 212(1):56-61.

_____, S. Wanichweacharungruang and B. Albinsson. 2009. Photophysical characterization of cinnamates. **Photochem. Photobiol. Sci.** 8(10):1455-1460.

Kern, P.S., G.F. Gerberick, C.A. Ryan, I. Kimber, A. Aptula and D.A. Basketter. 2010. Local lymph node data for the evaluation of skin sensitization alternatives: a second compilation. **Dermatitis : contact, atopic, occupational, drug** 21(1):8-32.

Kimber, I., D.A. Basketter, G.F. Gerberick and R.J. Dearman. 2002. Allergic contact dermatitis. **Int. Immunopharmacol.** 2(2-3):201-211.

_____. and C. Weisenberger. 1989. A murine local lymph node assay for the identification of contact allergens. Assay development and results of an initial validation study. **Arch. Toxicol.** 63(4):274-282.

Kirschner, K.N., A.B. Yongye, S.M. Tschampel, J. González-Outeiriño, C.R. Daniels, B.L. Foley and R.J. Woods. 2008. GLYCAM06: a generalizable biomolecular force field. Carbohydrates. **J. Comput. Chem.** 29(4):622-655.

Klinubol, P., P. Asawanonda and S.P. Wanichwecharungruang. 2008. Transdermal penetration of UV filters. **Skin Pharmacol. Physiol.** 21(1):23-29.

Koo, J., M.S. Fish, G.N. Walker and J. Blake. 1944. 2,3-dimethoxycinnamic acid. **Org. Syn. Coll.** 4:327-328.

Lawtrakul, L., H. Viernstein and P. Wolschann. 2003. Molecular dynamics simulations of β-cyclodextrin in aqueous solution. **Int. J. Pharm.** 256(1–2):33-41.

Lee, C., W. Yang and R.G. Parr. 1988. Development of the Colle-Salvetti correlation-energy formula into a functional of the electron density. **Phys. Rev. B** 37(2):785-789.

Lendlein, A., H. Jiang, O. Junger and R. Langer. 2005. Light-induced shape-memory polymers. **Nature** 434:879-882.

Lengauer, T. and M. Rarey. 1996. Computational methods for biomolecular docking. **Curr. Opin. Struct. Biol.** 6(3):402-406.

Lewis, F.D., S.L. Quillen, J.E. Elbert, S. Schneider and P. Geiselhart. 1989. The singlet states of methyl cinnamate and methyl indenoate. **J. Photochem. Photobiol. A: Chem.** 47(2):173-179.

Li, Y., Y.J. Tseng, D. Pan, J. Liu, P.S. Kern, G.F. Gerberick and A.J. Hopfinger. 2006. 4D-fingerprint categorical QSAR models for skin sensitization based on the classification of local lymph node assay measures. **Chem. Res. Toxicol.** 20(1):114-128.

Li, Z.-H., Q. Wang, X. Ruan, C.-D. Pan and D.-A. Jiang. 2010. Phenolics and plant allelopathy. **Molecules** 15(12):8933-8952.

Litani-Barzilai, I., V. Bulatov, V.V. Gridin and I. Schechter. 2004. Detector based on time-resolved ion-induced voltage in laser multiphoton ionization and laser-induced fluorescence. **Anal. Chim. Acta** 501(2):151-156.

Liu, L. and Q.-X. Guo. 2002. The driving forces in the inclusion complexation of cyclodextrins. **J. Incl. Phenom.** 42(1-2):1-14.

_____. and _____. 2004. Use of quantum chemical methods to study cyclodextrin chemistry. **J. Incl. Phenom.** 50(1-2):95-103.

Luadthong, C., A. Tachaprutinun and S.P. Wanichwecharungruang. 2008. Synthesis and characterization of micro/nanoparticles of poly(vinylalcohol-co-vinylcinnamate) derivatives. **Eur. Polym. J.** 44(5):1285-1295.

Madi, F., D. Khatmi, N. Dhaoui, A. Bouzitouna, M. Abdaoui and A. Boucekkine. 2009. Molecular model of CENS piperidine β-CD inclusion complex: DFT study. **Compt. Rend. Chim.** 12(12):1305-1312.

Marques, M.A.L. and E.K.U. Gross. 2004. Time-dependent density functional theory. **Annu. Rev. Phys. Chem.** 55(1):427-455.

Meeto, W., S. Suramitr, V. Lukeš, P. Wolschann and S. Hannongbua. 2010. Effects of the CN and NH_2 substitutions on the geometrical and optical properties of model vinylfluorenes, based on DFT calculations. **J. Mol. Struct. - THEOCHEM** 939(1–3):75-81.

_____, _____, S. Vannarat and S. Hannongbua. 2008. Structural and electronic properties of poly(fluorene-vinylene) copolymer and its derivatives: time-dependent density functional theory investigation. **Chem. Phys.** 349(1–3):1-8.

Miller, M.D., D.M. Yourtee, A.G. Glaros, C.C. Chappelow, J.D. Eick and A.J. Holder. 2005. Quantum mechanical structure-activity relationship analyses for skin sensitization. **J. Chem. Inf. Model.** 45(4):924-929.

Monhaphol, T., B. Albinsson and S.P. Wanichwecharungruang. 2007. 2-Ethylhexyl-2,4,5-trimethoxycinnamate and di-(2-ethylhexyl)-2,4,5-trimethoxybenzal malonate as novel UVA filters. **J. Pharm. Pharmacol.** 59(2):279-288.

Nakatsuji, H. 1979. Cluster expansion of the wavefunction. Calculation of electron correlations in ground and excited states by SAC and SAC-CI theories. **Chem. Phys. Lett.** 67(2–3):334-342.

_____. 1983. Cluster expansion of the wavefunction, valence and rydberg excitations, ionizations, and inner-valence ionizations of CO_2 and N_2O studied by the SAC and SAC-CI theories. **Chem. Phys.** 75(3):425-441.

_____. 1978. Cluster expansion of the wavefunction. Excited states. **Chem. Phys. Lett.** 59(2):362-364.

Namuangruk, S., R. Fukuda, M. Ehara, J. Meeprasert, T. Khanasa, S. Morada, T. Kaewin, S. Jungsuttiwong, T. Sudyoadsuk and V. Promarak. 2012. D–D−π–A-type organic dyes for dye-sensitized solar cells with a potential for direct electron injection and a high extinction coefficient: synthesis, characterization, and theoretical investigation. **J. Phys. Chem. C** 116(49):25653-25663.

Nascimento, C., Jr., C.A. Anconi, J. Lopes, H.D. Santos and W. Almeida. 2007. An efficient methodology to study cyclodextrin clusters: application to α-CD hydrated monomer, dimer, trimer and tetramer. **J. Incl. Phenom.** 59(3-4):265-277.

Numanoglu, U., T. Sen, N. Tarimci, M. Kartal, O.M. Koo and H. Onyuksel. 2007. Use of cyclodextrins as a cosmetic delivery system for fragrance materials: linalool and benzyl acetate. **AAPS Pharm. Sci. Tech.** 8(4):34-42.

Park, B.K., A. Boobis, S. Clarke, C.E. Goldring, D. Jones, J.G. Kenna, C. Lambert, H.G. Laverty, D.J. Naisbitt, S. Nelson, D.A. Nicoll-Griffith, R.S. Obach, P. Routledge, D.A. Smith, D.J. Tweedie, N. Vermeulen, D.P. Williams, I.D. Wilson and T.A. Baillie. 2011. Managing the challenge of chemically reactive metabolites in drug development. **Nat. Rev. Drug Discov.** 10(4):292-306.

Patlewicz, G., M.W. Chen and C.A. Bellin. 2011. Non-testing approaches under REACH – help or hindrance? Perspectives from a practitioner within industry. **SAR QSAR Environ. Res.** 22(1-2):67-88.

Pattanaargson, S., N. Hongchinnagorn, P. Hirunsupachot and Y. Sritana-anant. 2004a. UV absorption and photoisomerixation of *p*-methoxycinnamate grafted silicone. **Photochem. Photobiol.** 80(2):322-325.

_____. and P. Limphong. 2001. Stability of octyl methoxycinnamate and identification of its photo-degradation product. **Int. J. Cosmet. Sci.** 23(3):153-160.

Pattanaargson, S., T. Munhapol, P. Hirunsupachot and P. Luangthongaram. 2004b. Photoisomerization of octyl methoxycinnamate. **J. Photochem. Photobiol. A: Chem.** 161(2–3):269-274.

Peach, M.J.G., P. Benfield, T. Helgaker and D.J. Tozer. 2008. Excitation energies in density functional theory: An evaluation and a diagnostic test. **J. Chem. Phys.** 128(4):044118-044118.

Petersilka, M., U.J. Gossmann and E.K.U. Gross. 1996. Excitation energies from time-dependent density-functional theory. **Phys. Rev. Lett.** 76(8):1212-1215.

Poolmee, P., M. Ehara, S. Hannongbua and H. Nakatsuji. 2005. SAC-CI theoretical investigation on electronic structure of fluorene-thiophene oligomers. **Polymer** 46(17):6474-6481.

_____, _____, and H. Nakatsuji. 2011. Photophysical properties and vibrational structure of ladder-type penta *p*-phenylene and carbazole derivatives based on SAC-CI calculations. **Theor. Chem. Acc.** 130(2-3):161-173.

Promkatkaew, M., S. Suramitr, T.M. Karpkird, S. Namuangruk, M. Ehara and S. Hannongbua. 2009. Absorption and emission spectra of ultraviolet B blocking methoxy substituted cinnamates investigated using the symmetry-adapted cluster configuration interaction method. **J. Chem. Phys.** 131(22):224306-224310.

Rehab, A. and N. Salahuddin. 1999. Photocrosslinked polymers based on pendant extended chalcone as photoreactive moieties. **Polymer** 40(9):2197-2207.

Roberts, D.W., A.O. Aptula and G. Patlewicz. 2006a. Electrophilic chemistry related to skin sensitization. Reaction mechanistic applicability domain classification for a published data set of 106 chemicals tested in the mouse local lymph node assay. **Chem. Res. Toxicol.** 20(1):44-60.

Roberts, D.W., A.O. Aptula and G. Patlewicz. 2006b. Mechanistic applicability domains for non-animal based prediction of toxicological endpoints. QSAR analysis of the schiff base applicability domain for skin sensitization. **Chem. Res. Toxicol.** 19(9):1228-1233.

_____, _____, and _____. 2011. Chemistry-based risk assessment for skin sensitization: quantitative mechanistic modeling for the S_NAr domain. **Chem. Res. Toxicol.** 24(7):1003-1011.

_____, R. Fraginals, J.P. Lepoittevin and C. Benezra. 1991. Refinement of the relative alkylation index (RAI) model for skin sensitization and application to mouse and guinea-pig test data for alkyl alkanesulphonates. **Arch. Dermatol. Res.** 283(6):387-394.

_____, G. Patlewicz, P.S. Kern, F. Gerberick, I. Kimber, R.J. Dearman, C.A. Ryan, D.A. Basketter and A.O. Aptula. 2007. Mechanistic applicability domain classification of a local lymph node assay dataset for skin sensitization. **Chem. Res. Toxicol.** 20(7):1019-1030.

_____, T.W. Schultz, E.M. Wolf and A.O. Aptula. 2009. Experimental reactivity parameters for toxicity modeling: application to the acute aquatic toxicity of S_N2 electrophiles to tetrahymena pyriformis. **Chem. Res. Toxicol.** 23(1):228-234.

Rodil, R., M. Moeder, R. Altenburger and M. Schmitt-Jansen. 2009. Photostability and phytotoxicity of selected sunscreen agents and their degradation mixtures in water. **Anal. Bioanal. Chem.** 395(5):1513-1524.

Runge, E. and E.K.U. Gross. 1984. Density-functional theory for time-dependent systems. **Phys. Rev. Lett.** 52(12):997-1000.

Saha, B., M. Ehara and H. Nakatsuji. 2007. Investigation of the electronic spectra and excited-state geometries of poly(*para*-phenylene vinylene) (PPV) and poly(*para*-phenylene) (PP) by the symmetry-adapted cluster configuration interaction (SAC-CI) method. **J. Phys. Chem. A** 111(25):5473-5481.

Sarveiya, V., J. Templeton and H.E. Benson. 2004. Inclusion complexation of the sunscreen 2-hydroxy-4-methoxy benzophenone (oxybenzone) with hydroxypropyl-β-cyclodextrin: effect on membrane diffusion. **J. Incl. Phenom.** 49(3-4):275-281.

Sasiwilaskorn, S., P. Klinubol, A. Tachaprutinun, T. Udomsup and S.P. Wanichwecharungruang. 2008. Oligoesters based on poly(p-alkoxycinnamate) and poly(pentaethylene glycol cinnamate) as potential UV filters. **J. Appl. Polym. Sci.** 109(6):3502-3510.

Scalia, S., A. Casolari, A. Iaconinoto and S. Simeoni. 2002. Comparative studies of the influence of cyclodextrins on the stability of the sunscreen agent, 2-ethylhexyl-*p*-methoxycinnamate. **J. Pharm. Biomed. Anal.** 30(4):1181-1189.

Scalia, S., A. Molinari, A. Casolari and A. Maldotti. 2004. Complexation of the sunscreen agent, phenylbenzimidazole sulphonic acid with cyclodextrins: effect on stability and photo-induced free radical formation. **Eur. J. Pharm. Sci.** 22(4):241-249.

Scalmani, G., M.J. Frisch, B. Mennucci, J. Tomasi, R. Cammi and V. Barone. 2006. Geometries and properties of excited states in the gas phase and in solution: Theory and application of a time-dependent density functional theory polarizable continuum model. **J. Chem. Phys.** 124(9):094107-094115.

Schaafsma, G., E.D. Kroese, E.L.J.P. Tielemans, J.J.M. Van de Sandt and C.J. Van Leeuwen. 2009. REACH, non-testing approaches and the urgent need for a change in mind set. **Regul. Toxicol. Pharma.** 53(1):70-80.

Serpone, N., D. Dondi and A. Albini. 2007. Inorganic and organic UV filters: their role and efficacy in sunscreens and suncare products. **Inorg. Chim. Acta** 360(3):794-802.

Shimada, D., R. Kusaka, Y. Inokuchi, M. Ehara and T. Ebata. 2012. Nonradiative decay dynamics of methyl-4-hydroxycinnamate and its hydrated complex revealed by picosecond pump-probe spectroscopy. **Phys. Chem. Chem. Phys.** 14(25):8999-9005.

Singh, T.S., S. Mitra, A.K. Chandra, N. Tamai and S. Kar. 2008. A combined experimental and theoretical study on photoinduced intramolecular charge transfer in *trans*-ethyl *p*-(dimethylamino) cinamate. **J. Photochem. Photobiol. A: Chem.** 197(2–3):295-305.

Smith, G.J. and I.J. Miller. 1998. The effect of molecular environment on the photochemistry of *p*-methoxycinnamic acid and its esters. **J. Photochem. Photobiol. A: Chem.** 118(2):93-97.

Snor, W., E. Liedl, P. Weiss-Greiler, H. Viernstein and P. Wolschann. 2009. Density functional calculations on meloxicam-β-cyclodextrin inclusion complexes. **Int. J. Pharm.** 381(2):146-152.

Sprenger, W.W., W.D. Hoff, J.P. Armitage and K.J. Hellingwerf. 1993. The eubacterium Ectothiorhodospira halophila is negatively phototactic, with a wavelength dependence that fits the absorption spectrum of the photoactive yellow protein. **J. Bacteriol.** 175(10):3096-3104.

Stepan, A.F., D.P. Walker, J. Bauman, D.A. Price, T.A. Baillie, A.S. Kalgutkar and M.D. Aleo. 2011. Structural alert/reactive metabolite concept as applied in medicinal chemistry to mitigate the risk of idiosyncratic drug toxicity: a perspective based on the critical examination of trends in the top 200 drugs marketed in the United States. **Chem. Res. Toxicol.** 24(9):1345-1410.

Stumpf, W.E. 2006. The dose makes the medicine. **Drug Discov. Today** 11(11–12):550-555.

Suramitr, S., S. Phalinyot, P. Wolschann, R. Fukuda, M. Ehara and S. Hannongbua. 2011. Photophysical properties and photochemistry of *EE*-, *EZ*-, and *ZZ*-1,4-dimethoxy-2,5-bis[2-(thien-2-yl)ethenyl] benzene in solution: theory and experiment. **J. Phys. Chem. A** 116(3):924-937.

Szejtli, J. 1996. Inclusion of guest molecules, selectivity and molecular recognition by cyclodextrins, pp. 189-203. *In* J. Szejtli and T. Osa, eds. **Cyclodextrin; Comprehensive Supramolecular Chemistry,** Vol. 3, Elsevier Science, Amsterdam.

_____. 1998. Introduction and general overview of cyclodextrin chemistry. **Chem. Rev.** 98(5):1743-1754.

Tomasi, J., B. Mennucci and R. Cammi. 2005. Quantum mechanical continuum solvation models. **Chem. Rev.** 105(8):2999-3094.

Valero, R., J.R.B. Gomes, D.G. Truhlar and F. Illas. 2008. Good performance of the M06 family of hybrid meta generalized gradient approximation density functionals on a difficult case: CO adsorption on MgO(001). **J. Chem. Phys.** 129(12):124710-124717.

Valle, D. and E.M. Martin. 2004. Cyclodextrins and their uses: a review. **Process Biochem.** 39(9):1033-1046.

Womack, E.B. and J. McWhirter. 1955. Phenyl cinnamate. **Org. Syn. Coll.** 3:714-715.

Yanai, T., D.P. Tew and N.C. Handy. 2004. A new hybrid exchange-correlation functional using the coulomb-attenuating method (CAM-B3LYP). **Chem. Phys. Lett.** 393(1–3):51-57.

Zaleśny, R., K. Matczyszyn, A. Kaczmarek, W. Bartkowiak and P. Cysewski. 2007. Experimental and theoretical investigations of spectroscopic properties of azobenzene derivatives in solution. **J. Mol. Model.** 13(6-7):785-791.

Zhang, Y.-D., R.D. Hreha, G.E. Jabbour, B. Kippelen, N. Peyghambarian and S.R. Marder. 2002. Photo-crosslinkable polymers as hole-transport materials for organic light-emitting diodes. **J. Mater. Chem.** 12(6):1703-1708.

Zhao, Y. and D.G. Truhlar. 2011. Applications and validations of the Minnesota density functionals. **Chem. Phys. Lett.** 502(1-3):1-13.

Zuniga, C.A., S. Barlow and S.R. Marder. 2010. Approaches to solution-processed multilayer organic light-emitting diodes based on cross-linking. **Chem. Mater.** 23(3):658-681.

APPENDIX

1. Oral Presentation

Malinee Promkatkaew, Songwut Suramitr, Thitinun Karpkird, and Supa Hannongbua. Absorption and Emission properties of the F, OH and NO_2 Substituted Cinnamates: A TD-DFT Investigation. The Seventh Congress of the International Society for Theoretical Chemical Physics (ISTCP-VII), Waseda University, Tokyo, Japan. 2–8 September 2011

ISTCP-VII WASEDA, 2011

7th Congress of the International Society for Theoretical Chemical Physics

Book of Abstracts and Program

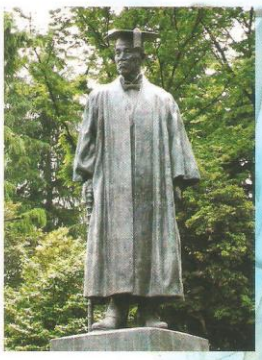

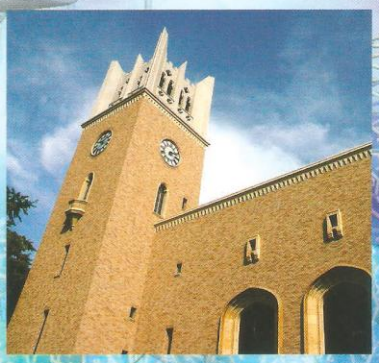

Waseda University
Tokyo, Japan
September 2-8, 2011

Chairs

Honorary Chair
János Ladik

Congress Chairs
Hiromi Nakai (Chair)
Erkki J. Brändas (Co-chair)

Coordinating Chair
Jean Maruani

7B1-6C

Absorption and Emission properties of the F, OH and NO_2 Substituted Cinnamates: A TD-DFT Investigation

Malinee Promkatkaew,[1,2] Songwut Suramitr,[1,2] Thitinun Karpkird,[1,3] Supa Hannongbua[1,2*]

[1]*Department of Chemistry, Faculty of Science, Kasetsart University, Thailand*

[2]*Center of Nanotechnology, Kasetsart University, Thailand*

[3]*Functional Compounds Special Research Unit (FCSRU), Kasetsart University, Thailand,*

The absorption and emission properties of F, OH and NO_2 substituted at *ortho*-, *meta*-, and *para*-positions of cinnamate derivatives were investigated by using the density functional theory (DFT) and time-dependent DFT (TD-DFT) calculations. The ground (S_0) and excited (S_1) state geometries were obtained at the B3LYP/6-31G(d) and TD-B3LYP/6-31G(d) methods, respectively. Based upon the optimized structures of the S_0 and S_1 states, the TD-B3LYP/6-311G(d,p) calculations were performed to compute the absorption and emission energies of the various substituted cinnamates. The results shown that all compounds had the local minimum at the planar structure conformation except for the NO_2 substituted at *ortho*-position. In the S_1 geometry, the bond length alternation (BLA) values of F and OH compounds decreases correspond to a fully delocalized electronic system, whereas, those of NO_2 increases indicate high delocalization degree of π-bond along the molecules. The calculated absorption and emission spectra in gas phase and methanol were agreed well with the experimental spectrum. The main electronic transition of cinnamates at *ortho*- and *meta*-positions of F and OH substitution correspond to the electronic excitation from HOMO-1 to LUMO. Whereas, those of NO_2 substitution correspond to the electronic excitation form HOMO to LUMO+1. In addition, the main electronic transition of cinnamates at *para*-positions of F, OH and NO_2 substitution correspond to the electronic excitation from HOMO to LUMO. Moreover, the predicted radiative lifetimes of cinnamate derivatives which discuss the origin of the stoke shift were also investigated. Our TD-DFT investigation can provide a useful insight into the optical and electronic properties of these molecules and a useful tool for designing and developing the novel UV absorbers.

Keywords: Cinnamate, Density functional theory (DFT), Time-dependent DFT (TD-DFT)

[1] Karpkird, T.M., S. Wanichweacharungruang and B. Albinsson. *Photochem. Photobiol. Sci.* **2009**, *8(10)*, 1455.

[2] Promkatkaew M., S. Suramitr, T.M. Karpkird, S. Namuangruk, M. Ehara, and S. Hannongbua. *J. Chem. Phys.* **2009**, *131*, 224309-1.

[3] Suramitr S., W. Meeto, P. Wolschann and S. Hannongbua. *Theor. Chem. Acc.* **2010**, *125*, 35.

Malinee Promkatkaew, Supa Hannongbua and Matthew Paul Gleeson. Skin Sensitization Prediction Based on Quantum Chemical Calculations: A Non-animal Model for the S_NAr Domain Chemicals. International Symposium of Homogeneous Chemical Reactivity, Mito Campus, Ibaraki University, Japan. 14–15 June, 2013

International Symposium of

Homogeneous Chemical Reactivity

(June 14th-15th, 2013)

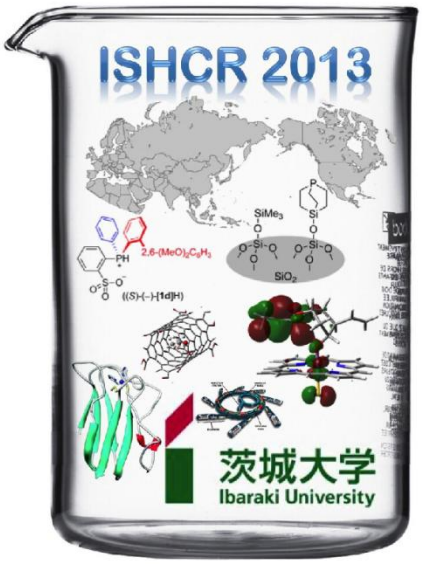

Mito Campus, Ibaraki University, Japan

Skin Sensitization Prediction Based on Quantum Chemical Calculations: A Non-animal Model for the S_NAr Domain Chemicals

Malinee Promkatkaew, Supa Hannongbua and Matthew Paul Gleeson*
Department of Chemistry, Faculty of Science, and Center of Nanotechnology, Kasetsart University, Bangkok 10900, Thailand
Corresponding author details: paul.gleeson@ku.ac.th

Skin sensitization is an important toxicological end point under REACH legislation. The possibility that chemicals used in the workplace or in consumer products might cause skin sensitization is now considered unacceptable. The mouse local lymph node assay (LLNA) was developed in the 1990s is an *in vivo* test used for skin sensitization hazard identification and characterization. In order to reduce both the cost and numbers of animals test, an approach based on physical organic chemistry has been widely investigated. Chemicals are classified into reaction mechanistic domains (i.e. Michael acceptors, S_NAr electrophiles, S_N2 electrophiles, Shiff base formers and Acylating agents), and quantitative models or read-across methods are derived for each.

This work is concerned with the nucleophilic aromatic substitution (S_NAr) reaction domain. Electronphiles able to react by an S_NAr mechanism have been recognized as some of the most potent skin sensitizers and have been used extensively in research studies on the biology of skin sensitization. A set of 23 halo- and pseudohalobenzenes, 13 of which are reported skin sensitizers and 10 of which are reported nonsensitizers, has been investigated by quantum chemical calculations using the M062x/6-31+G(d,p) method. A model cysteine based nucleoephile has been simulated using $-SCH_3$. The reaction coordinate associated with the mucleophilic attack by $–SCH_3$ on the 23 chemicals were evaluated. The barriers and enthalphies were subsequently used to successfully discriminate the sensitizers/reactive molecules from nonsensitizers/unreactive molecule of 23 S_NAr compounds.

References

[1] D. W. Roberts, A. O. Aptula, and G. Patlewicz, Electrophilic Chemistry Related to Skin Sensitization. Reaction Mechanistic Applicability Domain Classification for a Published Data Set of 106 Chemicals Tested in the Mouse Local Lymph Node Assay, *Chem. Res. Toxicol.* **2007**, *20,* 44-60.

[2] O. Mekenyan, D. W. Roberts, and W. Karcher, Molecular Orbital Parameters as Predictors of Skin Sensitization Potential of Halo- and Pseudohalobenzenes Acting as S_NAr Electrophiles *Chem. Res. Toxicol.* **1997**, *10*, 994-1000.

[3] D. W. Roberts, A. O. Aptula, and G. Y. Patlewicz, Chemistry-Based Risk Assessment for Skin Sensitization: Quantitative Mechanistic Modeling for the S_NAr Domain, *Chem. Res. Toxicol.* **2011**, *24*, 1003-1011.

2. Poster Presentation

Malinee Promkatkaew, Songwut Suramitr, Thitinun Karpkird, Maahiro Ehara and Supa Hannongbua. Structural, Electronic, and UV Absorption Properties of Various Substituted Cinnamic Acids and Cinnamates, Based on TD-DFT and SAC-CI Investigations. The 15th Asian Chemical Congress (15ACC). Resort World Sentosa, Singapore. 19–23 August 2013

Structural, Electronic, and UV Absorption Properties of Various Substituted Cinnamic Acids and Cinnamates, Based on TD-DFT and SAC-CI Investigations

Malinee Promkatkaew[1,2], Songwut Suramitr[1,2], Thitinun Karpkird[1], Masahiro Ehara[3], and Supa Hannongbua[1,2*]

[1]Department of Chemistry, Faculty of Science, Kasetsart University, Bangkok 10900, Thailand
[2]Center of Nanotechnology, Kasetsart University, Bangkok 10900, Thailand
[3]Institute for Molecular Science and Research Center for Computational Science, 38 Nishigo-naka, Myodaiji, Okazaki 444-8585, Japan
Co-responding author: *ehara@ims.ac.jp (ME) and *fscisph@ku.ac.th (SP) Tel. +66-2-5625555 ext. 2111

Introduction

Cinnamic acid and cinnamate derivatives have been widely used in sunscreen products due to their ability to absorb in the UVA (320-400 nm) and UVB (280-320 nm) ranges. To improve the UV blocking function and photostability, chemical modification is necessary. In this work, structural, electronic, and UV absorption properties of various substituted cinnamic acids and cinnamates have been investigated by using the time-dependent density functional theory (TD-DFT) and symmetry-adapted cluster-configuration interaction (SAC-CI) methods. To investigate *cis–trans* photoisomerization, the potential energy curves of the ground (S_0) and excited (S_1) states of the hydroxy derivatives were examined.

Methodology

Structural and electronic properties of the **hydroxy-**, **nitro-**, and **fluoro**-group substituted at ***ortho***-, ***meta***-, and ***para***-positions of **cinnamic acids (1A-9A)** and **cinnamates (1E-9E)** have been investigated theoretically. For cinnamate derivatives, ethylhexyl side chain was replaced with the methoxy group to reduce the computation time. **Ground-state (S_0) geometries** were fully optimized using the **B3LYP/6-31G(d)** method. To simulate the absorption spectra, the vertical excitation energies were calculated using the **TD-DFT** with **B3LYP/6-311G(d,p)** and **CAM-B3LYP/6-311G(d,p)** and **SAC-CI** with **SAC-CI/D95(d)**. Solvent effects were evaluated using the PCM in methanol solution.

Results and Discussions

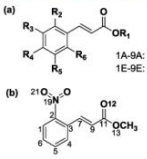

Compound	R_2	R_3	R_4	R_5	R_6
1	OH	H	H	H	H
2	H	OH	H	H	H
3	H	H	OH	H	H
4	NO_2	H	H	H	H
5	H	NO_2	H	H	H
6	H	H	NO_2	H	H
7	F	H	H	H	H
8	H	F	H	H	H
9	H	H	F	H	H

Figure 1 Molecular structures of (a) substituted **cinnamic acids (1A-9A)** and **methyl cinnamates (1E-9E)** and (b) the calculated model compounds and atom numbering of ***ortho***-**nitro methyl cinnamate (4E).**

Table 1 Absorption wavelengths (nm) in gas phase and in methanol solution for **cinnamic acids (1A-9A)** using **TD-B3LYP**, **TD-CAM-B3LYP**, **SAC-CI** compared with the experimental values.

	Gas phase						In methanol						*Exp.*
	B3LYP		CAM-B3LYP		SAC-CI		B3LYP		CAM-B3LYP		SAC-CI		MeOH
	λ_{abs}	|Error|	λ_{abs}	|Error|	λ_{abs}	|Error|	λ_{abs}	|Error|	λ_{abs}	|Error|	λ_{abs}	|Error|	
1A	313	11	288	36	320	4	332	8	302	22	336	12	324
	273	5	254	24	275	3	285	7	261	17	284	6	278
2A	317	0	280	37	309	8	331	14	289	28	320	3	317
	273	10	258	25	274	9	283	0	265	18	282	1	283
3A	295	5	277	23	298	2	312	12	290	10	313	13	300
4A	260	13	295	22	267	6	270	3	314	41	279	6	273
5A	260	14	280	6	270	4	276	2	293	19	277	3	274
6A	313	31	283	1	286	4	337	55	300	18	303	21	282
7A	288	23	270	5	274	9	296	31	277	12	279	14	265
8A	272	6	265	1	272	6	278	12	272	6	279	13	266
9A	282	13	267	2	271	2	291	22	275	6	279	10	269

Table 2 Absorption wavelengths (nm) in gas phase and in methanol solution for **methyl cinnamates (1E-9E)** using **TD-B3LYP**, **TD-CAM-B3LYP**, **SAC-CI** compared with the experimental values.

	Gas phase						In methanol						*Exp.*
	B3LYP		CAM-B3LYP		SAC-CI		B3LYP		CAM-B3LYP		SAC-CI		MeOH
	λ_{abs}	|Error|	λ_{abs}	|Error|	λ_{abs}	|Error|	λ_{abs}	|Error|	λ_{abs}	|Error|	λ_{abs}	|Error|	
1E	312	20	288	44	323	9	332	0	302	30	341	9	332
	273	7	253	27	275	5	285	5	261	19	285	5	280
2E	313	12	278	47	310	15	331	6	289	36	323	2	325
	273	12	258	27	273	12	284	1	265	20	281	4	285
3E	295	19	277	37	299	15	313	1	291	23	315	1	314
4E	261	20	296	15	268	13	271	10	315	34	279	2	281
5E	261	21	281	1	269	13	277	5	294	12	277	5	282
6E	315	11	285	19	282	22	339	35	301	3	298	6	304
7E	287	1	269	19	272	16	296	8	277	11	279	9	288
8E	271	13	265	19	269	15	279	5	273	11	278	6	284
9E	282	3	266	13	269	10	292	13	275	4	278	1	279

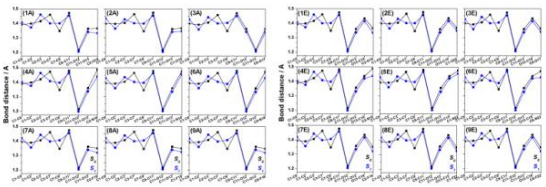

Figure 2 Bond lengths of substituted **cinnamaic acids (1A-9A)** and **methyl cinnamates (1E-9E)** in **ground (S_0) and excited (S_1) states** calculated using the **B3LYP/6-31G(d)** and **CIS/D95(d)** methods, respectively.

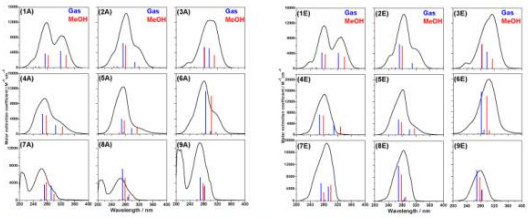

Figure 3 Absorption spectra of **cinnamaic acids (1A-9A)** and **methyl cinnamates (1E-9E)** calculated using the **SAC-CI/D95(d)** method in the **gas phase (blue)** and in **methanol (red)** compared with the experimental spectra.

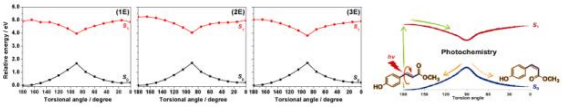

Figure 4 Potential energy curves (PECs) of the **ground (S_0) and excited (S_1) states** for the **hydroxycinnamates (1E-3E)** calculated using the **MP2/6-31G(d)** and **CIS/6-31G(d)//CIS(D)/6-31G(d)** methods, respectively.

Conclusions

Characteristics of the absorption spectra in the UVB region were reasonably reproduced in both peak position and intensity by the SAC-CI calculations, and the transition character of these 18 derivatives is analyzed in detail. Hydroxy derivatives have broad absorption bands in the UVA and UVB regions. The agreement of the SAC-CI results with the experimental values is better than the previous TD-DFT calculations. The shape of theoretical spectrum and the peak splitting are also different between SAC-CI and TD-DFT for some derivatives. This indicates that the accurate calculations based on wave function theory are necessary for the reliable analysis and assignments of the absorption spectrum in the present case. Potential energy curves of the S_0 and S_1 states of hydroxy derivatives were examined. *Ortho* and *meta* derivatives have an energy barrier to the conical intersection resulting in fluorescence, whereas *para* derivatives show nonradiative decay because they have no energy barrier. Hydroxy derivatives were found to be excellent UV absorbers because of their broad absorption in both the UVA and UVB regions. The obtained results provide a useful insight into the detailed information for further designing and developing the superior UV absorber compounds.

Acknowledgments

This work has been supported in part by the Thailand Research Fund (RTA5380010). M.P. is grateful to the Royal Golden Jubilee PhD Program (Grant No. 3.C.KU/52/B.1) for a scholarship. TRF is grateful for research supporting to S.S. (MRG5480273) and to T.K. (RDG5230004). M.E. acknowledges support from the Japan Society for the Promotion of Science (JSPS) and the Computational Materials Science Initiative (CMSI), Japan. The Japan Student Services Organization (JASSO), Outbound Research Student Exchange (ORSE), Faculty of Science, Kasetsart University, Kasetsart University Research and Development Institute (KURDI), National Nanotechnology Center (NANOTEC), Laboratory of Computational and Applied Chemistry (LCAC), the Commission on Higher Education, Ministry of Education [through the "National Research University Project of Thailand (NRU)" and "National Center of Excellence for Petroleum, Petrochemical Technology and Advance Materials (NCEPPAM)"], Institute for Molecular Science (IMS) and Research Center for Computational Science are gratefully acknowledged for partial support and research facilities.

References

[1] S. Pattanaargson and P. Limphong, *Int. J. Cosmet Sci.*, 2001, 23, 153-160.
[2] T. M. Karpkird, S. Wanichweacharungruang, B. Albinsson, *Photochem. Photobiol. Sci.* 2009, 8, 1455.
[3] M. Promkatkaew, S. Suramitr, T. M. Karpkird, S. Namuangruk, M. Ehara and S. Hannongbua, *J. Chem. Phys.*, 2009, 131, 224306.
[4] M. Promkatkaew, S. Suramitr, T. Karpkird, M. Ehara and S. Hannongbua, *Int. J. Quan. Chem.*, 2013, 113, 542-554.

Malinee Promkatkaew, Songwut Suramitr, Thitinun Karpkird, Maahiro Ehara and Supa Hannongbua. Photophysical Properties and Photochemistry of Substituted Cinnamates for UVB Blocking: Effect of Hydroxy, Nitro, and Fluoro Substitutions at *ortho*, *meta*, and *para* Positions. The VIIIth congress of the International Society of Theoretical Chemical Physics (ISTCP-VIII), Budapest, Hungary. 25–31 August 2013

Photophysical Properties and Photochemistry of Substituted Cinnamates for UVB Blocking: Effect of Hydroxy, Nitro, and Fluoro Substitutions at *ortho*, *meta*, and *para* Positions

Malinee Promkatkaew,[1,2,3] Songwut Suramitr,[1,2] Thitinun Karpkird,[1]
Masahiro Ehara,[3,4*] and Supa Hannongbua[1,2*]

[1]Department of Chemistry, Faculty of Science, Kasetsart University, Bangkok 10900, Thailand
[2]Center of Nanotechnology, Kasetsart University, Bangkok 10900, Thailand
[3]The Graduate University for Advanced Studies (SOKENDAI), Okazaki 444-8585, Japan
[4]Institute for Molecular Science and Research Center for Computational Science, 38 Nishigo-naka, Myodaiji, Okazaki 444-8585, Japan
*Co-responding author: *ehara@ims.ac.jp (ME) and *fscisph@ku.ac.th (SP) Tel. +66-2-5625555 ext. 2111

Introduction

Cinnamate derivatives, an important class of organic UV filters, are widely used as UVB (280-320 nm) blocking compounds in cosmetic sunscreens. To improve the UV blocking function and photostability, chemical modification is necessary. In this work, absorption and fluorescence spectra were performed by the direct SAC-CI method to elucidate the characteristics of the spectra of these compounds over a wide energy range. Relaxation in the excited state was examined by the fluorescence measurement including oxygen quenching and the photostability was examined using UVB irradiation. *Cis-trans* photoisomerization pathways that lead to the nonradiative decay were also investigated. Based on the comprehensive analysis, the effective substitution in the cinnamate derivatives was proposed.

Methodology

Photophysical properties and photochemistry of substituted cinnamates have been investigated theoretically. This series includes monohydroxy-, -nitro, and -fluoro derivatives at the *ortho*, *meta*, and *para* positions (1E-9E). Ethylhexyl side chain was replaced with the methoxy group to reduce the computation time. Ground-state (S_0) and first excited-state (S_1) geometries were fully optimized using the B3LYP/6-31G(d) and CIS/D95(d) methods, respectively. To simulate the absorption and fluorescence spectra, the vertical excitation energies were calculated using the SAC-CI/D95(d). To calculate the solvent effect with the SAC-CI method, the excitation energies and oscillator strengths including the solvent effect with the help of the PCM-TDDFT calculations.

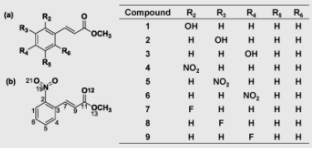

Compound	R_2	R_3	R_4	R_5	R_6
1	OH	H	H	H	H
2	H	OH	H	H	H
3	H	H	OH	H	H
4	NO_2	H	H	H	H
5	H	NO_2	H	H	H
6	H	H	NO_2	H	H
7	F	H	H	H	H
8	H	F	H	H	H
9	H	H	F	H	H

Fig. 1 Molecular structures of (a) substituted methyl cinnamates (1E-9E) and (b) the calculated model compounds and atom numbering of *ortho*-nitro methyl cinnamate (4E).

Results and Discussions

Table 1 Excitation Energies (E_{ex}), Absorption Wavelengths (λ_{abs}), Oscillator Strengths (f) and Dipole Moments (μ) in the Gas Phase and in Methanol Solution for Nine Substituted Methyl Cinnamates (1E-9E) Calculated Using the Direct SAC-CI Method.

		SAC-CI/D95(d)							Exp.
	State	E_{ex} (eV)	λ_{abs} (nm)	f	Excitation character	μ (D)[a]	$E_{ex(sol)}$[b]	$f_{(sol)}$[b]	(nm)
1E	X^1A'					(2.99)			
	$1^1A'$	3.84	323	0.267	H→L (34%), H-1→L (16%)	4.28	3.63	0.198	332
	$2^1A'$	4.50	275	0.273	H-1→L (33%), H→L (22%)	4.00	4.35	0.244	280
	$1^1A''$	4.79	259	0.000	H-3→L (32%), H-3→L+10 (12%)	0.13	5.03	0.000	
2E	X^1A'					(3.30)			
	$1^1A'$	4.00	310	0.082	H→L (28%), H-1→L (23%)	2.32	3.83	0.002	325
	$2^1A'$	4.55	273	0.431	H→L (58%), H-1→L (48%)	5.00	4.42	0.396	285
	$1^1A''$	4.75	261	0.000	H-3→L (37%), H-3→L+10 (14%)	0.13	4.97	0.000	
3E	X^1A'					(2.31)			
	$1^1A'$	4.15	299	0.287	H→L (33%), H→L+2 (23%)	4.27	3.93	0.160	314
	$2^1A'$	4.37	284	0.407	H→L (28%), H→L+2 (27%)	4.96	4.35	0.433	
	$1^1A''$	4.83	257	0.000	H-3→L (36%), H-3→L+14 (14%)	0.12	5.06	0.000	
4E	X^1A'					(5.88)			
	$1^1A'$	4.01	309	0.166	H→L (35%), H-1→L (15%)	3.30	3.77	0.137	
	$1^1A''$	4.21	295	0.000	H-3→L (31%), H-3→L+1 (18%)	0.11	4.32	0.000	
	$2^1A'$	4.63	268	0.351	H-1→L (26%), H→L+1 (23%)	4.47	4.44	0.334	281
5E	X^1A'					(5.40)			
	$1^1A'$	4.12	301	0.080	H→L (31%), H-1→L (16%)	2.26	3.93	0.101	
	$1^1A''$	4.36	284	0.000	H-4→L+1 (26%), H-4→L (22%)	0.10	4.48	0.000	
	$2^1A'$	4.61	269	0.262	H→L+1 (46%), H-1→L (43%)	3.87	4.47	0.213	282
6E	X^1A'					(4.20)			
	$1^1A'$	4.27	290	0.062	H-1→L (36%), H→L+1 (18%)	1.95	4.06	0.048	
	$1^1A''$	4.33	286	0.000	H-4→L (29%), H-4→L+1 (17%)	0.11	4.53	0.000	
	$2^1A'$	4.39	282	0.762	H→L (78%), H-1→L (17%)	6.77	4.15	0.679	304
7E	X^1A'					(3.09)			
	$1^1A'$	4.23	293	0.242	H→L (30%), H-1→L (25%)	3.88	4.13	0.282	
	$1^1A''$	4.37	284	0.000	H-3→L (28%), H-3→L+2 (28%)	0.11	4.59	0.000	
	$2^1A'$	4.56	272	0.307	H→L (28%), H-1→L (28%)	4.21	4.44	0.143	288
8E	X^1A'					(2.54)			
	$1^1A'$	4.33	286	0.038	H-1→L (34%), H→L+1 (25%)	1.51	4.27	0.066	
	$1^1A''$	4.38	283	0.000	H-3→L (42%), H-3→L+2 (23%)	0.10	4.59	0.000	
	$2^1A'$	4.60	269	0.626	H→L (70%), H→L+1 (17%)	5.99	4.46	0.472	284
9E	X^1A'					(1.27)			
	$1^1A'$	4.38	283	0.171	H→L+1 (28%), H→L (25%)	3.21	4.36	0.191	
	$1^1A''$	4.45	278	0.000	H-3→L (43%), H-3→L+2 (23%)	0.11	4.67	0.000	
	$2^1A'$	4.61	269	0.542	H→L (37%), H→L+1 (19%)	5.57	4.47	0.414	279

[a] Values in parentheses show the dipole moment of the ground state (XA').
[b] Solvent effect is calculated by PCM-TD-CAM-B3LYP in methanol solution from Ref. 4.

$$\Delta E_{i\to a,(sol)}^{SAC\text{-}CI} = \Delta E_{i\to a,(vac)}^{SAC\text{-}CI} + \Delta\Delta E_{i\to a,(sol)}^{TD\text{-}CAM-B3LYP} \quad (1)$$

$$f_{i\to a,(sol)}^{SAC\text{-}CI} = f_{i\to a,(vac)}^{SAC\text{-}CI} + \frac{\Delta E_{i\to a,(vac)}^{SAC\text{-}CI}}{\Delta E_{i\to a,(vac)}^{TD\text{-}CAM\text{-}B3LYP}} + f_{i\to a,(sol)}^{TD\text{-}CAM-B3LYP} \quad (2)$$

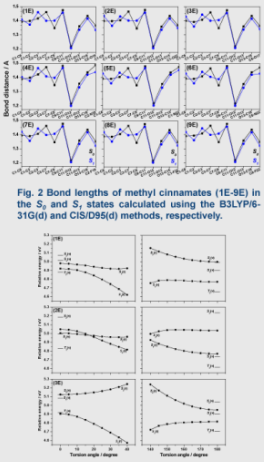

Fig. 2 Bond lengths of methyl cinnamates (1E-9E) in the S_0 and S_1 states calculated using the B3LYP/6-31G(d) and CIS/D95(d) methods, respectively.

Fig. 4 Excited state PECs for hydroxy methyl cinnamates (1E-3E). PECs of $S_1(r)$ and $S_2(r)$ were obtained by CIS(D)/6-31G(d)//CIS/6-31G(d) with fixed the torsion angle ω (C_2-C_7=C_8-C_{11}). The energy levels of $S_1(v)$, $S_2(v)$ and $T_1(v)$ were obtained by CIS(D)/6-31G(d).

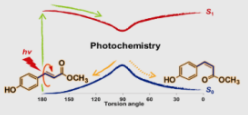

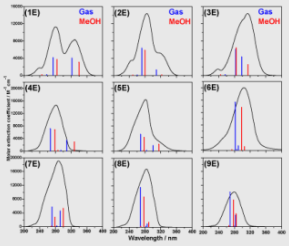

Fig. 3 Absorption spectra of methyl cinnamates (1E-9E) calculated using the direct SAC-CI method in the gas phase (blue) and in methanol solution (red) compared with the experimental spectra.

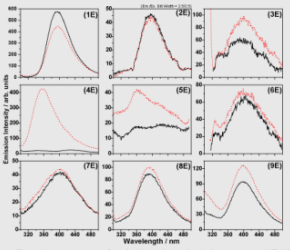

Fig. 5 Emission spectra of substituted methyl cinnamates (1E-9E) in the presence of oxygen (black line) and under nitrogen (red line).

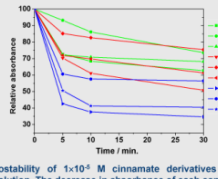

Fig.6 Photostability of 1×10^{-5} M cinnamate derivatives (1E-9E) in methanol solution. The decrease in absorbance of each compound was monitored at its maximum absorption as indicated.

Conclusions

Absorption spectra of these compounds were satisfactorily reproduced by the direct symmetry-adapted cluster-configuration interaction (SAC-CI) method with the experimental absorption bands. Emission spectra with oxygen quenching suggest that the emission or relaxation of some derivatives with an electron-withdrawing group (nitro and fluoro derivatives) occurs via a triplet state, whereas those with an electron-donating group (hydroxy derivatives) occur via a singlet excited state. We also examined the S_1 and S_2 potential energy curves (PECs) of the hydroxy derivatives, which lead to the conical intersection. Derivatives substituted at the *meta* position has an energy barrier to the conical intersection in S_1 and therefore show relatively strong fluorescence, whereas those at the *para* position show weak fluorescence without an energy barrier, leading to nonradiative decay. Among the derivatives, hydroxy derivatives were found to be excellent UV absorbers because of their broad absorption in both the UVA/UVB regions as well as their higher photostability. The present work provides important information for the design of UVB blocking compounds and for the possibility of photoactive molecules in the UV–Vis wavelength domain.

References

[1] S. Pattanaargson and P. Limphong, *Int. J. Cosmet Sci.*, 2001, 23, 153-160.
[2] T. M. Karpkird, S. Wanichweacharungruang, B. Albinsson, *Photochem. Photobiol. Sci.* 2009, 8, 1455.
[3] M. Promkatkaew, S. Suramitr, T. M. Karpkird, S. Namuangruk, M. Ehara and S. Hannongbua, *J. Chem. Phys.*, 2009, 131, 224306.
[4] M. Promkatkaew, S. Suramitr, T. Karpkird, M. Ehara and S. Hannongbua, *Int. J. Quan. Chem.*, 2013, 113, 542-554.

Acknowledgments

This work has been supported in part by the Thailand Research Fund (RTA5380010). M.P. is grateful to the Royal Golden Jubilee PhD Program (Grant No. 3.C.KU/52/B.1) for a scholarship. TRF is grateful for research supporting to S.S. (MRG5480273) and to T.K. (RDG5230004). M.E. acknowledges support from the Japan Society for the Promotion of Science (JSPS) and the Computational Materials Science Initiative (CMSI), Japan. The Japan Student Services Organization (JASSO), Outbound Research Student Exchange (ORSE), Faculty of Science, Kasetsart University, Kasetsart University Research and Development Institute (KURDI), National Nanotechnology Center (NANOTEC), Laboratory of Computational and Applied Chemistry (LCAC), the Commission on Higher Education, Ministry of Education [through the "National Research University Project of Thailand (NRU)" and "National Center of Excellence for Petroleum, Petrochemical Technology and Advance Materials (NCEPPAM)"], Institute for Molecular Science (IMS) and Research Center for Computational Science are gratefully acknowledged for partial support and research facilities.

Malinee Promkatkaew, Thitinun Karpkird, Peter Wolschann and Supa Hannongbua. Theoretical Investigation on the Inclusion of Methoxycinnamic Acid and Cyclodextrin by Performing Quantum Chemical Calculations and Molecular Dynamics Simulations. The 7th Asian Cyclodextrin Congress, Bangkok, Thailand. 27–29 November 2013

Theoretical Investigation on the Inclusion of Methoxycinnamic Acid and Cyclodextrin by Performing Quantum Chemical Calculations and Molecular Dynamics Simulations

Malinee Promkatkaew[1,2], Thitinun Karpkird[1], Peter Wolschann[3,4], and Supa Hannongbua[1,2]

[1]*Department of Chemistry, Faculty of Science, Kasetsart University, Bangkok 10900, Thailand*
[2]*Center of Nanotechnology, Kasetsart University, Bangkok 10900, Thailand*
[3]*Department of Pharmaceutical Technology and Biopharmacy University of Vienna, Austria*
[4]*Institute of Theoretical Chemistry, University of Vienna, Austria*

Introduction

Octyl methoxycinnamate (OMC) is widely used as UVB filter in sunscreen and many cosmetic formulations. OMC can absorb the UVB (280-320 nm) and UVA-II (320-340 nm). The photoisomerization of *trans*-OMC to *cis*-OMC causing a decrease of absorption efficiency. A photostability study of methoxycinnamoyl moieties attached to the cyclodextrins indicated that size matching played an important role in the molecular recognition process of the methoxycinnamoyl modified cyclodextrins. The inclusion complexation could improve photostability of the cinnamoyl moieties in an aqueous solution and are not cytotoxic compared to their parent methoxycinnamic acids.

Results and Discussion

Table 1 Torsion angles θ (deg.) of CA when bound to CDs

Complex	Gas Phase		Water (PCM)	
	Inside	Outside	Inside	Outside
[1] *p*CA-αCD	-4.32	-164.67	-4.32	-165.26
[2] *p*CA-βCD	-172.37	-163.67	-170.96	-165.06
[3] 245CA-βCD	-168.11	-173.51	-168.90	-174.60
[4] 246CA-βCD	-167.73	-168.94	-167.49	-167.30
[5] 246CA-γCD	171.72	-159.30	171.16	-163.31

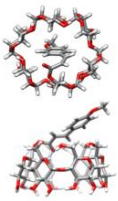

Table 2 Interaction energies of CA located inside and outside CD

Complex	Gas Phase	Water (PCM)
	ΔE (kcal/mol)	ΔE (kcal/mol)
[1] *p*CA-αCD	10.33	7.05
[2] *p*CA-βCD	5.64	2.91
[3] 245CA-βCD	-2.11	0.06
[4] 246CA-βCD	-5.93	-4.57
[5] 246CA-γCD	8.01	4.12

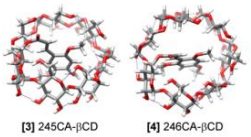

Figure 1 Structures of the M06-2x/6-31G(d,p) energy minima obtained for complex **[3]** 245CA-βCD : Head (left) and Tail (right) orientations

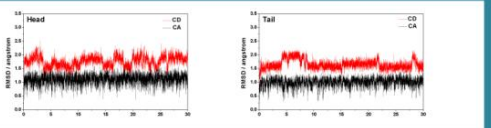

Figure 2 Root mean square displacement (RMSD) for complex **[3]** 245CA-βCD : Head (left) and Tail (right) orientations

Conclusions

The calculated results reveal that CA and CDs can form stable inclusion complexes in both the gas phase and water and their stability depends on molecular size and shape complementation. DFT and MD results show clearly that the Tail orientation of CA inserted into the cavity of CD is more favorable than the Head orientation. The calculated UV-Vis spectra show clearly that the Tail orientation of inclusion complex between CA and CD is most stable orientations and can absorb in both UVB and UVA regions which is similar to the parent CA. The agreement between theoretical results and experimental data can be a potent way to determine the geometry of supramolecular system. We expect that the theoretical results would provide valuable information for developing effective UV blocking compound.

Methods of Calculations

Five host-guest inclusion complexes between methoxycinnamic acid (CA) and cyclodextrins (CD) including **[1]** *p*CA-αCD, **[2]** *p*CA-βCD, **[3]** 245CA-βCD, **[4]** 246CA-βCD, and **[5]** 246CA-γCD. The geometries of all five complexes were studied by using quantum chemical calculations. All possible conformers have been considered and analyzed the structural and energetic behaviors. Whereas, molecular dynamics simulations were investigated the most photostability complex **[3]** 245CA with βCD, the most widely used one of the natural CDs.

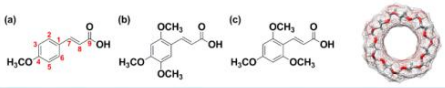

Table 3 Binding (ΔE_b) and deformation (ΔE_d) energies (kcal/mol) between methoxycinnamic acid and cyclodextrins both in gas phase and water

Complex	Gas Phase				Water (PCM)			
	ΔE_b	ΔE_d	ΔE_d(H)	ΔE_d(G)	ΔE_b	ΔE_d	ΔE_d(H)	ΔE_d(G)
	Head orientation							
[1] *p*CA-αCD	-20.65	-26.80	1.60	4.54	-18.04	-23.72	1.50	4.18
[2] *p*CA-βCD	-21.42	-35.11	1.73	11.95	-17.57	-30.40	2.36	10.47
[3] 245CA-βCD	-24.07	-37.46	4.01	9.38	-15.11	-26.16	4.37	6.67
[4] 246CA-βCD	-18.35	-29.57	4.73	6.49	-13.30	-25.78	5.01	7.47
[5] 246CA-λCD	-21.01	-28.13	2.56	4.56	-16.53	-20.22	1.95	1.74
	Tail orientation							
[1] *p*CA-αCD	-27.38	-35.82	2.57	5.87	-19.75	-26.65	2.05	4.85
[2] *p*CA-βCD	-30.69	-40.19	1.02	8.48	-22.07	-29.18	0.40	6.72
[3] 245CA-βCD	-37.96	-52.61	2.35	12.30	-25.58	-37.18	1.80	9.80
[4] 246CA-βCD	-37.23	-52.83	4.88	10.72	-24.49	-37.45	3.81	9.14
[5] 246CA-λCD	-35.41	-50.22	4.69	10.12	-24.17	-35.45	3.75	7.53

Table 4 Excitation energies (E_{ex}), absorption wavelengths (λ_{abs}), and oscillator strengths (f) in the gas phase and in DMSO for methoxyinnamic acid, cyclodextrins and host-guest inclusion complexes calculated using the TD-M06-2X/6-31G(d,p) method compared with the experimental data.

Compound		State	Gas Phase			DMSO (PCM)			*Exp.*
			E_{ex} (eV)	λ_{abs} (nm)	f	E_{ex} (eV)	λ_{abs} (nm)	f	(nm)
Guest	*p*CA	S_1	4.61	269	0.789	4.41	281	0.917	320
	245CA	S_1	4.05	306	0.521	3.86	321	0.629	350
		S_2	4.97	250	0.213	4.85	256	0.226	290
	246CA	S_1	4.50	276	0.724	4.26	291	0.842	320
Host	αCD	S_1	8.18	152	0.000	8.27	150	0.003	
	βCD	S_1	8.17	152	0.001	8.26	150	0.004	
	γCD	S_1	8.16	152	0.002	8.26	150	0.005	

Complex	State	Gas Phase			DMSO (PCM)		
		E_{ex} (eV)	λ_{abs} (nm)	f	E_{ex} (eV)	λ_{abs} (nm)	f
[1] (a) Inside	S_1	4.94	251	0.189	4.87	255	0.349
(b) Outside	S_1	4.51	275	0.671	4.38	283	0.795
(c) Head	S_1	4.71	263	0.399	4.53	273	0.538
(d) Tail	S_1	4.31	288	0.464	4.30	289	0.582
[2] (a) Inside	S_1	4.69	264	0.254	4.51	275	0.612
(b) Outside	S_1	4.41	281	0.729	4.29	289	0.869
(c) Head	S_1	4.50	276	0.539	4.35	285	0.683
(d) Tail	S_1	4.16	298	0.591	4.14	299	0.732
[3] (a) Inside	S_1	4.12	301	0.335	3.98	311	0.419
	S_3	4.97	249	0.148	4.83	257	0.041
(b) Outside	S_1	3.96	313	0.546	3.83	324	0.654
	S_2	4.89	254	0.202	4.83	257	0.211
(c) Head	S_1	4.25	292	0.281	4.07	305	0.354
	S_2	4.89	253	0.013	4.94	251	0.068
(d) Tail	S_1	3.72	334	0.348	3.71	335	0.440
	S_2	4.70	264	0.126	4.71	263	0.147
[4] (a) Inside	S_1	4.43	280	0.486	4.23	293	0.620
(b) Outside	S_1	4.35	285	0.756	4.19	296	0.889
(c) Head	S_1	4.60	269	0.405	4.43	280	0.503
(d) Tail	S_1	4.17	297	0.450	4.12	301	0.575
[5] (a) Inside	S_1	4.28	289	0.568	4.08	304	0.718
(b) Outside	S_1	4.28	289	0.679	4.18	297	0.815
(c) Head	S_1	4.51	275	0.532	4.35	285	0.650
(d) Tail	S_1	4.18	296	0.480	4.12	301	0.608

References

1. Karpkird T., Wanichweacharungruang S., *Journal of Photochemistry and Photobiology A: Chemistry* (2010), 212, 56-61.
2. Snor W., Liedl E., Weiss-Greiler P., Viernsteinb H., Wolschann P., *International Journal of Pharmaceutics* (2009), 381, 146-152.
3. Pan W., Zhang D., Zhan J., *Journal of Hazardous Materials* (2011), 192, 1780-1786.

Acknowledgments

This work has been supported in part by the Royal Golden Jubilee PhD Program (Grant No. 3.C.KU/52/B.1), Thailand Research Fund (RTA5380010), Faculty of Science, Kasetsart University, Kasetsart University Research and Development Institute (KURDI), National Nanotechnology Center (NANOTEC), Laboratory of Computational and Applied Chemistry (LCAC), the Commission on Higher Education, Ministry of Education [through the "National Research University Project of Thailand (NRU)" and "National Center of Excellence for Petroleum, Petrochemical Technology and Advance Materials (NCEPPAM)"].

CURRICULUM VITAE

NAME : Ms. Malinee Promkatkaew

BIRTH DATE : April 2, 1985

BIRTH PLACE : Chiang-Rai, Thailand

EDUCATION

YEAR	INSTITUTE	DEGREE/DIPLOMA
2007	Naresuan Univ.	B.Sc.(Biology)
2009	Kasetsart Univ.	M.S.(Chemistry)

AWARDS

1. Outstanding Poster Presentation Award, The Pure and Applied Chemistry International Conference (PACCON 2009), Naresuan University, Phitsanulok, Thailand, January 14–16, 2009.
2. 2nd Outstanding Master Thesis Award, The Graduate School Kasetsart University 2009.

SCHOLARSHIPS

M.Sc. (2007–2008)	The National Center of Excellence for Petroleum, Petrochemicals and Advanced Materials (NCE-PPAM)
M.Sc. (2008–2009)	The Thailand Graduated Institute of Science and Technology (TGIST)
Apr.–May 2009	The Bilateral Research Cooperation (BRC) Faculty of Science, Kasetsart University
Ph.D. (2009–2013)	The Royal Golden Jubilee PH.D. Program (3.C.KU/52/B.1)
Oct.–Dec. 2011	The Outbound Research Student Exchange (ORSE), Faculty of Science, Kasetsart University
Oct. 2011–Feb. 2012	The Japan Student Services Organization (JASSO)

PUBLICATIONS

1. Malinee Promkatkaew, Songwut Suramitr, Thitinun Karpkird, Supason Wanichweacharungrang, Masahiro Ehara, and Supa Hannongbua. 2014. Photophysical and Photochemical Properties of the Substituted Cinnamates and Cinnamic Acids for UVB Blocking Function: Effect of Hydroxy, Nitro, and Fluoro Substitutions at *ortho*-, *meta*-, and *para*-Positions. **Photochemical and Photobiological Sciences**. 13: 583-594.

2. Malinee Promkatkaew, Duangkamol Gleeson, Supa Hannongbua and M. Paul Gleeson. 2014. Skin Sensitization Prediction Using Quantum Chemical Calculations: A Theoretical Model for the S_NAr Domain. **Chemical Research in Toxicology**. 27(1): 51-60.

3. Malinee Promkatkaew, Songwut Suramitr, Thitinun Karpkird, Masahiro Ehara, and Supa Hannongbua. 2013. Absorption and Emission Properties of Various Substituted Cinnamic Acids and Cinnamates, Based on TDDFT Investigation. **International Journal of Quantum Chemistry**. 113(4): 542-554.

4. Masahiro Ehara, Biswajit Saha, Potjaman Poolmee, Malinee Promkatkaew, Supa Hannongbua, Yun-peng Lu, and Hiroshi Nakatsuji. 2012. Electronic Structure and Optical Properties of Conjugated Molecules: SAC-CI Study. **International Conference of Computational Methods in Sciences and Engineering 2009, AIP Conference Proceeding.** 1504: 279-290.

5. Masahiro Ehara, Lu Yun-peng, Malinee Promkatkaew, and Supa Hannongbua. 2012. Electronic Structure and Optical Properties of Conjugated Molecules: SAC-CI Study. **International Conference of Computational Methods in Sciences and Engineering 2009, AIP Conference Proceeding.** 1504: 848-851.

6. M. Paul Gleeson, Sandeep Modi, Andreas Bender, Richard L. Marcese Robinson, Johannes Kirchmair, Malinee Promkatkaew, Supa Hannongbua and Robert C. Glen. 2012. The Challenges Involved in Modeling Toxicity Data In Silico: A Review. **Current Pharmaceutical Design**. 18(9): 1266-1291.

7. Malinee Promkatkaew, Songwut Suramitr, Thitinun Monhaphol Karpkird, Supawadee Namuangruk, Masahiro Ehara, and Supa Hannongbua. 2009. Absorption and Emission Spectra of UVB Blocking Methoxy Substituted Cinnamates Investigated Using the Symmetry-Adapted Cluster Configuration Interaction Method. **Journal of Chemical Physics**. 131(22): 224309-1-10.